1.0

2.8   2.5
3 2   2.2
36
4 0   2.0

1.1

1.8

1.25   1.4   1.6

MICROCOPY RESOLUTION TEST CHART
NATIONAL BUREAU OF STANDARDS 1963 A.

REPORT DOCUMENTATION PAGE		READ INSTRUCTIONS BEFORE COMPLETING FORM
1. REPORT NUMBER 81-11D	2. GOVT ACCESSION NO. AD A10R014	3. RECIPIENT'S CATALOG NUMBER
4. TITLE (and Subtitle) Molecular Dynamics Calculations for Sodium using Pseudopotential Theory.		5. TYPE OF REPORT & PERIOD COVERED THESIS/DISSERTATION
		6. PERFORMING ORG. REPORT NUMBER
7. AUTHOR(s) Richard E. Swanson		8. CONTRACT OR GRANT NUMBER(s)
9. PERFORMING ORGANIZATION NAME AND ADDRESS AFIT STUDENT AT: Univ of New Mexico		10. PROGRAM ELEMENT, PROJECT, TASK AREA & WORK UNIT NUMBERS
11. CONTROLLING OFFICE NAME AND ADDRESS AFIT/NR WPAFB OH 45433		12. REPORT DATE Apr 81
		13. NUMBER OF PAGES 173
14. MONITORING AGENCY NAME & ADDRESS(if different from Controlling Office)		15. SECURITY CLASS. (of this report) UNCLASS
		15a. DECLASSIFICATION DOWNGRADING SCHEDULE

LEVEL

16. DISTRIBUTION STATEMENT (of this Report)

APPROVED FOR PUBLIC RELEASE; DISTRIBUTION UNLIMITED

17. DISTRIBUTION STATEMENT (of the abstract entered in Block 20, if different from Report)

23 NOV 1981

18. SUPPLEMENTARY NOTES

APPROVED FOR PUBLIC RELEASE: IAW AFR 190-17

FREDRIC C. LYNCH, Major, USAF
Director of Public Affairs
Air Force Institute of Technology (ATC)
Wright-Patterson AFB, OH 45433

19. KEY WORDS (Continue on reverse side if necessary and identify by block number)

20. ABSTRACT (Continue on reverse side if necessary and identify by block number)

ATTACHED

DD FORM 1473 EDITION OF 1 NOV 65 IS OBSOLETE

UNCLASS

81 11 30 016

MOLECULAR DYNAMICS CALCULATIONS FOR SODIUM
USING PSEUDOPOTENTIAL THEORY

Richard E. Swanson

B.S., Physics, United States Air Force Academy, 1970

M.S., Physics, The Ohio State University, 1971

Ph.D., Physics, University of New Mexico, 1981

We study the equation of state of sodium using the molecular dy-namics technique whereby the classical motion of a system of ions is solved with the aid of computers. The interaction potential between pairs of sodium ions consists of coulomb and Born-Mayer repulsion terms and an effective ion-ion interaction derived from pseudopotential theory. This theory includes the effects of electron gas screening, exchange, and correlation. We use a model pseudopotential with param-eters fit to experimental low-temperature data. By using this technique, we are able to begin with an atomic description of a simple metal and proceed to calculate its macroscopic thermodynamic properties.

We calculate equation-of-state points consisting of the total in-ternal energy in volume and temperature space. For our study, the volume ranges from 10% expansion to 10% compression of the normal den-sity and the temperature ranges from 0 to 600 Kelvin. We are able to calculate directly values of the function that contains the anharmonic contributions to the energy. We report the results for calculations of solid sodium in the hexagonal close-packed (hcp) and body-centered cubic (bcc) phases, and of liquid sodium.

At high temperatures the molecular dynamics system melts. We cool the liquid sodium back to low temperatures and it forms a metastable glassy state for which we are able to calculate equation-of-state points. We study the dynamics of the melt transition and define a region where

partial melting occurs. The upper limit that we place on the melting temperature is consistent with the observed value and the calculated heat of fusion, diffusion coefficient, and atomic distributions agree well with experiment.

We illustrate the unique capabilities of the molecular dynamics technique by inducing a dynamic bcc-to-hcp martensitic phase change. We change the shape of the calculational volume, which pushes the bcc sodium structure over a potential hill. It then spontaneously transforms to the more stable hcp structure.

The results of this study demonstrate that the molecular dynamics technique, coupled with an interaction potential that adequately describes the ion-ion interaction in a simple metal, can be used to calculate the macroscopic properties of such systems.

AFIT RESEARCH ASSESSMENT

The purpose of this questionnaire is to ascertain the value and/or contribution of research accomplished by students or faculty of the Air Force Institute of Technology (ATC). It would be greatly appreciated if you would complete the following questionnaire and return it to:

AFIT/NR
Wright-Patterson AFB OH 45433

RESEARCH TITLE: Molecular Dynamics Calculations for Sodium using Pseudopotential Theory

AUTHOR: Richard E. Swanson

RESEARCH ASSESSMENT QUESTIONS:

1. Did this research contribute to a current Air Force project?

( ) a. YES ( ) b. NO

2. Do you believe this research topic is significant enough that it would have been researched (or contracted) by your organization or another agency if AFIT had not?

( ) a. YES ( ) b. NO

3. The benefits of AFIT research can often be expressed by the equivalent value that your agency achieved/received by virtue of AFIT performing the research. Can you estimate what this research would have cost if it had been accomplished under contract or if it had been done in-house in terms of manpower and/or dollars?

( ) a. MAN-YEARS _____ ( ) b. $_____

4. Often it is not possible to attach equivalent dollar values to research, although the results of the research may, in fact, be important. Whether or not you were able to establish an equivalent value for this research (3. above), what is your estimate of its significance?

( ) a. HIGHLY ( ) b. SIGNIFICANT ( ) c. SLIGHTLY ( ) d. OF NO
SIGNIFICANT SIGNIFICANT SIGNIFICANCE

5. AFIT welcomes any further comments you may have on the above questions, or any additional details concerning the current application, future potential, or other value of this research. Please use the bottom part of this questionnaire for your statement(s).

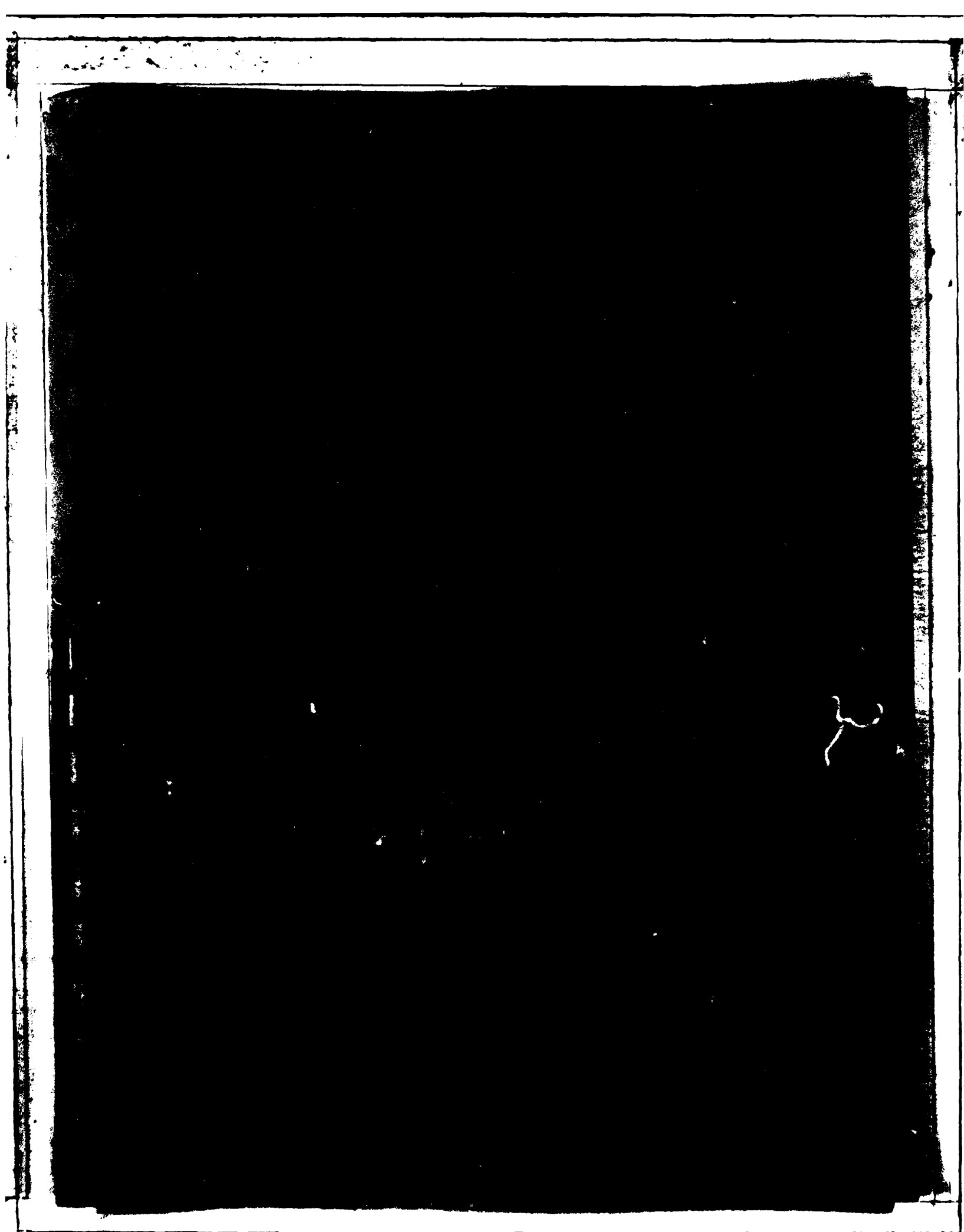NAME   GRADE   POSITION

ORGANIZATION   LOCATION

STATEMENT(s):

MOLECULAR DYNAMICS CALCULATIONS FOR SODIUM
USING PSEUDOPOTENTIAL THEORY

Richard E. Swanson
B.S., Physics, United States Air Force Academy, 1970
M.S., Physics, The Ohio State University, 1971
Ph.D., Physics, University of New Mexico, 1981

We study the equation of state of sodium using the molecular dy-
namics technique whereby the classical motion of a system of ions is
solved with the aid of computers. The interaction potential between
pairs of sodium ions consists of coulomb and Born-Mayer repulsion terms
and an effective ion-ion interaction derived from pseudopotential
theory. This theory includes the effects of electron gas screening,
exchange, and correlation. We use a model pseudopotential with param-
eters fit to experimental low-temperature data. By using this technique,
we are able to begin with an atomic description of a simple metal and
proceed to calculate its macroscopic thermodynamic properties.

We calculate equation-of-state points consisting of the total in-
ternal energy in volume and temperature space. For our study, the
volume ranges from 10% expansion to 10% compression of the normal den-
sity and the temperature ranges from 0 to 600 Kelvin. We are able to
calculate directly values of the function that contains the anharmonic
contributions to the energy. We report the results for calculations of
solid sodium in the hexagonal close-packed (hcp) and body-centered
cubic (bcc) phases, and of liquid sodium.

At high temperatures the molecular dynamics system melts. We cool
the liquid sodium back to low temperatures and it forms a metastable
glassy state for which we are able to calculate equation-of-state points.
We study the dynamics of the melt transition and define a region where

partial melting occurs. The upper limit that we place on the melting temperature is consistent with the observed value and the calculated heat of fusion, diffusion coefficient, and atomic distributions agree well with experiment.

We illustrate the unique capabilities of the molecular dynamics technique by inducing a dynamic bcc-to-hcp martensitic phase change. We change the shape of the calculational volume, which pushes the bcc sodium structure over a potential hill. It then spontaneously transforms to the more stable hcp structure.

The results of this study demonstrate that the molecular dynamics technique, coupled with an interaction potential that adequately describes the ion-ion interaction in a simple metal, can be used to calculate the macroscopic properties of such systems.

MOLECULAR DYNAMICS CALCULATIONS FOR SODIUM

USING PSEUDOPOTENTIAL THEORY

BY

RICHARD E. SWANSON

B.S., United States Air Force Academy, 1970

M.S., The Ohio State University, 1971

DISSERTATION

Submitted in Partial Fulfillment of the

Requirements for the Degree of

Doctor of Philosophy in Physics

The University of New Mexico

Albuquerque, New Mexico

April 1981

ACKNOWLEDGMENTS

I gratefully acknowledge the support ot the Air Force Institute of Technology, the United States Air Force Academy, the Los Alamos National Laboratory, and the University of New Mexico, whose cooperation made the time and facilities available for this study.

I especially appreciate the continued support of Dr. C. L. Mader who encouraged and helped me through this entire effort, and the support of Dr. J. F. Barnes who was instrumental in setting up this program.

This effort was guided by the advice and technical experience of Dr. G. K. Straub, Dr. B. L. Holian, and Dr. D. C. Wallace whose support, help, and ideas were used on a continuing basis.

I was fortunate to have scientists such as Dr. M. S. Shaw, Dr. J. D. Johnson, Dr. G. I. Kerley, and J. D. Kershner available for discussions.

I especially thank Louise Criss who provided moral encouragement throughout the effort and edited and typed the text. Thanks also go to Sharon Crane who graciously helped with the text.

My most heartfelt appreciation goes to my wife, Leigh, who steadfastly and lovingly took over my duties at home during this busy time and encouraged me throughout the effort. Special thanks go to Serena and her new brother, Shane, who arrived two days before I defended this dissertation and reminded me of the more important aspects of life.

MOLECULAR DYNAMICS CALCULATIONS FOR SODIUM

USING PSEUDOPOTENTIAL THEORY

BY

RICHARD E. SWANSON

ABSTRACT OF DISSERTATION

Submitted in Partial Fulfillment of the
Requirements for the Degree of

Doctor of Philosophy in Physics

The University of New Mexico
Albuquerque, New Mexico

MOLECULAR DYNAMICS CALCULATIONS FOR SODIUM
USING PSEUDOPOTENTIAL THEORY

Richard E. Swanson
B.S., Physics, United States Air Force Academy, 1970
M.S., Physics, The Ohio State University, 1971
Ph.D., Physics, University of New Mexico, 1981

We study the equation of state of sodium using the molecular dynamics technique whereby the classical motion of a system of ions is solved with the aid of computers. The interaction potential between pairs of sodium ions consists of coulomb and Born-Mayer repulsion terms and an effective ion-ion interaction derived from pseudopotential theory. This theory includes the effects of electron gas screening, exchange, and correlation. We use a model pseudopotential with parameters fit to experimental low-temperature data. By using this technique, we are able to begin with an atomic description of a simple metal and proceed to calculate its macroscopic thermodynamic properties.

We calculate equation-of-state points consisting of the total internal energy in volume and temperature space. For our study, the volume ranges from 10% expansion to 10% compression of the normal density and the temperature ranges from 0 to 600 Kelvin. We are able to calculate directly values of the function that contains the anharmonic contributions to the energy. We report the results for calculations of solid sodium in the hexagonal close-packed (hcp) and body-centered cubic (bcc) phases, and of liquid sodium.

At high temperatures the molecular dynamics system melts. We cool the liquid sodium back to low temperatures and it forms a metastable glassy state for which we are able to calculate equation-of-state points. We study the dynamics of the melt transition and define a region where

partial melting occurs. The upper limit that we place on the melting temperature is consistent with the observed value and the calculated heat of fusion, diffusion coefficient, and atomic distributions agree well with experiment.

We illustrate the unique capabilities of the molecular dynamics technique by inducing a dynamic bcc-to-hcp martensitic phase change. We change the shape of the calculational volume, which pushes the bcc sodium structure over a potential hill. It then spontaneously transforms to the more stable hcp structure.

The results of this study demonstrate that the molecular dynamics technique, coupled with an interaction potential that adequately describes the ion-ion interaction in a simple metal, can be used to calculate the macroscopic properties of such systems.

CONTENTS

LIST OF FIGURES

Figure   Page

LIST OF TABLES

I.   INTRODUCTION

Pseudopotential theory has proved useful in studying many properties of simple metals (for example, see Refs. 1-7). It is a method for solving the Schrödinger equation which contains the essential features of the behavior of the electrons in these metals.

Molecular dynamics is a technique for studying the classical behavior of a many-particle system. Newton's second law is solved from the force between pairs of interacting particles where the force is determined by the gradient of the interaction potential between pairs of particles. The interaction potentials most commonly used in molecular dynamics calculations are empirically determined (for example, the Lennard-Jones potential). While such potentials are easy to use and adequately represent the behavior of some systems, they are not appropriate to the interactions between the ions in a simple metal.

We propose to use an effective ion-ion interaction potential derived using the pseudopotential method in our molecular dynamics calculations. By doing this we are able to start with the atomic description of the simple metal and proceed to calculate macroscopic thermodynamic properties. This effective interaction potential is long range and requires the inclusion of approximately 170 neighbors for each particle when the forces are calculated.

Additionally, the crystal potential energy of the effective interaction is only a fraction (about (0.2%) of the total energy of the crystal. The volume-dependent energy terms (such as the electron-gas kinetic energies and the exchange and correlation energies) are primarily responsible for holding the crystal together. These terms are

calculated separately and added to the structure-dependent energy, which
is calculated by the molecular dynamics program.

In the "Background" section of this paper we describe the theory
for both the pseudopotential method and the molecular dynamics technique.
This discussion has been developed elsewhere, as referenced in the text,
and we include the features important to our study for completeness.

In Sec. III and IV we describe the calculation of the effective
ion-ion interaction for sodium and the setup of our molecular dynamics
calculations. We outline in detail the necessary steps for determining
the parameters and run conditions necessary to perform these calculations.

In Sec. V we develop the equations necessary for the calculation of
the volume-dependent energy terms, mentioned above, that must be added
to the structure-dependent terms to arrive at the total system energy.

In these first five sections, we describe the technique for using
the quantum mechanical results of pseudopotential theory in a classical
trajectory calculation of the motion of the ions of sodium. Using this
technique, we calculate equation-of-state points consisting of the sys-
tem energies at given volumes and temperatures for solid sodium in the hcp
and bcc phases and for liquid sodium. We are able to define the equa-
tion of state for a "glassy" sodium, which is the liquid extended to a
metastable low-temperature state. The results of these calculations
are direct measurements of the anharmonic contributions to the system
energy for these systems.

One of the major advantages of the molecular dynamics technique is
the ability to follow the dynamics of the system studied. We discuss
the melting of sodium and are able to define a transition region of
partial melting. The calculated heats of fusion and upper limit to the

melting temperature are in agreement with observed values. We are also able to calculate the atomic distributions and diffusion coefficients for sodium.

As a final result and as a demonstration of the unique capabilities of molecular dynamics calculations, we present a calculation of the dynamics of the bcc→hcp phase change in sodium. We artificially change the shape of the calculational volume. This pushes the meta-stable low-temperature bcc structure over a potential hill. The system is then able to spontaneously relax into the preferred hcp structure with an accompanying increase in temperature.

Our results indicate that the technique described in this paper adequately represents the behavior of sodium in the volume (10% expansion to 10% compression) and temperature (0-600 K) ranges studied.

II. BACKGROUND

This section discusses the necessary theoretical background for development of the technique described in the introduction, by which we will study the sodium equation of state. Section II.A discusses the pseudopotential method and culminates with an expression for the total effective ion-ion interaction. Section II.B describes the molecular dynamics technique and the applicable equations.

A. The Pseudopotential Method

W. calculate the ion motion in a simple metal. A simple metal is one for which the conduction electrons behave very nearly as if they comprise a free-electron gas.[1,2] We assume that the metal consists of ions and conduction electrons. The ions are composed of the nuclei and the core electrons. An ion core does not overlap with other ion cores. The core electron states are assumed to be the same as the respective states in a free atom.[1,3]

In this section we describe the pseudopotential method, which is a technique for solving the Schrödinger equation for the energy of the conduction electrons. In Sec. II.A.1 we express the electron energy in terms of the pseudopotential. In II.A.2 we restructure the equation to express the electron energy in terms of an effective ion-ion interaction. In Secs. II.A.3 - II.A.5 we incorporate a local approximation to the pseudopotential and modify the theory to include electron screening, exchange, and correlation effects. In Sec. II.A.6 we develop the model pseudopotential that we will use for this study, and in Sec. II.A.7 we add the coulomb and core repulsion terms to obtain the total ion-ion interaction, which will be used in the molecular dynamics calculations.

1.   Conduction Electron Energy. The total Hamiltonian, H_{TOT}, for a system of N ions and N' electrons, neglecting external interactions, is

$$H_{TOT} = H_I + H_e \tag{1}$$

with subscript e denoting electrons and subscript I denoting ions, where

$$H_I = \sum_{\ell} \frac{\vec{P}_\ell^2}{2m_I} + \sum_{\ell} \sum_{k > \ell} V_I(\vec{R}_\ell - \vec{R}_k)$$

$$= T_I + V_I$$

$$H_e = \sum_{i} \frac{\vec{P}_i^2}{2m_e} + \sum_{i} \sum_{j > i} V_e(\vec{r}_i - \vec{r}_j) + \sum_{i} \sum_{\ell} V_{I-e}(\vec{r}_i, \vec{R}_\ell)$$

$$= T_e + V_e + V_{I-e}$$

$\ell, k = 1, \cdots N$

$i, j = 1, \cdots N'$

$\vec{r}_i$ = electron positions

$\vec{R}_\ell$ = ion positions

T = kinetic energy

m = mass

V_I = ion-ion potential interaction

V_e = electron-electron potential interaction

V_{I-e} = ion-electron potential interaction

The Schrödinger equation is

$$H_{TOT} \psi_{TOT} = E_{TOT} \psi_{TOT} \cdot \tag{2}$$

The solution of this equation is intractable, and we simplify it with another well-known assumption--the adiabatic, or Born-Oppenheimer, approximation. The essence of this approximation is that the electrons readjust themselves so rapidly to a change in ion configuration that the ions are regarded as fixed when solving for the electron energies. This uncouples the electron part of the equation from the ion part. Therefore, the total wave function is separable and is written as

$$\Psi_{TOT} = \Psi_I \Psi_e \quad .$$

We may solve the electron problem for fixed ion positions to obtain

$$H_e \Psi_e = E_e \Psi_e \quad . \tag{3}$$

This substituted in Eq. (2) yields

$$H_{TOT} \Psi_{TOT} = (T_I + V_I + H_e)\Psi_I \Psi_e = E_{TOT} \Psi_I \Psi_e$$
$$= T_I \Psi_I \Psi_e + V_I \Psi_I \Psi_e + E_e \Psi_I \Psi_e \quad , \tag{4}$$

where

$$T_I \Psi_I \Psi_e = \sum_\ell \frac{\vec{P}_\ell^{\,2}}{2m} \Psi_I \Psi_e = -\sum_\ell \frac{\hbar^2}{2m} \frac{\partial^2}{\partial \vec{R}_\ell^{\,2}} \Psi_I \Psi_e$$

$$= -\Psi_e \sum_\ell \frac{\hbar^2}{2m_I} \frac{\partial^2}{\partial \vec{R}_\ell^{\,2}} \Psi_I - \frac{\hbar^2}{2m_I} \sum_\ell \left(2 \frac{\partial \Psi_e}{\partial \vec{R}_\ell} \frac{\partial \Psi_I}{\partial \vec{R}_\ell} + \Psi_I \frac{\partial^2 \Psi_e}{\partial \vec{R}_\ell^{\,2}} \right) \quad .$$

The last two terms in this expression are neglected in the adiabatic approximation because they contribute negligibly to the system energy.[4,5] Thus, we can write

$$H_{TOT} \Psi_{TOT} = \Psi_e (T_I + V_I + E_e)\Psi_I = E_{TOT} \Psi_I \Psi_e$$

or

$$(H_I + E_e)\Psi_I = E_{TOT}\Psi_I \quad , \tag{5}$$

and we see that the adiabatic approximation allows consideration of the electron problem separately from the ion problem. The conduction electron energy becomes an effective potential energy of the ions.[3] We now solve the electron problem,

$$H_e\Psi_e = E_e\Psi_e \quad .$$

We assume the self-consistent field, or one-electron, approximation, where the potential $(V(\vec{r}))$ that an electron moves in is calculated in a self-consistent manner.[1] We write

$$H_e = T_e + V(\vec{r}) \quad ,$$

where $V(r)$ is the self-consistent field and we write the Schrödinger equation for a single electron as:[1]

$$H_e\psi = [T_e + V(\vec{r})]\psi = E_e\psi$$

Following the notation in Ref. 6, we use the index t to denote core electron states and j to denote the state centered at ion position R_j. We have

$$[T_e + V(\vec{r})]\psi_{t,j} = E_{t,j}\psi_{t,j} \quad , \tag{6}$$

where the $\psi_{t,j}$ are the same as for the free atom, according to our first assumption.

With the above equation established within the constraints of the assumptions mentioned, we now restructure it in terms of the pseudopotential formulation. First we expand the electron wave functions

in terms of a basis of functions that are constructed to be orthogonal to the core states. Following Harrison,[1,6] we use the notation

$$|\vec{k}\rangle \equiv \Omega^{-\frac{1}{2}} e^{i\vec{k}\cdot\vec{r}} \text{ , a normalized plane wave,}$$

$$|t,j\rangle \equiv \psi_t(\vec{r} - \vec{R}_j) \text{ , a normalized core function} \text{ centered at ion position } R_j,$$

and

$$\langle t,j|\vec{k}\rangle = \Omega^{-\frac{1}{2}} \int d^3r \ \psi_t(\vec{r} - \vec{R}_j) e^{i\vec{k}\cdot\vec{r}} \ .$$

Then we write the basis functions, called orthogonalized plane waves, as

$$OPW_k = (1 - P)|\vec{k}\rangle \ ,$$

where P is the projection operator, which projects any function onto the core states[1] (note that $\langle t,j|t',j'\rangle = \delta_{tt'}\delta_{jj'}$),

$$P = \sum_j |t,j\rangle\langle t,j| \ . \tag{7}$$

We expand the conduction electron wave function in terms of the orthogonalized plane waves to obtain

$$\psi = (1 - P)\sum_k a_k |k\rangle \ , \tag{8}$$

where a_k are the expansion coefficients. If we substitute ψ in the Schrödinger equation, the solution could be attempted using the standard orthogonalized plane wave method. We are attempting a different approach and will restructure the equation. We introduce the pseudowavefunction,

$$\phi = \sum_k a_k |k\rangle \tag{9}$$

so that

$$\psi = (1 - P)\phi \ . \tag{10}$$

We note that ϕ is an expansion of free electron states and that $\phi = \psi$ outside the cores because the projection operator is zero there.[6] Substituting in the Schrödinger equation yields

$$T_e(1 - P)\phi + V(\vec{r})(1 - P)\phi = E(1 - P)\phi \quad ,$$

and rearranging gives

$$T_e\phi + V(\vec{r})\phi - [T_e + V(r)]P\phi + EP\phi = E\phi \quad ,$$

so that

$$T_e\phi + W\phi = E\phi \quad , \tag{11}$$

where we have defined the operator,

$$W = V(\vec{r}) - [T_e + V(\vec{r})]P + EP \equiv \text{the pseudopotential operator.}$$

Using

$$[T_e + V(\vec{r})]P = \sum_{t,j} E_{t,j}|t,j\rangle\langle t,j| \quad ,$$

we have

$$W = V(\vec{r}) + \sum_{t,j} (E - E_{t,j})|t,j\rangle\langle t,j| \quad , \tag{12}$$

which is the pseudopotential equation.[6]

As Harrison[1,6] notes, the pseudopotential has several interesting properties. It is nonlocal in that it depends on all ion positions and states. It is an operator and is not restricted to multiplying the wave function. Its form is not unique and the pseudowavefunctions are not unique. That is, an arbitrary number of core states can be added to the pseudowavefunctions and they will still solve the Schrödinger

equation. Also, Harrison shows that $(E - E_{t,j})$ may be replaced by any function of the energies and the core states $[f(E,t,j)]$ and the solution will remain unchanged. There exist many valid forms that will yield correct energies and wave functions.[6]

The pseudopotential property of importance here is that it can be considered small. $V(r)$ is negative, P is positive, and $(E - E_{t,j})$ is positive so that the terms in Eq. (12) tend to cancel.[6] Experimental evidence corroborates that, in simple metals, the conduction electrons behave much like free electrons.

Given that W is small, we may use perturbation theory to solve for the electron energies. We note here that, even though the W form is arbitrary, if the problem were solved exactly (i.e. to all orders in W), the correct solution would always be obtained. However, using perturbation theory, the W form will affect the result and the validity of the form used must be determined by the results obtained when applied to a specific problem.[6]

Using perturbation theory, we calculate the electron energy in the state k to the second order,[6]

$$E_k = \varepsilon_k + \langle \vec{k}|W|\vec{k} \rangle + \sum_q{}' \frac{\langle \vec{k}|W|\vec{k} + \vec{q} \rangle \langle \vec{k} + \vec{q}|W|\vec{k} \rangle}{\varepsilon_k - \varepsilon_{k+q}} \quad , \qquad (13)$$

where

$$\varepsilon_k = \frac{\hbar^2 k^2}{2m} \qquad (14)$$

are the free-electron kinetic energies. The prime on the summation indicates that the $q=0$ term is omitted from the sum. We also may calculate the first-order pseudowavefunctions as

$$\phi_k = |\vec{k}> + \sum_q a_{qk} |k + q> \quad , \tag{15}$$

where

$$a_{qk} = \frac{<\vec{k} + \vec{q}|W|\vec{k}>}{\epsilon_k - \epsilon_{k+q}} \quad , \quad q \neq 0 \quad . \tag{16}$$

The q = 0 term, which does not immediately concern us, is determined in Ref. 2 by normalization.

Given an appropriate pseudopotential, we evaluate this expression and sum over all occupied electron states to determine the electron energy.

$$E_e = \sum_k n_k E_k \tag{17}$$

$$n_k = \begin{cases} 1 & k \text{ is occupied} \\ 0 & k \text{ is not occupied} \end{cases}$$

This particular result helps solve the ion motion problem (see Eq. 5). In evaluating the conduction electron energy we must consider the electron self-energy terms that are counted twice in Eq. (17). This will be discussed appropriately in the ensuing sections.

2. Effective Ion-Ion Interaction. We evaluate now the matrix elements in the perturbation expansion for the electron energies [Eq. (13)]. In Eq. (12) and its discussion, the general expression for the pseudopotential was shown to be

$$W = V(\vec{r}) + \sum_{t,j} f(E,t,j)|t,j><t,j| \quad . \tag{18}$$

$V(\vec{r})$ contains the potential field due to the ions, $V_I(\vec{r})$, which may be written as the sum of contributions from individual ions[1] at positions $\vec{r}_j$.

$$V_I(\vec{r}) = \sum_j v_I(\vec{r} - \vec{r}_j) \quad . \tag{19}$$

The ion screening, according to Harrison[1] may be superimposed at the ion sites and will be spherically symmetric. We have already written the core states as

$$|t,j\rangle = \psi_t(\vec{r} - \vec{r}_j) \quad .$$

If we require that the function $f(E,t,j)$ depends only on the core states through the index t, we may separate the pseudopotential and write it as a sum of contributions from individual ion sites as[1]

$$W = \sum_j w(\vec{r} - \vec{r}_j) \quad . \tag{20}$$

This assumption is essential to the pseudopotential matrix element calculation.

Now we are able to factor the matrix elements. Choosing W of Eq. (20) as our pseudopotential allows factoring out the structure-dependent term. We write

$$\langle \vec{k} + \vec{q}|W|k\rangle = \frac{1}{\Omega} \int e^{-i(\vec{k}+\vec{q})\cdot\vec{r}} \sum_j w(\vec{r} - \vec{r}_j) e^{i\vec{k}\cdot\vec{r}} \, d^3r \quad .$$

Changing the summation and integration order and factoring out $e^{-iq\cdot r_j}$,

$$\langle \vec{k} + \vec{q}|W|k\rangle = \frac{1}{\Omega} \sum_j e^{-i\vec{q}\cdot\vec{r}_j} \int e^{-i(\vec{k}+\vec{q})\cdot(\vec{r}-\vec{r}_j)} w(\vec{r} - \vec{r}_j) e^{ik\cdot(\vec{r}\cdot\vec{r}_j)} \, d^3r \quad .$$

The integral is just the integration of an individual potential with respect to the position of that particular ion. The sum contains the information about the system structure, so we write

$$S(q) = \text{structure factor} \equiv \frac{1}{N} \sum_j e^{i\vec{q}\cdot\vec{r}_j} \quad , \tag{21}$$

and we define

$$\langle \vec{k} + \vec{q} | w | k \rangle = \text{form factor} \equiv \frac{1}{\Omega_0} \int e^{i(\vec{k}+\vec{q})\cdot\vec{r}} w(\vec{r}) e^{i\vec{k}\cdot\vec{r}} \tag{22}$$

where

$$\Omega_0 = \text{atomic volume} = \Omega/N \quad .$$

So the pseudopotential matrix element[1] becomes

$$\langle \vec{k} + \vec{q} | W | \vec{k} \rangle = S(\vec{q}) \langle \vec{k} + \vec{q} | w | \vec{k} \rangle \quad . \tag{23}$$

This factoring is critical to the development of the pseudopotential method. It allows simple solution of the seemingly intractable many-body problem.[1] The detailed ion positions enter only through the structure factor $S(\vec{q})$, and the ionic potential details enter only through the form factor.

We are ready to sum electron energies over the available states to determine the total electron energy. We rewrite Eq. (13) in terms of the structure and form factors as

$$E_k = \varepsilon_k + S(0)\langle \vec{k} | w | \vec{k} \rangle + \sum_q{}' \frac{S^*(\vec{q})S(\vec{q})\langle \vec{k} | w | \vec{k} + \vec{q} \rangle \langle \vec{k} + \vec{q} | w | \vec{k} \rangle}{\varepsilon_k - \varepsilon_{k+q}} \quad . \tag{24}$$

Note here that

$$S(0) = \frac{1}{N} \sum_{j=1}^{N} 1 = 1 \quad .$$

For free electrons in the ground state, the available energy states are described by the Fermi sphere of radius,

$$k_f = \left(\frac{3\pi^2 z}{\Omega_0}\right)^{1/3} \quad , \tag{25}$$

where k_f is the Fermi wavenumber. With the pseudopotential present, the energy surface is not spherical. However, when evaluating the energies to second order, we may neglect this higher order effect[1,2] and sum over the Fermi sphere. We divide by N to obtain the total electron energy per ion, $N^{-1}E_e$.

$$N^{-1}E_e = \frac{1}{N}\sum_{k<k_f} E_k = \frac{2\Omega_0}{(2\pi)^3}\int_0^{k_f} E(\vec{k})d^3k \quad , \tag{26}$$

where we have used the density of states in wave-number space to convert the sum to an integral, including a factor of 2 to account for spin states.[1]

We now evaluate the contributions to Eq. (26) of the three terms in Eq. (24). The first is

$$\frac{2\Omega_0}{(2\pi)^3}\int_0^{k_f}\varepsilon_k d^3k = \frac{2\Omega_0}{(2\pi)^3}\int_0^{k_f}\frac{\hbar^2 k^2}{2m}d^3k$$

$$= \frac{3}{5}z\frac{\hbar^2}{2m}k_f^2 = z\frac{3}{5}\varepsilon_f \quad , \tag{27}$$

which is the average kinetic energy of the electrons times the valence. The second term is

$$\frac{2\Omega_0}{(2\pi)^3}\int_0^{k_f}\langle\vec{k}|w|\vec{k}\rangle d^3k = \frac{2\Omega_0}{(2\pi)^3}\int_0^{k_f}\frac{\int_0^{k_f}\langle\vec{k}|w|\vec{k}\rangle d^3k}{\int_0^{k_f}d^3k}d^3k$$

$$= \frac{2\Omega_0}{(2\pi)^3}\frac{4\pi}{3}k_f^3\overline{\langle\vec{k}|w|\vec{k}\rangle} = z\overline{\langle\vec{k}|w|\vec{k}\rangle} \quad , \tag{28}$$

which is Z times the average value of $<k/w/k>$. Both of these terms depend on volume but not on the details of the ion positions, and they represent the free-electron energy.[1] Exchanging the order of the sum and integral, the third term is

$$\sum_{q}' S^*(\vec{q})S(\vec{q}) \frac{2\Omega_0}{(2\pi)^3} \int_0^{k_f} d^3k \frac{<\vec{k}|w|\vec{k}+\vec{q}><\vec{k}+\vec{q}|w|\vec{k}>}{\frac{\hbar^2}{2m}(k^2 - |\vec{k}+\vec{q}|^2)} \quad .$$

Here, we define the part of this expression that is a function of $|\vec{q}|$ only as the energy wave-number characteristic $F(q)$. It is determined by w, which is spherically symmetric, and k_f.

$$F(q) = \frac{2\Omega_0}{(2\pi)^3} \int_0^{k_f} d^3k \frac{<\vec{k}|w|\vec{k}+\vec{q}><\vec{k}+\vec{q}|w|\vec{k}>}{\frac{\hbar^2}{2m}(k^2 - |\vec{k}+\vec{q}|^2)} \tag{29}$$

The third term is called the band-structure energy, E_{bs}, and is written

$$E_{bs} = \sum_{q}' S^*(\vec{q})S(\vec{q})F(q) \quad . \tag{30}$$

Note that $F(q)$ depends on the volume but not on the detailed ion arrangement, which is determined by the structure factor. This band structure energy interests us when we calculate the effects of an ion position change in a constant volume situation. It may be considered an effective (indirect) interaction between ions.[1]

To show this in a more direct manner we restructure the expression for E_{bs},

$$E_{bs} = \sum_{q}' S^*(\vec{q})S(\vec{q})F(q) = \sum_{q}' \frac{1}{N^2} F(q) \sum_{i=1}^{N} \sum_{j=1}^{N} e^{-i\vec{q}\cdot(\vec{r}_i - \vec{r}_j)} \quad .$$

Note that

$$\sum_{i=j}^{N} e^{-i\vec{q}\cdot(\vec{r}_i-\vec{r}_j)} = \sum_{i=j=1}^{N} 1 = N \quad ,$$

so that

$$E_{bs} = \sum_{q}' \frac{1}{N^2} F(q)\left(N + \sum_{i,j}' e^{-i\vec{q}\cdot(\vec{r}_i-\vec{r}_j)}\right) \quad ,$$

where the prime on the summation indicates exclusion of the $i = j$ term. Therefore,

$$E_{bs} = \frac{1}{2N} \sum_{i,j}' V_{IND}(\vec{r}_j - \vec{r}_i) + \frac{1}{N} \sum_{q}' F(q) \quad . \tag{31}$$

The second term here is volume dependent and we define

$$V_{IND}(\vec{r}) = \frac{2}{N} \sum_{q}' F(q) e^{i\vec{q}\cdot\vec{r}} \quad . \tag{32}$$

We have written the structure-dependent terms as a summation over the ions of an effective potential that is dependent only on the positions of the ions through $(\vec{r}_j - \vec{r}_i)$. V_{IND} is the effective interaction between the ions for which we have been looking and which we now must evaluate.

Replacing the summation of Eq. (32) by an integral,

$$\sum_{q} \to \frac{\Omega}{(2\pi)^3} \int d^3q \quad ,$$

we evaluate the angular parts of the integral over q space to obtain

$$V_{IND}(\vec{r}) = \frac{\Omega_0}{\pi^2} \int_0^\infty F(q) \frac{\sin qr}{qr} q^2 \, dq \quad . \tag{33}$$

This is a two-body, central force interaction between ions that may be added to the direct ion-interaction terms when calculating the ion motion.

   3. The Local Approximation. Anticipating that we will approximate the pseudopotential by a real model potential with adjustable parameters, $w(r)$, we make the "local approximation," which will simplify the rest of the development.[2] We assume that w is independent of q and we neglect its nonlocal, operator character. Therefore. we can write

$$\langle \vec{k} + q | w(\vec{r}) | \vec{k} \rangle = \frac{1}{\Omega_0} \int w(\vec{r}) e^{-i\vec{q} \cdot \vec{r}} \, d^3r = w_q \quad . \tag{34}$$

Additionally, the true wavefunction now equals the pseudowavefunction to first order within a normalization constant and can be written[2]

$$\psi_k = |k\rangle + \sum_q{}' a_{qk} |\vec{k} + \vec{q}\rangle \quad . \tag{35}$$

   We now evaluate the energy wave-number characteristic in the local approximation. $w(q)$ is taken out of the integral of Eq. (29) so that

$$F(q) = \frac{2\Omega_0}{(2\pi)^3} |w_q|^2 \frac{2m}{\hbar^2} \int \frac{d^3k}{k^2 - |\vec{k} + \vec{q}|^2} \quad .$$

The integral is evaluated[2] over the Fermi sphere as

$$\int \frac{d^3k}{k^2 - |\vec{k} + \vec{q}|^2} = \frac{-\pi^2 k_f^2 \hbar^2 \eta^2}{me^2} (\epsilon(q) - 1) \quad , \tag{36}$$

where

$$\epsilon(q) - 1 = \frac{me^2}{2\pi k_f h^2 \eta^2}\left(\frac{1 - \eta^2}{2\eta} \ell n \left|\frac{1 + \eta}{1 - \eta}\right| + 1\right)$$

and

$$\eta = \frac{q}{2k_f} \quad , \tag{37}$$

which yields[1]

$$F(q) = \frac{-\Omega_0 q^2}{8\pi e^2}|w_q|^2[\epsilon(q) - 1] \quad . \tag{38}$$

$\epsilon(q)$ is the static Hartree dielectric function for free electrons. It has a logarithmic singularity at $q = 2k_f$, which will affect significantly the calculated interaction potential form.

Constructing the local pseudopotential by following the notations of Ref. 2, we write

$$W = W_B + W_s + W_x \quad , \tag{39}$$

where W_B is the "bare-ion" pseudopotential, the local potential by which the electrons interact with ions. W_s is the Hartree screening contribution, which includes only the coulomb interactions with the other conduction electrons determined self-consistently.[1] W_x contains contributions due to exchange and correlation. W_B will be chosen later as an appropriate model potential. W_s is determined accurately in the next section. W_x must be approximated and is discussed in Sec. II.A.5.

4. Self-Consistent Screening. Within the adiabatic approximation, we treat the conduction electrons as though responding in an

electrostatic sense to the total potential W. The self-consistent electron contribution, W_s, due to the resulting charge density, $d(\vec{r})$ may be calculated using Poisson's equation. (We are following Wallace's method[2].)

$$\vec{\nabla}^2 \phi(r) = -4\pi e\; d(\vec{r}) \quad , \tag{40}$$

where

$$W_s(\vec{r}) = e\phi(r)$$

and

$$d(\vec{r}) = \text{electron density}$$

so that

$$\vec{\nabla}^2 W_s(\vec{r}) = -4\pi e^2 d(r) \quad .$$

We now expand $W_s(\vec{r})$ and $d(\vec{r})$ in Fourier series

$$\vec{\nabla}^2 W_s(\vec{r}) = \vec{\nabla}^2 \sum_q W_{sq}\, e^{i\vec{q}\cdot\vec{r}} = -\sum_q q^2 W_{sq}\, e^{i\vec{q}\cdot\vec{r}} = -4\pi e^2\; d(r)$$

$$= -4\pi e^2 \sum_q d_q\, e^{iq\cdot r} \quad .$$

The subscript q denotes the qth Fourier coefficient. Thus the expansion coefficients for W_s and d are related through

$$W_{sq} = \left(\frac{4\pi e^2}{q^2}\right) d_q \quad . \tag{41}$$

To calculate the screening contribution we must calculate the charge density, remembering that we are calculating the electron energies to

second order and the wavefunction to first order in perturbation theory. The charge density is given by

$$d(\vec{r}) = \sum_{k} n_k \psi_k^* \psi_k \quad , \tag{42}$$

where the sum is over all electron states and n_k is the occupation number, which is one when the state is occupied and zero when unoccupied.[2] Using Eq. (35), which is the expression for ψ_k accurate to first order, we calculate[2], keeping only first-order terms,

$$\psi_k^* \psi_k = \Omega^{-1} \left[1 + \sum_{q}' (a_{-qk}^* + a_{qk}) e^{i\vec{q} \cdot \vec{r}} \right] \quad . \tag{43}$$

We identify the Fourier coefficient d_q, defined by

$$d(\vec{r}) = \sum_{q} d_q \, e^{i\vec{q} \cdot \vec{r}}$$

as

$$d_0 = \Omega^{-1} \sum_{k} n_k = \Omega^{-1} NZ = \Omega_0^{-1} Z$$

$$d_q = 2\Omega^{-1} \sum_{k} n_k a_{qk} \quad , \quad q \neq 0 \quad . \tag{44}$$

Substituting the value for a_{qk}, yields

$$d_q = 2\Omega^{-1} \sum_{k} n_k \frac{W_q}{\epsilon_k - \epsilon_{k+q}} = \frac{mW_q}{\hbar^2 \pi^3} \int \frac{d^3 k}{k^2 - |\vec{k} + \vec{q}|^2} \quad , \tag{45}$$

where we have used the density in wave-number space with a factor of 2 for spin to convert the sum to an integral and the zero order electron energy,

$$\epsilon_k = \frac{\hbar^2}{2m} k^2 \quad . \tag{46}$$

We can calculate the Fermi energy E_f and Fermi wave number k_f to second order due to the local pseudopotential perturbation.[2] This exercise results in zero-order terms for E_f and k_f, followed by second-order corrections. First-order corrections do not appear. This result allows us to take the integral $\int d^3k$ over the zero-order Fermi sphere and ensures that the results will still be good to first order. We evaluate the integral

$$\int \frac{d^3k}{k^2 - |\vec{k} + \vec{q}|^2}$$

over the Fermi sphere as we did in Sec. 1.A.3 and calculate[2]

$$d_q = \frac{q^2 W_q}{4\pi e^2} [1 - \varepsilon(q)] \quad , \tag{47}$$

where $\varepsilon(q)$ is the static Hartree dielectric function given by Eq. (37).

Substituting into Eq. (41), we find the result for the Fourier coefficients of W_s is

$$W_{sq} = W_q [1 - \varepsilon(q)] \quad . \tag{48}$$

Momentarily, we are neglecting W_x of Eq. (39), so

$$W_q = W_{Bq} + W_{sq} \quad ,$$

and we see that

$$W_q = W_{Bq}/\varepsilon(q) \quad , \tag{49}$$

so that $\varepsilon(q)$ plays the role of the dielectric function.[1]

Now that we are including the coulomb energy of the conduction electrons, we must reevaluate the expression for the structure-dependent

part of the total band structure energy, Eq. (30). In this equation we have double-counted the electron self-energy E_{ee} and must subtract it to get the correct result. That is,

$$E_{bs} = \sum_q{}' S^*(q)S(q)F'(q) - \frac{1}{N} E_{ee} \quad . \tag{50}$$

The prime on $F'(q)$ indicates evaluation of a more appropriate energy wave-number characteristic, which can be used in Eq. (33) for V_{IND}.

The electrostatic electron self-energy per ion is given by

$$\frac{1}{N} E_{ee} = \frac{1}{2N} \int d^3r \; d(\vec{r}) \; W_s(\vec{r}) \quad , \tag{51}$$

which (neglecting the $q = 0$ term) can be written[2] in terms of Fourier coefficients as

$$\frac{1}{N} E_{ee} = \frac{\Omega}{2N} \sum_g{}' d_q \; W_{s-q} \quad . \tag{52}$$

$$W_{sq} = \left(\frac{4\pi e^2}{q^2}\right) d_q \tag{53}$$

so that

$$\frac{1}{N} E_{ee} = \frac{\Omega_0}{8\pi e^2} \sum_q{}' q^2 W_{sq} W_{s-q} \quad . \tag{54}$$

From Eq. (20), we have

$$W(\vec{r}) = \sum_j w(|\vec{r} - \vec{r}_j|) \quad ,$$

and we can show that

$$W_q = S(q) w_q \quad , \tag{55}$$

where

$$W_q = \frac{1}{\Omega} \int W(r) e^{-i\vec{q} \cdot \vec{r}} \, d^3 r \quad , \tag{56}$$

$$w_q = \frac{1}{\Omega_0} \int w(r) e^{-i\vec{q} \cdot \vec{r}} \, d^3 r \quad , \tag{57}$$

and, as in Eq. (21),

$$S(q) = S_q = \frac{1}{N} \sum_j e^{-i\vec{q} \cdot \vec{r}_j}$$

which yields

$$\frac{1}{N} E_{ee} = \frac{\Omega_0}{8\pi e^2} \sum_q{}' S_q S_{-q} \, q^2 |w_{sq}|^2 \quad . \tag{58}$$

We may substitute this into Eq. (50), using the relations between W_q, W_{sq}, and W_{Bq} to arrive at

$$E_{bs} = \sum_q{}' S_q S_{-q} \frac{\Omega_0 q^2}{8\pi e^2} |w_{Bq}|^2 \frac{\epsilon(q) - 1}{\epsilon(q)} \quad .$$

The appropriate energy wave-number characteristic for use in Eq. (33) to calculate V_{IND} is, therefore,

$$F(q) = \frac{-\Omega_0 q^2}{8\pi e^2} |w_{Bq}|^2 \frac{\epsilon(q) - 1}{\epsilon(q)} \quad . \tag{59}$$

This expression accounts for the self-consistent screening of the electron gas, within the order of our perturbation calculation.

    5. Exchange and Correlation. We include approximately the exchange and correlation effects in the screening calculation. We follow the

discussion in Ref. 2. The screening calculation outlined in the preceding section yields the appropriate result with the inclusion of an additional interaction due to exchange and correlation, W_x, so that

$$W_q = W_{Bq} + W_{sq} + W_{xq} \quad .$$

We assume that there exists an average interaction $I(q)$ within the electron gas,[2]

$$W_{xq} = I(q) \, d_q \quad . \tag{60}$$

Then, using Eq. (41),

$$W_{sq} + W_{xq} = \left[\frac{4\pi e^2}{q^2} + I(q) \right] d_q = \frac{4\pi e^2}{q^2} \, [1 - f(q)] \, d_q \quad , \tag{61}$$

where

$$f(q) = \frac{-q^2}{4\pi e^2} \, I(q) \quad , \tag{62}$$

and we parallel the screening calculation algebra to obtain

$$W_q = \frac{W_{Bq}}{1 + [\epsilon(q) - 1][1 - f(q)]} \quad . \tag{63}$$

We recalculate the electron self-energy appropriately [see Eq. (51)] from

$$E_{ee} = \frac{\Omega}{2N} \sum_q{}' \, dq(W_{s-q} + W_{x-q}) \tag{64}$$

and reevaluate the energy wave-number characteristic. This all follows the development in the preceding section, with the additional $[1 - f(q)]$ term to keep track of. The result is

$$F(q) = \frac{-\Omega_0 q^2}{8\pi e^2} |w_{Bq}|^2 \frac{\varepsilon(q) - 1}{1 + [\varepsilon(q) - 1][1 - f(q)]} \quad . \tag{65}$$

Heine[7] discusses the formalism that we have just outlined and states that the form of the equation may be justified, using exact many-body theory.

To determine an appropriate form for $f(q)$, we consider the calculation of the effective interaction between quasi-particles in an interacting electron gas. As discussed in Ref. 8, in the random-phase approximation and the high-density limit, a partial matrix element summation of "ring" Feynman diagrams is appropriate. The effective interaction potential is calculated to be

$$V_{eff\ q} = \frac{4\pi e^2}{q^2 + k_s^2} \quad , \tag{66}$$

which in real space is a screened coulomb interaction in the Thomas-Fermi approximation,[8]

$$V_{eff}(\vec{r}) \propto \frac{e^2}{r} e^{-k_s r} \quad . \tag{67}$$

Sham[9] follows Hubbard's[10] treatment and replaces $V_{eff\ q}$ by

$$V_{eff\ q} = \frac{4\pi e^2}{q^2 + k_f^2 + k_s^2} \quad , \tag{68}$$

where k_f is some average of the Fermi vector. Hubbard also proposes that the effect of exchange on the screening in the high-q limit should be to cancel half the direct coulomb contribution to the screening. We will write[2,7,10,11]

$$V_{eff\ q} = I(q) = -\frac{1}{2}\left(\frac{4\pi e^2}{q^2 + \xi k_f^2}\right), \tag{69}$$

where we have replaced $k_f^2 + k_s^2$ by ξk_f^2. This is in accord with Wallace.[2] ξ is an adjustable parameter that we will determine later to ensure that $I(q)$ has the correct $q \to 0$ limit.[2]

The final form for $f(q)$ to be used in Eq. (65) is, therefore,

$$f(q) = \frac{1}{2}\frac{q^2}{q^2 + \xi k_f^2}. \tag{70}$$

We have specified the terms in the energy wave-number characteristic [Eq. (65)], including exchange and correlation effects within our level of approximation. Heine[7] discusses the exchange and correlation effects and states that the uncertainties arising from the approximations used in determining Eq. (70) are greater than the uncertainties in the pseudopotential. We continue by choosing an appropriate local bare-ion potential W_{Bq} to complete our determination of $F(q)$ and V_{IND}.

6. A Model Pseudopotential. We approximate the local bare-ion pseudopotential, $w_B(r)$, by a simple model which behaves like the potentials in the real metal. $w_B(r)$ is composed of two contributions,[2]

$$w_B(r) = w_z(r) + w_c(r). \tag{71}$$

$w_z(r)$ is due to the coulomb attraction of the ion and has the form

$$w_z(r) = \frac{-ze^2}{r}$$

with Fourier transform (i.e., the w_{zq} matrix element)

$$w_{zq} = \frac{-4\pi z e^2}{\Omega_0 q^2} \quad . \tag{72}$$

$w_c(r)$ is a localized potential confined to the core region. It approximates the repulsion due to the core electrons and tends to cancel the coulomb part within the core. An appropriate choice for $w_c(r)$ is of the form of the s-state core functions,[1,2]

$$w_c(\vec{r}) = e^{-\delta r} \quad .$$

The Fourier transform of this is

$$w_{cq} = \frac{8\pi\delta}{\Omega_0} \left[\frac{1}{(\delta^2 + q^2)^2} \right] \quad .$$

We introduce the arbitrary constants β and ρ such that

$$w_{cq} = \frac{\beta}{\Omega_0} \left[\frac{1}{(1 + q^2\rho^2)^2} \right] \quad . \tag{73}$$

The form that we will use for the matrix element of the bare ion potential in Eq. (65) is, therefore,

$$w_{Bq} = \frac{1}{\Omega_0} \left[\frac{-4\pi z e^2}{q^2} + \frac{\beta}{(1 + q^2\rho^2)^2} \right] \quad . \tag{74}$$

7. Total Ion-Ion Interaction. For a molecular dynamics calculation we are interested in the total ion-ion interaction potential. We have just calculated the effective interaction V_{IND} due to the presence of the nearly free electron gas in a simple metal. To this we must add the coulomb replusion between the ions,[5]

$$\frac{z^2 e^2}{r} \tag{75}$$

and the exchange repulsion between two ion cores,

$$\alpha_B e^{-\gamma_B r} \tag{76}$$

which is a Born-Mayer repulsive central potential.[2] α_B and γ_B are empirically determined constants.

Therefore, we may summarize the results of this development by writing down the ion-ion interaction potential, which will be used in our molecular dynamics calculations:

$$\phi(r) = \frac{z^2 e^2}{r} + \alpha_B e^{-\gamma_B r} + V_{IND}(r) \quad , \tag{77}$$

where

$$V_{IND}(r) = \frac{\Omega_0}{\pi^2} \int_0^\infty F(q) \frac{\sin qr}{qr} q^2 \, dq \quad , \tag{78}$$

$$F(q) = \frac{-\Omega_0 q^2}{8\pi e^2} |w_{Bq}|^2 \frac{\varepsilon(q) - 1}{1 + [\varepsilon(q) - 1][1 - f(q)]} \quad , \tag{79}$$

$$\varepsilon(q) - 1 = \frac{me^2}{2\pi k_f \hbar^2 \eta^2} \left(\frac{1 - \eta^2}{2\eta} \ln \left| \frac{1 + \eta}{1 - \eta} \right| + 1 \right) \quad , \quad \eta = \frac{q}{2k_f} \quad , \tag{80}$$

$$f(q) = \frac{q^2}{2(q^2 + \xi k_f^2)} \quad , \tag{81}$$

and

$$w_{Bq} = \frac{1}{\Omega_0} \left[\frac{-4\pi z e^2}{q^2} + \frac{\beta}{(1 + q^2 \rho^2)^2} \right] \quad . \tag{82}$$

The determination of the constants α_B, γ_B, ξ, β, and ρ will be discussed in Sec. III.

B. Molecular Dynamics

We have calculated an effective interaction potential for the ions in a simple metal [Eq. (77)]. We use this as the potential of inter-action between pairs of classical particles and will solve for the ion motion in the metal using the molecular dynamics technique. In this section we present the equations that are solved by high-speed com-puters to yield ion positions and velocities. We derive the conserva-tion of energy and momentum in a molecular dynamics system, describe sys-tem size and boundary effects, and discuss the methods of calculating thermodynamic properties from the molecular dynamics results.

1. Central Difference Equations. For a three-dimensional array of N identical particles, we solve the set of classical Newtonian equa-tions,

$$m\ddot{\vec{r}}_i(t) = \vec{F}_i(t) \quad , \tag{83}$$

where

    i = particle number = $1, 2, \cdots, N$,

    $\vec{r}_i$ = particle position (x_i, y_i, z_i) ,

    m = particle mass, and

    $\vec{F}_i$ = force on the ith particle.

The dots denote time differentiation. The force on the ith particle is determined generally by the positions of the other particles, and thus the equations are coupled. We develop the difference equations used in the molecular dynamics program to solve this system of equations. Con-sider, for simplicity, only the x-direction. The y- and z-direction equations are identical.

In the x-direction

$$m\ddot{x}_i(t) = F_{xi}(t) \quad . \tag{84}$$

Performing a Taylor series expansion on Δt, the new position at $t + \Delta t$ is

$$x_i(t + \Delta t) = x_i(t) + \Delta t\, \dot{x}_i(t) + \frac{1}{2}(\Delta t)^2 \ddot{x}_i(t) + \cdots , \tag{85}$$

and similarly,

$$x_i(t - \Delta t) = x_i(t) - \Delta t\, x_i(t) + \frac{1}{2}(\Delta t)^2 \ddot{x}_i(t) + \cdots . \tag{86}$$

Adding these equations yields

$$x_i(t + \Delta t) = -x_i(t - \Delta t) + 2x_i(t) + (\Delta t)^2 \ddot{x}_i(t) + \cdots . \tag{87}$$

Subtracting gives

$$\dot{x}_i(t) = \frac{x_i(t + \Delta t) - x_i(t - \Delta t)}{2\Delta t} \quad . \tag{88}$$

These equations constitute a straightforward central difference scheme that is appropriate to the solution of the $\underline{i}$th particle position and velocity and is accurate to the order of $(\Delta t)^3$.

We work easily in terms of displacements defined at the time interval midpoints as

$$\Delta x_i(t + \frac{\Delta t}{2}) = x_i(t + \Delta t) - x_i(t) \quad . \tag{89}$$

With this definition, and expanding $x_i(t \pm \Delta t/2)$ in a Taylor series about $\Delta t/2$, the following difference equations are calculated as

$$\Delta x_i(t + \frac{\Delta t}{2}) = \Delta x_i(t - \frac{\Delta t}{2}) + (\Delta t)^2 \frac{F_{xi}(t)}{m} \quad , \tag{90}$$

$$x_i(t + \Delta t) = x_i(t) + \Delta x_i(t + \frac{\Delta t}{2}) \quad , \text{ and} \tag{91}$$

$$x_i(t + \frac{\Delta t}{2}) = \frac{\Delta x_i[t + (\Delta t/2)]}{\Delta t} \quad , \tag{92}$$

where we have used $\ddot{x}_i(t) = F_{xi}(t)/m$.

These are the equations used in the molecular dynamics program to solve the coupled system of differential equations. The force of the ith particle is calculated by assuming additive interactions between pairs between the ith particle and its neighbors.

$$F_{xi}(t) = \sum_{j=1}^{N}{}' F_{xij}(t) \quad . \tag{93}$$

The prime on the summation indicates that the j=i term is omitted. F_{xij} is the x-component of the force on the ith particle due to the jth particle and

$$F_{xij} = -F_{xji} \tag{94}$$

by Newton's third law. For this study we calculate the force by taking the negative gradient of the ion-ion interaction potential determined through pseudopotential theory [Eq. (77)].

The computer program that solves the difference equations is easily understood.* After determining the initial positions and velocities of the particles (see Sec. IV), all the particle forces are calculated

---

*The molecular dynamics computer program used in this study was developed by B. L. Holian and G. K. Straub of the Los Alamos National Laboratory.

based on the current positions. With $F_{xi}(t)$ thus calculated, $\Delta x_i(t + \Delta t/2)$, $x_i(t + \Delta t)$, and $\dot{x}_i(t + \Delta t/2)$ are evaluated readily by Eqs. 90-92. With $x_i(t + \Delta t)$ known, the time step is advanced and $F_{xi}(t + \Delta t)$ is calculated. In this manner, the trajectories of all N-particles are calculated exactly at any time [within $(\Delta t)^3$]. The particle positions and velocities may be evaluated to obtain a time history of the system being studied.

2. **Conservation of Momentum and Energy.** The difference equations just described can be shown to explicitly conserve momentum and energy.[*] In a system of N identical particles interacting by way of a conservative, additive force between pairs, where

$$F_{xi}(t) = m\ddot{x}_i(t) = \frac{-\partial\phi(x_i)}{\partial x_i} \quad , \tag{95}$$

and ϕ is the additive potential between pairs, we can demonstrate conservation of momentum, P, by showing that

$$P(t + \frac{\Delta t}{2}) = P(t - \frac{\Delta t}{2})$$

or

$$\sum_{i=1}^{N} m\dot{x}_i(t + \frac{\Delta t}{2}) = \sum_{i=1}^{N} m\dot{x}_i(t - \frac{\Delta t}{2}) \quad . \tag{97}$$

Using the difference equations [Eqs. (90)-(92)] we evaluate

$$\sum_{i=1}^{N} x_i(t + \frac{\Delta t}{2}) = \frac{1}{\Delta t}\sum_{i=1}^{N} \Delta x_i(t + \frac{\Delta t}{2}) = \frac{1}{\Delta t}\sum_{i=1}^{N} \left[\Delta x_i(t - \frac{\Delta t}{2}) + \frac{F_{xi}}{m}(\Delta t)^2\right] \quad .$$

---

[*]Based on a calculation by Brad Lee Holian of the Los Alamos National Laboratory.

Also,

$$\sum_{i=1}^{N} F_{xi} = \sum_{i=1}^{N}\sum_{j=1}^{N} F_{xij} = \sum_{i=1}^{N}\sum_{j>1}^{N}{}' (F_{xij} + F_{xji}) \quad .$$

But, by Newton's third law

$$F_{xij} = F_{xji} \quad ,$$

so that this sum is zero and we have shown in Eq. (97) that

$$\sum_{i=1}^{N} m\dot{x}_1(t + \frac{\Delta t}{2}) = \sum_{i=1}^{N} m\dot{x}_1(t - \frac{\Delta t}{2}) \quad ,$$

which proves that momentum is conserved to within the accuracy of the difference equations.

Similarly, we calculate the total energy to demonstrate conservation of energy.

E = total energy = potential (PE) + kinetic (KE) energy.

We calculate the change in potential energy,

$$\Delta PE = PE(t + \frac{\Delta t}{2}) - PE(t - \frac{\Delta t}{2}) \quad , \tag{98}$$

and compare it with the change in kinetic energy,

$$\Delta KE = KE(t + \frac{\Delta t}{2}) - KE(t - \frac{\Delta t}{2}) \quad . \tag{99}$$

The change in potential energy is

$$\Delta PE = \sum_{i=1}^{N} [\phi_i(t + \frac{\Delta t}{2}) - \phi_i(t - \frac{\Delta t}{2})] \quad .$$

ϕ_i is the potential energy of the $\underline{i}$th particle defined as

$$\phi_i(t) = \sum_{j=1}^{N}{}' \phi_{ij}(t)$$

and

$$\phi_{ij} = \phi(|\vec{r}_j - \vec{r}_i|) \quad .$$

Expanding in Taylor series yields

$$\Delta PE = \sum_{i=1}^{N} \left\{ [\phi_i(t) + \frac{\Delta t}{2} \dot{\phi}_i(t) + \frac{1}{2} (\frac{\Delta t}{2})^2 \ddot{\phi}_i(t) + O(\Delta t)^3] \right.$$

$$\left. - [\phi_i(t) - \frac{\Delta t}{2} \dot{\phi}_i(t) + \frac{1}{2} (\frac{\Delta t}{2})^2 \ddot{\phi}_i(t) + O(\Delta t)^3] \right\}$$

$$= \sum_{i=1}^{N} [\dot{\phi}_i(t)\Delta t + O(\Delta t)^3] \quad .$$

The potential is related to the force by

$$\dot{\phi}_i(t)\Delta t = \frac{d\phi(t)}{dt} \Delta t = \frac{d\phi(t)}{dx(t)} \frac{dx(t)}{dt} \Delta t = -F_i(t)\dot{x}(t) \Delta t \quad , \qquad (100)$$

so that

$$\Delta PE = \sum_{i=1}^{N} [-F_i(t)\dot{x}_i(t) \Delta t + O(\Delta t)^3] \quad . \qquad (101)$$

The change in kinetic energy is

$$\Delta KE = \frac{M}{2} \sum_{i=1}^{N} [\dot{x}_i(t + \frac{\Delta t}{2})^2 - \dot{x}_i(t - \frac{\Delta t}{2})^2] \quad .$$

We evaluate these terms by noting that

$$[\dot{x}_i(t + \tfrac{\Delta t}{2})^2 - \dot{x}_i(t - \tfrac{\Delta t}{2})^2] = [\dot{x}_i(t + \tfrac{\Delta t}{2}) + \dot{x}_i(t - \tfrac{\Delta t}{2})]$$

$$[\dot{x}_i(t + \tfrac{\Delta t}{2}) - \dot{x}_i(t - \tfrac{\Delta t}{2})] \qquad (102)$$

and by expanding using the Taylor series

$$\dot{x}_i(t + \tfrac{\Delta t}{2}) = \dot{x}_i(t) + \tfrac{\Delta t}{2}\ddot{x}_i(t) + \tfrac{1}{2}(\tfrac{\Delta t}{2})^2 \dddot{x}_i(t) + 0(\Delta t)^3$$

$$\dot{x}_i(t - \tfrac{\Delta t}{2}) = \dot{x}_i(t) - \tfrac{\Delta t}{2}\ddot{x}_i(t) + \tfrac{1}{2}(\tfrac{\Delta t}{2})^2 \dddot{x}_i(t) + 0(\Delta t)^3 \quad .$$

By adding and subtracting the second of these equations from the first, we get the needed factors in Eq. (102). By using

$$F_i(t) = m\ddot{x}_i$$

and some algebra, we arrive at

$$\Delta KE = \sum_{i=1}^{N} [F_i(t)\dot{x}_i(t) + 0(\Delta t)^3] \quad , \qquad (103)$$

and we see, from Eqs. 101 and 103, that

$$\Delta E = \Delta KE + \Delta PE = 0 + 0(\Delta t)^3 \quad . \qquad (104)$$

Thus we have shown explicitly that both momentum and energy are conserved by the difference equations.

3. Boundary Conditions and System Size. We now set up the system of N interacting particles. We perform our molecular dynamics calculation on this system, and from the resulting information, we infer the macroscopic properties of sodium. The system is obviously limited to

having N much less than a macroscopic (10^{24}) number. We must minimize the effects of finite system size by choosing appropriate boundary conditions, and we must recognize the N-dependence of our results.

To minimize the effects of finite system size, we choose periodic boundary conditions whereby the N-particle system is repeated periodically throughout space and thus may be considered an infinite system with the imposed periodicity. Figure 1 is a schematic of an N=3 system in two dimensions and its nearest repeated systems.[12] L is the length of the square system box and RMAX is the range of the potential. We use the minimum image convention, which means that a particle only interacts with the image of a neighbor that is nearest to it. That is, in Fig. 1, particle two will only interact with the image of particle three in the box to its right and no other "particle threes." This constrains us to keep the system length, L, in a given direction greater than twice the potential range so that not only will a particle never interact with its own image but it will not interact with more than one of its neighbor's images. The method for determining our particular system dimensions and the potential range is discussed in Sec. IV.

The N dependence of calculated system properties has only been determined for some simple cases. (See discussions in Refs. 12, 13, and 14.) Based on such studies, we expect a 1/N dependence. However, a generalized solution method does not exist.[12] Therefore, we must include sufficient particles in the system, and we check to see that the calculated results are not N dependent. If there is an N dependence we may be able to evaluate how to extrapolate our results to the macroscopic N limit. In our equilibrium property studies, we are not overly concerned because the N dependence is generally small for systems with
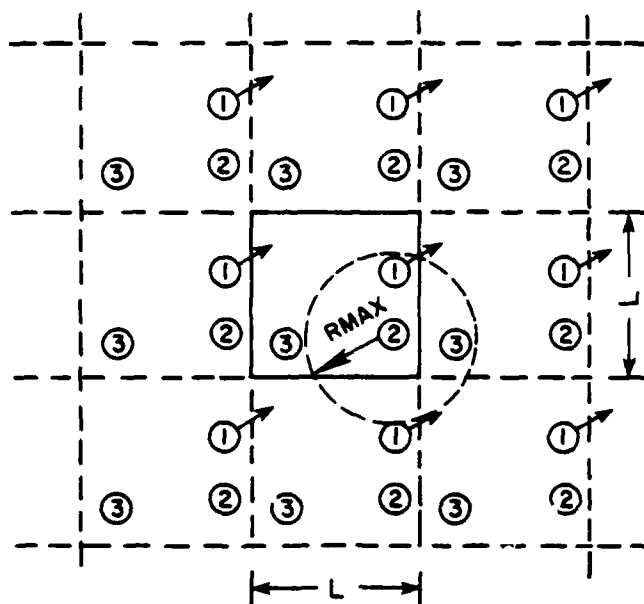
Fig. 1.
A two-dimensional system of N=3 particles in
an L x L box with periodic boundary conditions.
RMAX is the range of the potential. Note that
as particle ① moves out of the system it re-
appears by way of its periodic image.

n > 100 and we will be dealing with N > 600, owing to the long range of the pseudopotential. If we study nonequilibrium properties or effects relating to large numbers of particles, such as coexistence of phases, then the N dependence becomes more critical. We discuss N dependence effects as they affect our calculations in Sec. IV.

4. Thermodynamic Properties

When it is appropriate to calculate macroscopic equilibrium properties from an N-particle molecular dynamics system, we proceed by taking averages over time.[12] In a molecular dynamics calculation, the number N of particles, volume Ω of the system, and total energy E remain constant. With these constraints, the system forms a microcanonical ensemble. However, there is the additional constraint of constant linear momentum (M), so we would describe the system as having N, V, E, and M constant.[15] This must be taken into account when comparing molecular dynamics time averages with ensemble averages obtained using statistical mechanics or other calculational techniques such as Monte Carlo (see Refs. 12, 13, and 15 for discussion). We are not concerned immediately with such comparisons. The essential assumption regarding the appropriateness of the averages is that the system is ergodic. That is, all states of the system in phase space are mutually accessible[13] with equal probability, so that all time histories of the same system have equivalent statistical averages.[16] This assumption has never been proved, but experience shows it to be valid.[12] We assume that our time averages yield the appropriate statistical averages of the system's equilibrium properties.

We will now determine various properties of our system at a particular time, with the understanding that we will sample these properties many times during a molecular dynamics calculation and average them.

We calculate the average kinetic energy per particle of the system of N particles as

$$KE = \frac{1}{N} \sum_{i=1}^{N} \frac{1}{2} m(\dot{x}_i^2 + \dot{y}_i^2 + \dot{z}_i^2) \quad . \tag{105}$$

The average potential energy per particle is

$$\Phi = PE = \frac{1}{2N} \sum_{i=1}^{N} \sum_{j=1}^{N}{}' \phi(|\vec{r}_j - \vec{r}_i|) \quad , \tag{106}$$

where

$$\vec{r}_i = (x_i, y_i, z_i)$$

and $\phi(r)$ is the potential that describes the interaction between two particles. The factor of 1/2 is included to correct for double-summing of the potential energies.

Our system at equilibrium, obeying the laws of classical dynamics, will satisfy the Maxwell-Boltzmann law. The law states that the average of a property (P, for example) can be obtained by

$$\bar{P} = \frac{\int P dN}{N} = \frac{\int_{-\infty}^{\infty} \cdots \int e^{-E/kT} P \, dq_1 \cdots dp_{3N}}{\int_{-\infty}^{\infty} \cdots \int e^{-E/kT} \, dq_1 \cdots dp_{3N}} \quad ,$$

where E is the system energy, kT is Boltzmann's constant times the temperature, and the integration is over all points in phase space with positional coordinates q_i and momentum coordinates p_i.[17]

Using this law, we may calculate the distribution function for each velocity component as

$$\frac{dN_{\dot{x}}}{N} = \frac{1}{\sigma\sqrt{2\pi}} \exp\left(\frac{-\dot{x}^2}{2T^2}\right)$$

$$\sigma = \left(\frac{kT}{m}\right)^{\frac{1}{2}} , \tag{107}$$

and similarly for y and z. This is the Maxwell or normal distribu-
tion.[17] Then we calculate the average kinetic energy per particle as

$$KE = \frac{1}{2}(\overline{\dot{x}^2} + \overline{\dot{y}^2} + \overline{\dot{z}^2}) = \frac{3}{2} kT . \tag{108}$$

We are assuming that our system has no net motion, i.e. $\overline{\dot{x}} = \overline{\dot{y}} = \overline{\dot{z}} = 0$.
If there were net motion, we would calculate only the fluctuations
about this average motion and replace $\dot{x}^2$ by $(\dot{x} - \overline{\dot{x}})^2$. This connects
the kinetic energy per particle calculated using molecular dynamics and
the thermodynamic temperature of the system.

$$KE = \frac{1}{N} \sum_{i=1}^{N} \frac{1}{2} m(\dot{x}_i^2 + \dot{y}_i^2 + \dot{z}_i^2) = \frac{3}{2} kT . \tag{109}$$

We also accept this expression as the definition of kinetic temperature
to be used even when the system is not in equilibrium.[18]

Note that the N-particle molecular dynamic system may not be in
equilibrium. Also, the velocity distribution may not be normal. We may
investigate this, as far as the temperature and kinetic energy are con-
cerned, by seeing if the kinetic temperature is isotropic. That is,
we may for convenience define

$$\frac{1}{2} kT_x = \frac{1}{N} \sum_{i=1}^{N} \frac{1}{2} m\dot{x}_i^2 , \tag{110}$$

and, similarly, T_y and T_z. We require that $T_x = T_y = T_z$ for the system
to be in equilibrium. To investigate if the velocity distribution is
normal, we may calculate the kurtosis (which measures the "degree of
peaking") of the distribution in the molecular dynamics calculation.[19]
We calculate the kinetic temperatures and the kurtosis for example
calculations and discuss their implications in Sec. IV.

The volume of a molecular dynamics calculation as we apply it is
a constant and an input parameter. A given calculation will yield the
potential and kinetic energies and the calculated temperature. For
each calculation we have an equation-of-state point for the molecular
dynamics system consisting of a total internal energy (kinetic plus
potential) at a volume and temperature.

III. THE ION-ION INTERACTION POTENTIAL FOR SODIUM

In this section we discuss how the necessary parameters are determined for the calculation of the ion-ion interaction potential in Eq. (77). We use these parameters to calculate the functions in Eqs. (78) to (82) which specify the potential. Finally, we calculate the interaction potential and discuss how it is tabulated for use by the molecular dynamics program.

A. Determination of the Parameters

1. Determination of ξ. The constant ξ in the expression for the function $f(q)$ [Eq. (81)], which corrects the dielectric function to include exchange and correlation effects, may be determined analytically. In the long wavelength ($q \to 0$, or macroscopic) limit, the static dielectric constant is related to the electron gas compressibility, κ, as[11]

$$\varepsilon'(q) - 1 = \frac{4\pi N^2 e^2}{q^2} \kappa \quad , \quad q \to 0 \text{ limit} \tag{111}$$

where the prime distinguishes this dielectric constant from the Hartree dielectric constant of the noninteracting electron gas, $\varepsilon(q)$, defined by Eq. (80).

Note that

$$\frac{(\varepsilon'(q) - 1)^0}{(\varepsilon'(q) - 1)} = \frac{\kappa^0}{\kappa} \quad , \tag{112}$$

where the superscript zero indicates the values appropriate to a noninteracting electron gas. With some algebra and the formulas relating $f(q)$ and the dielectric constants [for example, Eq. (63)], this relation becomes

$$\frac{\kappa^0}{\kappa} = 1 - f(q)[\varepsilon'(q) - 1]^0 = 1 - f(q)[\varepsilon(q) - 1] \quad , \tag{113}$$

which is valid in the long wavelength limit.

From the expression for $\varepsilon(q)$, Eq. (80), we find[2]

$$\lim_{q \to 0} [\varepsilon(q) - 1] = \frac{4me^2 k_f}{\pi \hbar^2 q^2} - \frac{me^2}{3\pi \hbar^2 k_f} \quad , \tag{114}$$

so that

$$\frac{\kappa^0}{\kappa} = \lim_{q \to 0} [1 - f(q)(\varepsilon(q) - 1)]$$

$$= \lim_{q \to 0} \left[1 - \left(\frac{q^2}{2(q^2 + \xi k_f^2)} \right) \left(\frac{4me^2 k_f}{\pi \hbar^2 q^2} - \frac{me^2}{3\pi \hbar^2 k_f} \right) \right] \quad , \tag{115}$$

or

$$\frac{\kappa^0}{\kappa} = 1 - \frac{2me^2}{\xi k_f \pi \hbar^2} \quad . \tag{116}$$

This is the relation that determines ξ.

We calculate κ and κ^0 from the relation

$$\frac{1}{\kappa} = \Omega_0 \frac{\partial^2 E_0}{\partial^2 \Omega_0} \quad , \tag{117}$$

where E_0 is the electron gas ground-state energy. We write the energies in terms of r_s, which is defined as the radius of the sphere whose volume is the average conduction electron volume, so that

$$\frac{4}{3} \pi r_s^3 = \frac{\Omega_0}{z} \quad . \tag{118}$$

To calculate the compressibilities, we use the results from Sec. V for the ground-state energies of the noninteracting and interacting electron gas, E_0^0 and E_0, respectively.

$$E_0^0 = \frac{2.21}{r_s^2} \, Ry$$

$$E_0 = \left(\frac{2.21}{r_s^2} - \frac{0.916}{r_s} - 0.115 + 0.031 \, \ln r_s \right) R_y \quad .$$

With the help of the relations

$$\Omega_0^2 \left(\frac{\partial^2 E_0}{\partial \Omega_0^2} \right) = \frac{1}{9} \left(r_s^2 \frac{\partial^2 E_0}{\partial r_s^2} - 2 r_s \frac{\partial E_0}{\partial r_s} \right) \quad ,$$

$$\Omega_0 = z \frac{4}{3} \pi r_s^3 = \frac{3\pi^2 z}{k_f^3} \quad , \text{ and}$$

$$\frac{\hbar^2}{me^2} = 1 a_0 \quad ,$$

we may calculate κ^0/κ and use Eq. (116) to arrive at

$$\xi = 0.916/(0.458 + 0.012 \, r_s) \quad . \tag{119}$$

With the value $r_s = 3.939 \, a_0$ corresponding to an atomic volume of $256 \, a_0^3$ for sodium, we have

$$\xi = 1.81 \quad . \tag{120}$$

We notice here that ξ is volume-dependent and is treated as such in our calculations.

2. <u>Determination of γ_B, α_B, β, and ρ.</u> The remaining parameters γ_B, α_B, β, and ρ have been determined by fitting to available data.

We have chosen the value for γ_B in the Born-Mayer repulsive potential, Eq. (76), to have the value determined by simultaneously fitting calculated lattice energies to equation-of-state data for the family of alkali halide salts.[20] The value is

$$\frac{1}{\gamma_B} = 0.339 \times 10^{-8} \text{ cm} ,$$

so that

$$\gamma_B = 1.56 \, a_0^{-1} . \qquad (121)$$

Wallace[21] determined the values of α_B, β, and ρ by fitting the calculated expressions for the total adiabatic potential and its volume derivative to measurements of the equation-of-state properties of sodium. The data included were the binding energy, the ionization energy, and the bulk modulus at zero temperature and pressure. The requirement that the pressure be zero at zero temperature was also used. He found that these data could be fit with some arbitrariness remaining. This arbitrariness was removed by requiring that the calculated average of the phonon frequencies squared ($\langle \omega^2 \rangle$ as calculated by lattice dynamics) also be fit. The resulting parameters are

$$\alpha_B = 10.5 \text{ Ry} ,$$

$$\beta = 37. \text{ Ry } a_0^3 , \text{ and}$$

$$\rho = 0.50 \, a_0 .$$

We discuss in detail the total system energy calculation and equation-of-state value determination in Sec. V.

With these parameters determined, we have completely specified the effective ion-ion interaction potential of Eq. (77). We now proceed to calculate this potential and apply it to the molecular dynamics calculations.

B. Calculation of the Potential

We now calculate the ion-ion interaction potential for sodium, using Eqs. (77)-(82) and the parameter values determined in the previous section. For these calculations, which illustrate the factors involved in the ion-ion interaction, we use the observed zero temperature and pressure atomic volume for sodium of

$$\Omega_0 = 256 \ a_0^3 \quad ,$$

which yields a Fermi wave vector of

$$k_f = \left(\frac{3\pi^2 z}{\Omega_0}\right)^{1/3} = 0.4872 \quad .$$

1. $\varepsilon(q)$. The static Hartree dielectric function is calculated using Eq. (80) and the result is the solid line shown in Fig. 2. It acts as the dielectric function for an interacting electron gas without taking exchange and correlation into effect. It has large and small q limits given by[2]

$$\lim_{q \to \infty} \varepsilon(q) = 1 + \frac{16 \ me^2 k_f^3}{3\pi\hbar^2 q^4} \tag{123}$$

and

$$\lim_{q \to 0} \varepsilon(q) = \frac{4 \ me^2 k_f}{\pi\hbar^2 q^2} - \left(\frac{me^2}{3\pi\hbar^2 k_f} - 1\right) \quad . \tag{124}$$
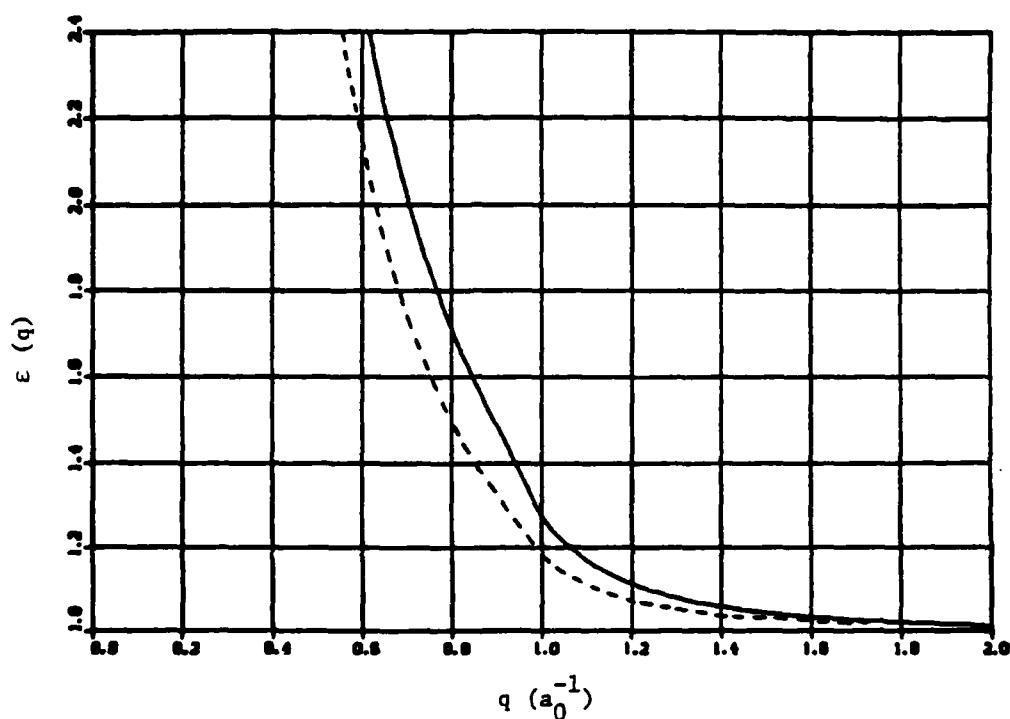
Fig. 2.
The solid line is the static Hartree dielectric function, $\epsilon(q)$,
as given by Eq. (80). The dashed line is the modified dielectric
function as given in the discussion following Eq. (125).

$\varepsilon(q)$ has a logarithmic infinity in its second derivative at $q = 2 k_f$, which will have an important effect on the interaction potential, as will be discussed later.

2. $f(q)$. The interpolation formula $f(q)$, which corrects the electron screening because of exchange and correlation effect, is given by Eq. (81) and is shown in Fig. 3. It varies smoothly from the expected $f(0) = 0$ long-range limit to the $f(\infty) = 1/2$ limit, where the screening effect is reduced by a factor of 2 because only electrons of anti-parallel spin should interact in this limit with exchange taken into account.[11] With $f(q)$ included, the relation between the total potential W and the bare-ion potential W_B Fourier coefficients is

$$W_q = W_{Bq}/[1 + (\varepsilon(q) - 1)(1 - f(q)] \quad , \tag{125}$$

so that the modified dielectric function is $1 + [\varepsilon(q) - 1][1 - f(q)]$. This function is shown as the dashed line in Fig. 2.

3. w_{Bq} and w_q. The local bare-ion pseudopotential matrix element w_{Bq}, discussed in Sec. I and given by Eq. (82) is the solid line in Fig. 4. The screened matrix element given by Eq. (125) is the dashed line in the same figure.

Note here that the screening effect is the cutting off of the long-range (small q) part of the potential, as expected. We also note that in the small q-limit

$$\lim_{q \to 0} W_q = \frac{-2}{3}\left(\frac{\hbar^2}{2m} k_f^2\right) = \frac{-2}{3} \varepsilon_f \cong -0.158 \text{ Ry} \quad , \tag{126}$$

where we have used the $\lim_{q \to 0} f(q) = 0$ and the small q-limit for the Hartree dielectric function given by Eq. 124.
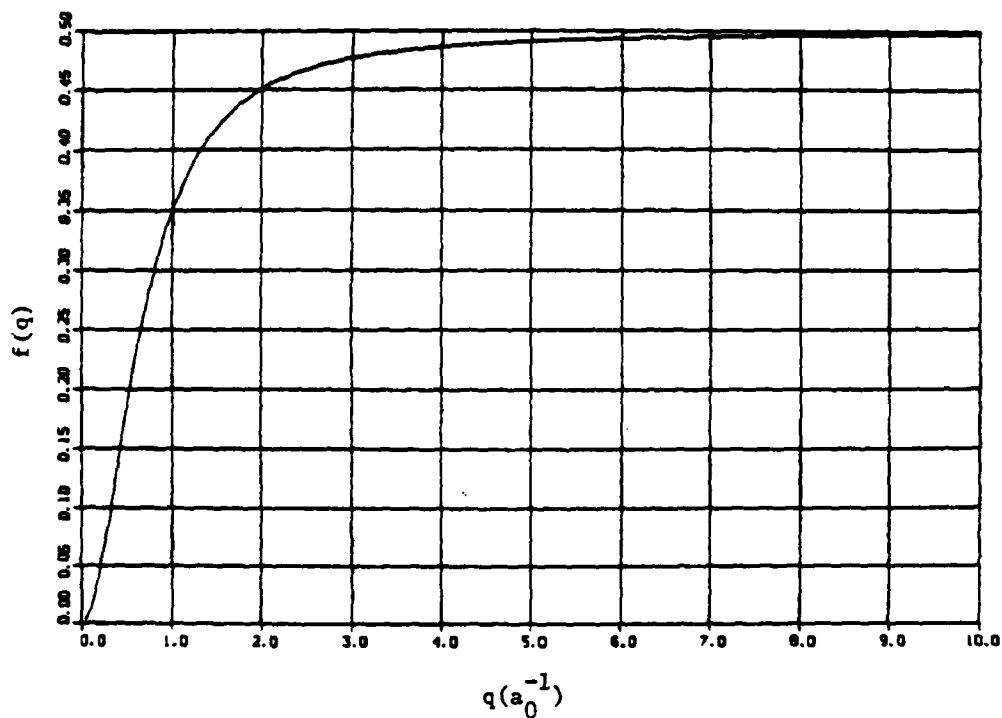
Fig. 3.
The interpolation formula for the approximate correction to the
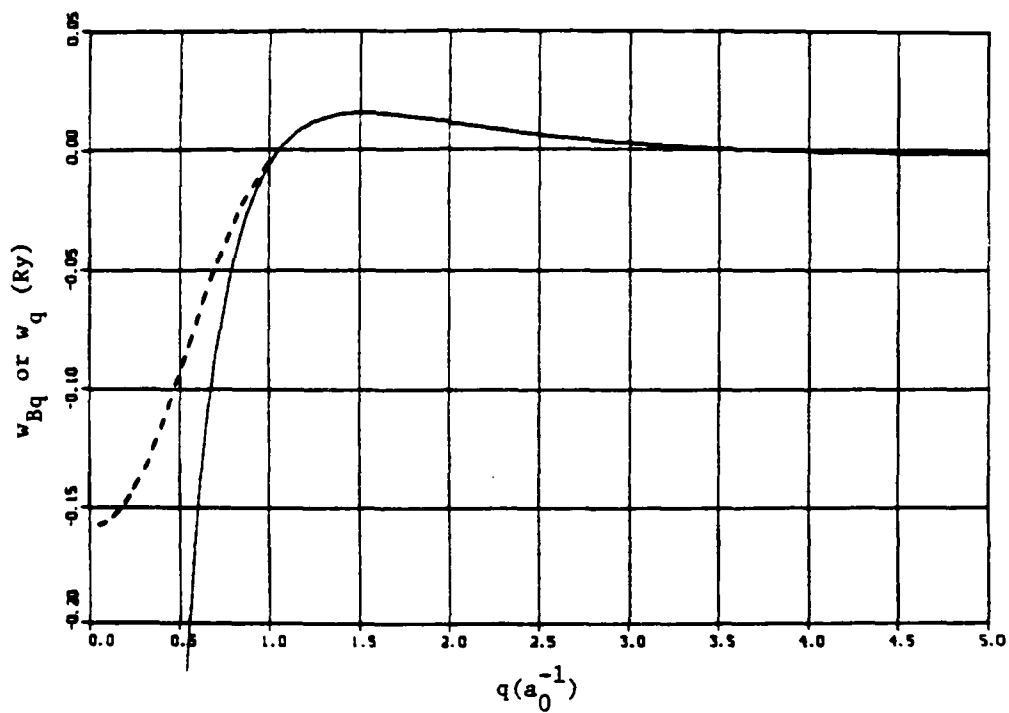electron screening due to exchange and correlation effects, f(q),
as given by Eq. (81).

Fig. 4.
The solid line is the local bare-ion pseudopotential matrix ele-
ment, w_{Bq}, given by Eq. (82). The dashed line is the screened
matrix element given by Eq. (125).

4. F(q). The energy wave-number characteristic given by Eq. (79) is calculated easily using the results above, and it is plotted as a function of q in Fig. 5. F(q) has more detail than this scale graph shows, such as a second negative "hump" at about $q = 5a_0^{-1}$ with a magnitude of 1.0×10^{-7} Ry.

In the large q-limit, F(q) goes to zero as

$$\lim_{q \to \infty} F(q) = - \frac{64 \; z^2 k_f^3}{3 \Omega_0} \; \frac{1}{q^6} \; , \tag{127}$$

and in the small q-limit, F(q) goes to negative infinity as

$$\lim_{q \to 0} F(q) = \frac{-2\pi z^2 e^2}{\Omega_0 q^2} \; . \tag{128}$$

5. $V_{IND}(r)$. We can evaluate the effective ion-ion interaction due to the presence of the electrons in the ion-electron system. We must evaluate the integral in Eq. (78), which is

$$V_{IND}(r) = \frac{\Omega_0}{\pi^2} \int_0^\infty F(q) \; \frac{\sin qr}{qr} \; q^2 dq \; . \tag{129}$$

It is instructive to look at plots of the argument of this integral; i.e.,

$$ARG = \frac{\Omega_0}{\pi^2} F(q) \; \frac{\sin qr}{qr} \; q^2 \; , \tag{130}$$

which are plotted for different r values in Fig. 6. This figure shows that the absolute value of the integral will decrease with increasing r because of the modulation of the sin (qr) term.
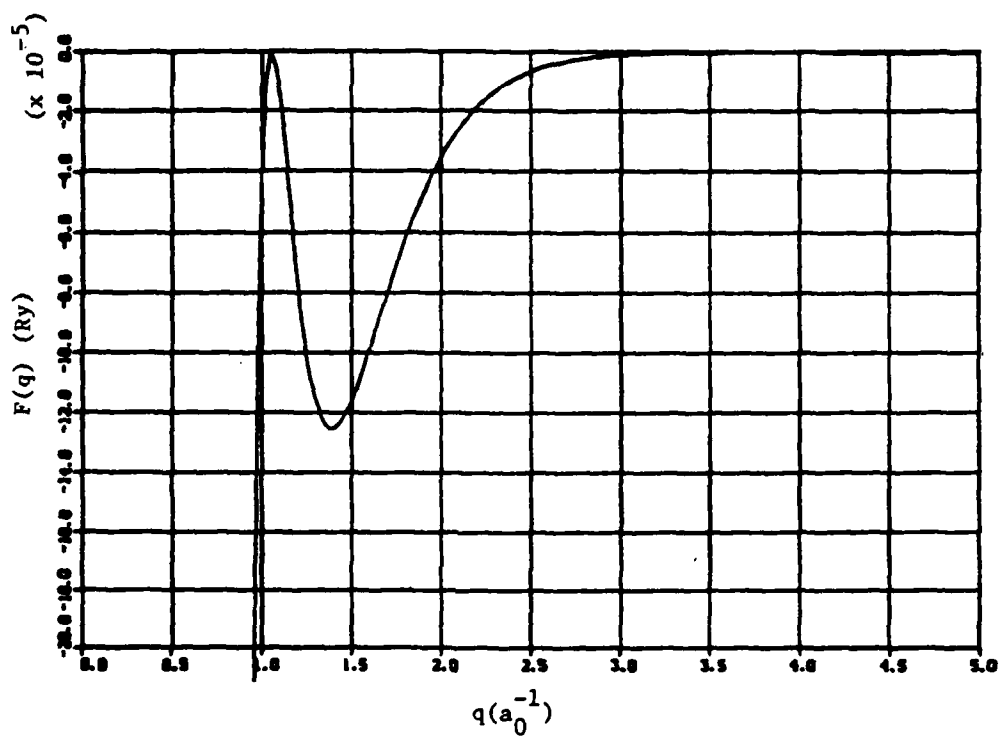
Fig. 5.
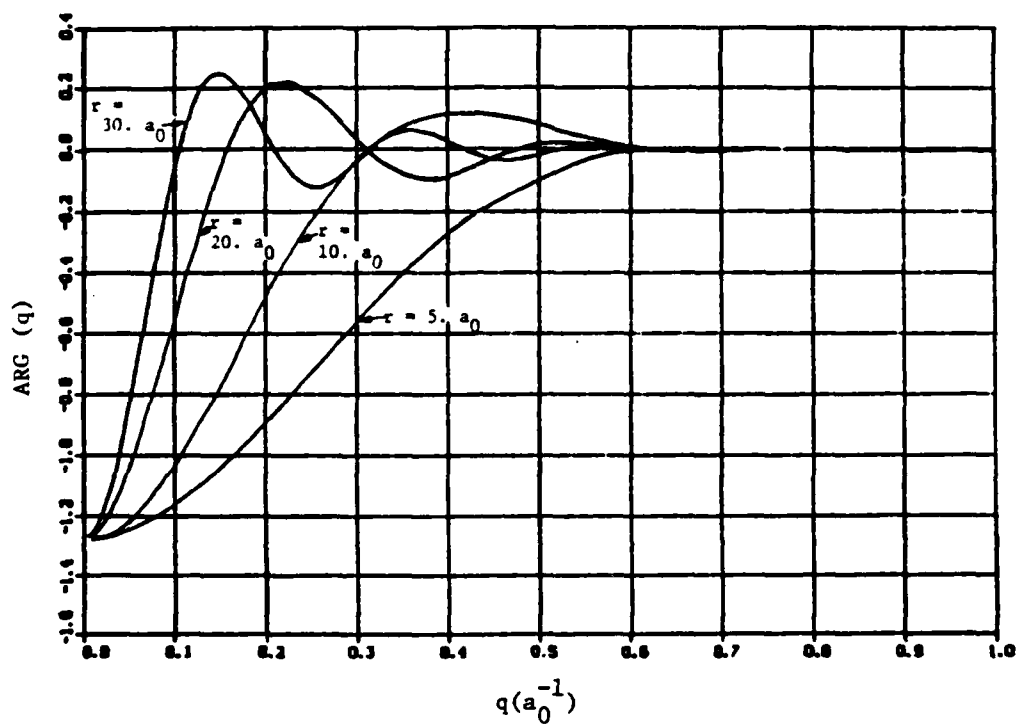The energy wavenumber characteristic, F(q), as given by Eq. (79).

Fig. 6.
Arguments of the effective ion-ion interaction integral as given
by Eq. (130) plotted for different r values.

The integral of this argument is evaluated numerically with the help of a Simpson's rule integration subroutine and the following relationship,

$$\int_0^\infty \text{ARG } dq = \int_0^b \text{ARG } dq + \int_b^\infty (\lim_{q\to\infty} \text{ARG}) \, dq \quad , \tag{131}$$

where the second integral is an analytical integral of the large q-limit of the argument.

Using the large q-limit for F(q) given by Eq. (127), we must evaluate

$$\int_b^\infty (\lim_{q\to\infty} \text{ARG}) \, dq = \frac{-64 \; z^2 k_f^3 r^3}{3\pi^2} \int_{br}^\infty \frac{\sin x}{x^5} \, dx \quad , \tag{132}$$

where we have changed variables in the integral from qr to x. This integral may be evaluated using standard integration formulas and the rational approximations to the sine integral of the form

$$\int_{br}^\infty \frac{\sin x}{x} \, dx \quad ,$$

given by Ref. 22.

In practice, the first integral in Eq. (131) is broken into NINT intervals, starting at A, with each B wide to ensure that the Simpson's rule integration is able to converge efficiently. The integrator uses a convergence criterion parameter, EPS, to determine the accuracy of each integration. The actual integration procedure is illustrated by

$$\int_0^\infty = \int_A^{A+B} + \int_{A+B}^{A+2B} + \cdots \int_{A+(NINT-1)B}^{A+(NINT)B} + \int_{A+(NINT)B}^\infty (\text{large q limit}) \quad . \tag{133}$$

Breaking up the interval allows investigation and correction for in-accuracies that may arise when Simpson's rule is used to evaluate integrals that have positive and negative areas canceling. We performed a convergence study of the $V_{IND}(r)$ integral and determined that the values

$$NINT = 20 \ ,$$
$$B = 1 \ ,$$
$$A = 1 \times 10^{-10} \ , \text{ and} \quad (134)$$
$$EPS = 1 \times 10^{-6}$$

yielded results accurate to about 10^{-5}, relative to the integral values we obtained for the well-converged solution. This value set was chosen to evaluate the integrals for use in the rest of the study. The function $V_{IND}(r)$ calculated in this manner is shown in Fig. 7 and as the solid line in Fig. 8.

We now investigate the $V_{IND}(r)$ behavior in the large r-limit.[*] To do this we expand Eq. (79) for $F(q)$ by letting

$$\frac{\varepsilon(q) - 1}{1 + [\varepsilon(q) - 1][1 - f(q)]} = \frac{x}{1 - f(q)x} \ , \quad (135)$$

where

$$x = 1 - \frac{1}{\varepsilon(q)} \ .$$

We note from the values of $f(q)$ and $\varepsilon(q)$ that $0 \leqslant f(q) < 1/2$ and $0 \leqslant x < 1$, so that $[f(q)x]^2 < 1$. We, therefore, may expand Eq. (135) as

---

[*]Based on a calculation by Galen K. Straub, Los Alamos National Laboratory.
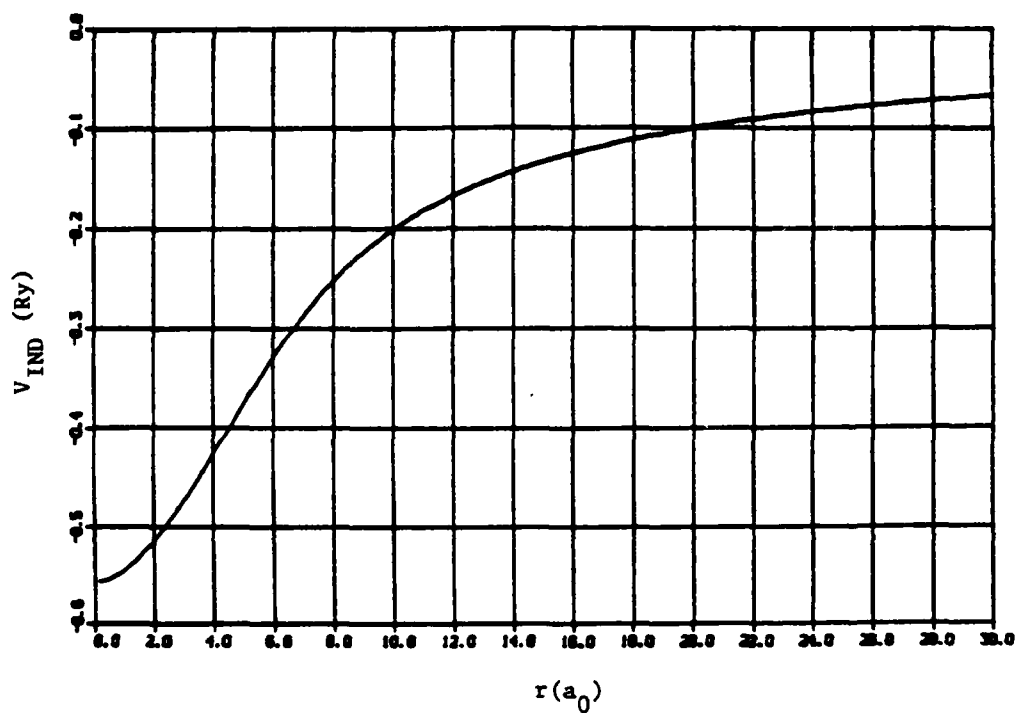
Fig. 7.
The effective ion-ion interaction, V_{IND}, as given by Eq. (78).
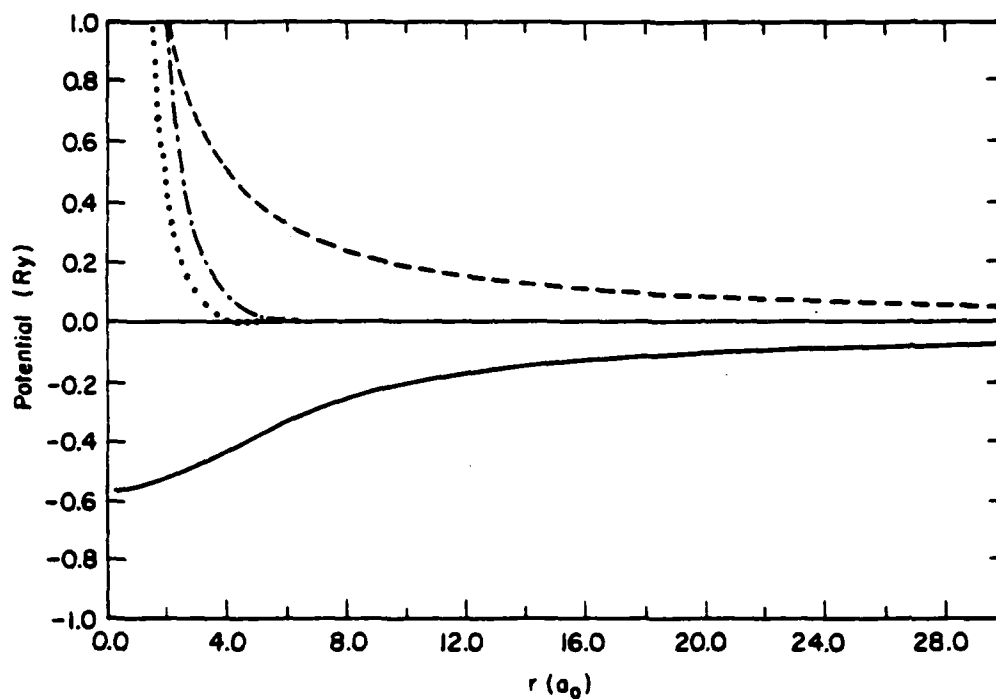
Fig. 8.
Plots of the effective ion-ion interaction, $V_{IND}(r)$ (solid line); the coulomb term, z^2e^2/r (dashed line); the Born-Mayer term, $\alpha_B e^{-\gamma_B r}$ (dotted line); and their sum, the total ion-ion interaction, $\Phi(r)$ (chain-dashed line) as given by Eq. (77).

$$\frac{x}{1 - f(q)x} = x[1 + f(q)x + f^2(q)x^2 + f^3(q)x^3 + \cdots]$$

$$= 1 - \frac{1}{\varepsilon(q)} + f(q)[1 - \frac{1}{\varepsilon(q)}]^2 + f^2(q)[1 - \frac{1}{\varepsilon(q)}]^3 + \cdots \quad . \quad (136)$$

We use this expansion and evaluate the contribution of each term to $V_{IND}(r)$ by evaluating the integral in Eq. (78). The contribution of the first term in Eq. (136) to $V_{IND}(r)$ is

$$\frac{-z^2 e^2}{r} + z \frac{\beta}{4\pi\rho^3} e^{-r/\rho} - O\left(\frac{1}{r^5}\right) \quad . \quad (137)$$

The second term in the expansion Eq. 136 yields the following integral.

$$\frac{\Omega_0}{\pi^2} \int_0^\infty \left(\frac{-\Omega_0 q^2}{8\pi e^2}\right) |w_{Bq}|^2 \left(\frac{1}{\varepsilon(q)}\right) \frac{\sin qr}{qr} q^2 \, dq \quad . \quad (138)$$

Now the infinite discontinuity effect in the static Hartree dielectric function, $\varepsilon(q)$, becomes apparent. Harrison[6] evaluates this expression by integrating by parts. He obtains vanishing contributions in the large r-limit for all terms except those containing the divergent second derivative of $\varepsilon(q)$. These yield a nonvanishing integral. The most singular term goes as $[\cos (2k_f r)]/r^3$, which is the leading term in the large r limit.

Using this result and Eq. (137), we see that the leading terms in the large r-limit of $V_{IND}(r)$ are

$$\lim_{r \to \infty} V_{IND}(r) \sim \frac{-z^2 e^2}{r} + \frac{\cos 2k_f r}{r^3} \quad . \quad (139)$$

The first term corresponds to the coulomb contribution of the bare ion potential and cancels the direct coulomb ion-ion interaction at large r. The second term represents the Friedel oscillations typical of screening caused by electrons in a system characterized by a sharp cutoff of momentum at the Fermi surface.[1,5,6] This term gives rise to the long-range oscillatory behavior of the ion-ion interaction.

6. $\phi(r)$. We calculate the total effective ion-ion interaction given by Eq. (77) as

$$\phi(r) = \frac{z^2 e^2}{r} + \alpha_B e^{-\gamma_B r} + V_{IND}(r) \quad . \tag{140}$$

The coulomb and Born-Mayer repulsive terms are plotted as the dashed and dotted lines, respectively, in Fig. 8. $V_{IND}(r)$ and $\phi(r)$ are also plotted in this figure. The nature of $\phi(r)$ is obscure in this figure, other than the cancellation of the coulomb repulsion by the leading $1/r$ term in the large r expansion of $V_{IND}(r)$ given by Eq. (139).

The nature of $\phi(r)$ is apparent from the plot in Fig. 9. We notice the dominant repulsion for $r < \sim 6.5\ a_0$, the minimum in the potential at $r \cong 8a_0$, and the long-range oscillatory behavior as discussed above. For convenience, we include here a plot of the force between pairs,

$$F(r) = \frac{-\partial \phi(r)}{\partial r} \tag{141}$$

in Fig. 10. The force is the value used directly in the molecular dynamics calculations to determine ion motion. Values for both the potential and force as a function of interatomic distance, r, are tabulated in Appendix A.

These, then, are the effective ion-ion interaction potential and force that will be used in our molecular dynamics calculations. We
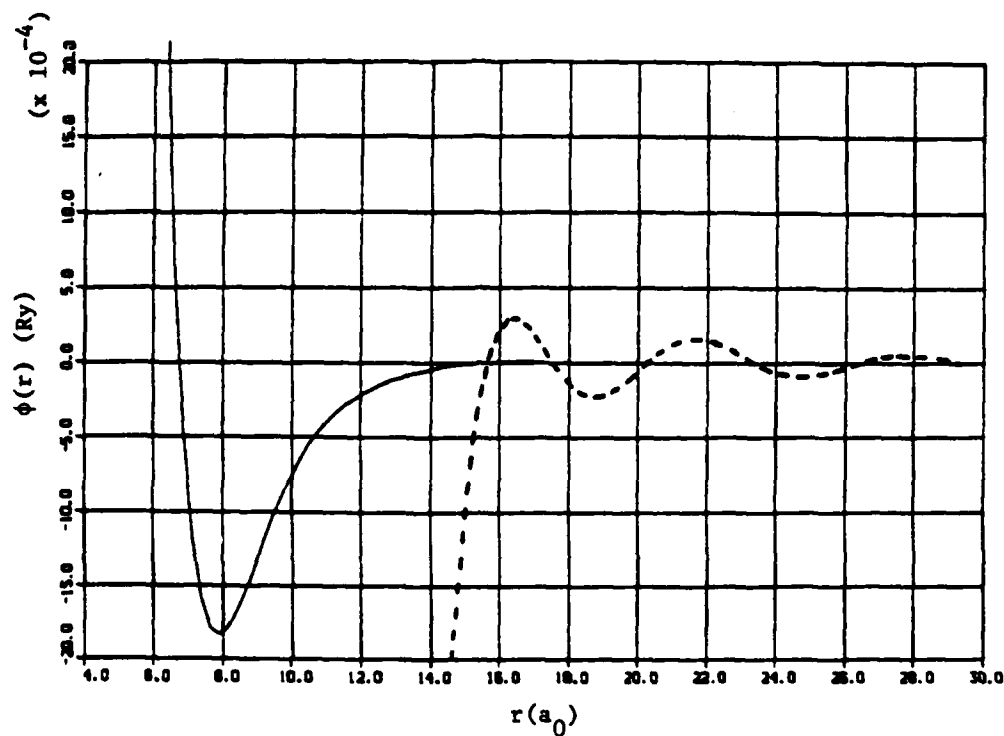
Fig. 9.
The total effective ion-ion interaction potential, $\phi(r)$, as given by Eq. (77). The dashed line is $\phi(r)$ multiplied by 100.
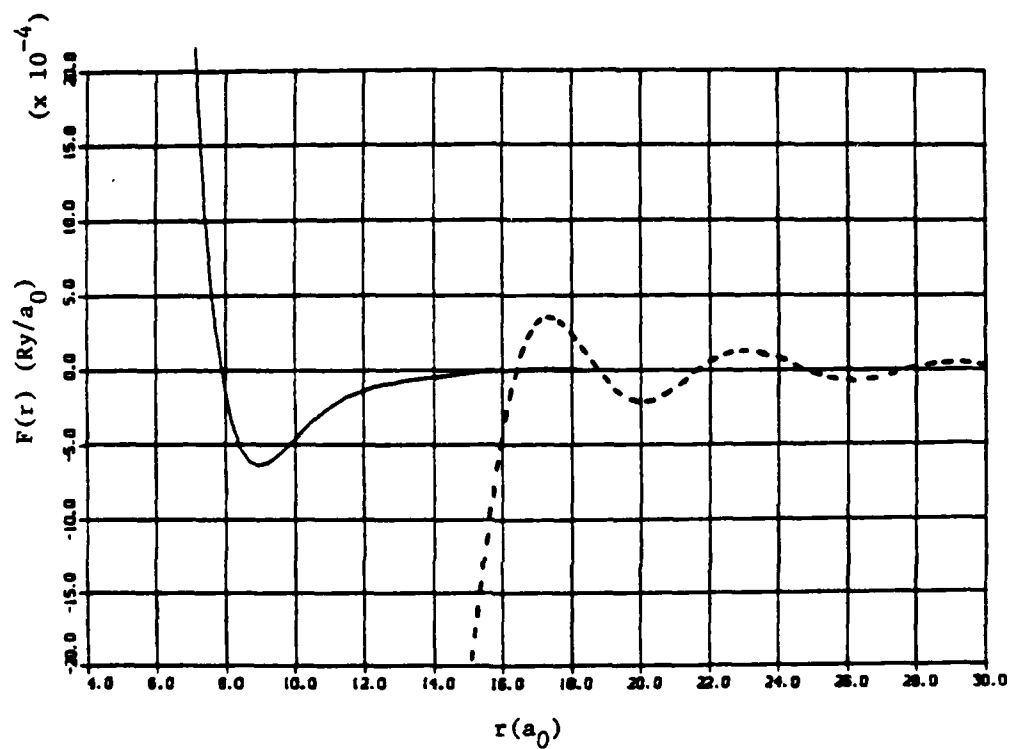
Fig. 10.
The effective pairwise force, F(r), as given by Eq. (141). The
dashed curve is F(r) multiplied by 100.

notice that they are dependent on the atomic volume Ω_0, through the Fermi wavenumber k_f, so that new functions are required at each sodium density calculated. Because the calculation of the potential and force functions is lengthy, we will tabulate the results and interpolate from the tables during a molecular dynamics calculation. This procedure is discussed in the next section.

C. Tabulation of the Potential and Force

Because each molecular dynamics calculation with the number of particles that we are considering is inherently costly, we want to make the potential and force information available in a manner which minimizes the number of operations required by the molecular dynamics program. To do this we tabulate the potential and force values and then look up the values as needed.

There is a tradeoff between different interpolation schemes. Some schemes are accurate for a relatively small number of points in the table, yet require many operations to obtain a value. The simplest of schemes, linear interpolation, requires a high point density but few calculations. Because, in a molecular dynamics program, we must perform many table lookups, and storage on the computer we are using (CDC 7600) is not a serious constraint, we have decided to use a linear interpolation scheme with enough points in the tables to ensure a negligible loss of accuracy owing to the table lookup.

The potential and force functions are dependent both on interatomic distance, R, and atomic volume, V. (For this discussion, we are using notation convenient to the notation used in the computer program.) Therefore, we must set up our tables and interpolate in both the R and V dimensions.

To illustrate table setup and the interpolation scheme, we will outline the procedure for determining the potential, POT, and force, F, once V and R have been specified.

The volume table is set up with a minimum volume VMIN, a maximum volume VMAX, and a certain number of table values NV (see Fig. 11). The constant interval between values is given by

$$DELV = \frac{VMAX - VMIN}{NV - 1} \quad . \tag{142}$$

The radius table is set up in a similar manner with RMIN, RMAX, NR, and DELR values specified.

V(IV) is the volume at the IVth position in the volume table, R(IR) is the radius at the IRth position in the volume table, and POT(IR,IV) is the potential at IR and IV, which are calculated from pseudopotential theory as discussed in Sec. III.B [and similarly for F(IR,IV)].

Now, given an arbitrary R and V within the table limits, we perform an integer divide (i.e., truncate the division to an integer) to get

$$IV = \frac{V - VMIN}{DELV} + 1 \quad , \tag{143}$$

so that we know that V is positioned between V(IV) and V(IV + 1) in the volume table.

At each of these volumes we find IR and IR + 1 and interpolate to find

POT1 = POT at IV and R ,
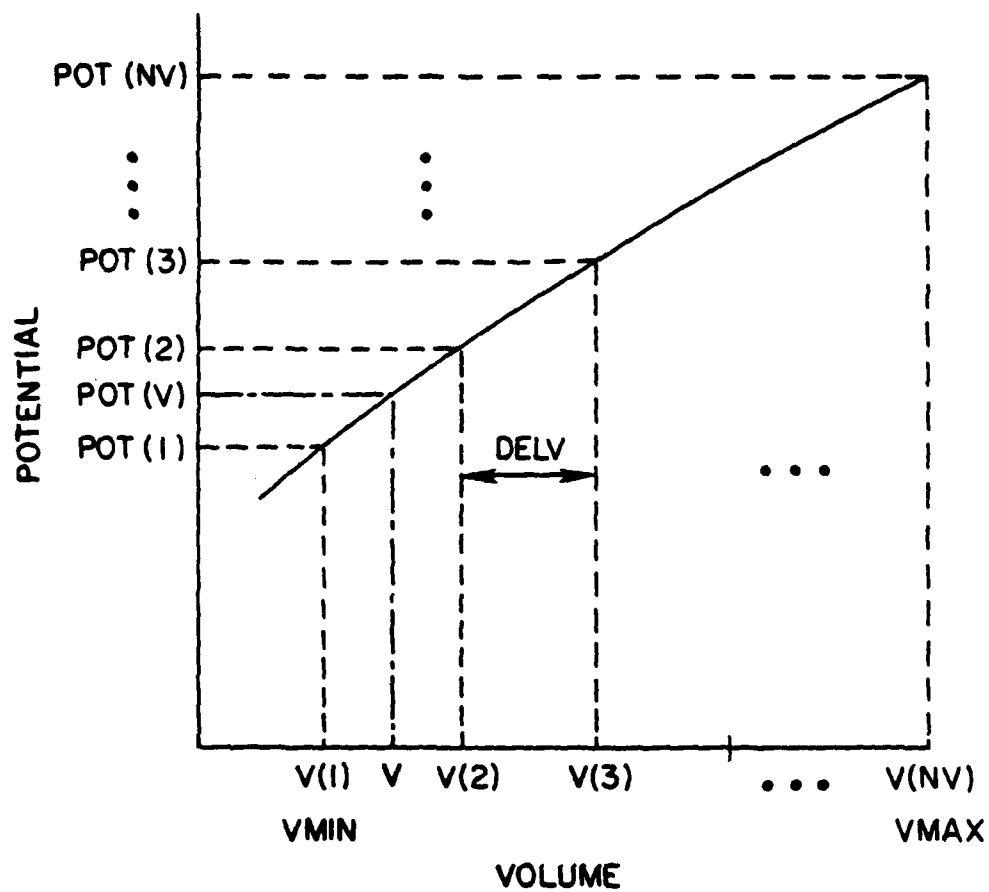
POT2 = POT at IV + 1 and R .

Fig. 11.
A schematic showing the arrangement of the volume-dependent table.
NV is the number of points in the table.

We may then interpolate on the volume to arrive at the value for the potential at V and R given by

$$POT = POT1 + \frac{V - V(IV)}{DELV} (POT2 - POT1) \quad , \tag{144}$$

and similarly for the force

$$F = F1 + \frac{V - V(IV)}{DELV} (F2 - F1) \quad . \tag{145}$$

We determined the appropriate density of points for these tables. Calculations of the potential and force at different volumes and constant radius showed an almost linear relationship, and five tables were adequate to cover a range from 10% compression to 10% expansion from normal density. For the R tables, a value of NR = 2000 was chosen, which yields interpolated values that are precise to about 10^{-4}, relative to calculated values. The RMIN and RMAX values include the expected interatomic distances.

The following values were chosen for the table setup.

$$\begin{aligned} RMIN &= 4.0 \ a_0 \\ RMAX &= 30.0 \ a_0 \\ NR &= 2000 \\ VMIN &= 230.01 \ a_0^3 \ (10\% \text{ compression}) \\ VMAX &= 281.12 \ a_0^3 \ (10\% \text{ expansion}) \\ NV &= 5 \end{aligned} \tag{146}$$

Curves obtained from the tables for the 10% compression and expansion volumes are shown in Fig. 12 to illustrate the density dependence of the potential.
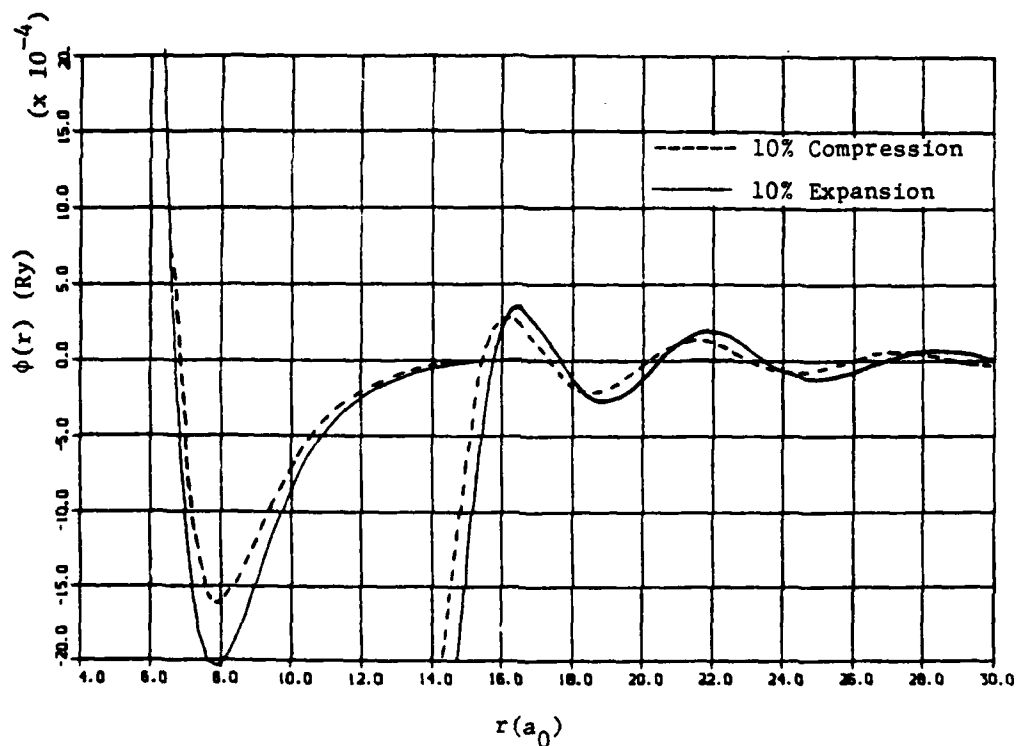
Fig. 12.
The total effective ion-ion interaction potential for the 10% compression ($\Omega_0 = 230$ a_0^3) and 10% expansion ($\Omega_0 = 280$ a_0^3) conditions. The oscillating curves at large r have been multiplied by 100.

IV. SETUP OF THE MOLECULAR DYNAMICS CALCULATIONS

We have described the molecular dynamics calculations and the pseudopotential method by which we calculate the effective pair inter-action between ions. A given molecular dynamics calculation proceeds as described in Sec. II.B, with the forces needed in Eq. (9C) read as required from the tables set up as described in Sec. III.C. In this section we discuss the setup of our particular calculations on sodium, and describe the units, initial conditions, and crystal configurations for the hexagonal close-packed (hcp) and body-centered (bcc) phases of sodium.

A. Units

We specify the energy ($E\emptyset$), distance ($X\emptyset$), and mass ($M\emptyset$) units for these calculations as

$$E\emptyset = 1 \text{ Rydberg} = Ry = 13.60559 \text{ eV} = 2.17971 \times 10^{-11} \text{ erg} = e^2/2a_0 \quad ,$$

$$X\emptyset = 1 \text{ Bohr radius} = a_0 = 0.529167 \times 10^{-8} \text{ cm} = 0.529167 \,\text{Å} = \hbar^2/me^2 \quad , \quad (147)$$

$$M\emptyset = 1 \text{ molecular weight of sodium} = 22.9898 \text{ g/mole} = 3.81731 \times 10^{-23} \text{ g} \quad .$$

Note that in these units, the mass of a sodium ion is unity. From these specified units we derive the time and velocity units as

$$t\emptyset = X\emptyset \left(\frac{M\emptyset}{E\emptyset}\right)^{\frac{1}{2}} = 7.00281 \times 10^{-15} \text{ s} \quad ,$$

and   (148)

$$v\emptyset = \frac{X\emptyset}{t\emptyset} = 0.755650 \text{ cm/}\mu\text{s} \quad .$$

Pressure is given in Ry/a_0^3. We will use kelvins (K) as our temperature unit with Boltzmann's constant given by

$$k = 6.33359 \times 10^{-6} \text{ Ry/K} \quad .$$

B. Initial Conditions

To solve the difference equations described in Sec. II.B, we must supply initial positions and velocities for the particles in the system, such that both the expected crystal configuration and approximate temperature are predetermined. In the next section we discuss the determination of the initial particle velocities. In the following two sections we describe the initial positions for hcp and bcc crystals of sodium.

1. Particle Velocities. We determine the initial velocities to satisfy the requirements that the center of mass velocity is zero and that the average of the velocities squared will give twice the temperature desired. We say twice here because, with the particles placed at their lattice positions, all initial energy will be kinetic and we expect about half to be partitioned to potential energy as the calculation proceeds and equilibrium is attained.

The computer program selects initial velocities by using a random number generator to choose the initial Δx, Δy, Δz for each particle to be between -1 and +1. These velocities are then scaled [see Eq. (109)] so that

$$KE = \frac{1}{N} \sum_{i=1}^{N} \frac{1}{2} m(\dot{x}_i^2 + \dot{y}_i^2 + \dot{z}_i^2) = 2 \left(\frac{3}{2} kT\right) , \qquad (149)$$

where the factor 2 is included according to the discussion above.

The initial velocity distribution is not normal. We expect that, as the calculation proceeds and the system approaches equilibrium, the distribution will become normal. This helps determine whether or not the system has attained equilibrium and will be discussed in Sec. IV.D.

Note also that the temperature is not specified precisely as an initial condition. We specify the initial conditions as outlined above, and when the system equilibrates, we calculate the system temperature from the average of the kinetic energy as given in Eq. (109).

2. hcp Initial Positions. We specify the initial particle positions for hexagonal close-packed crystals by placing the particles at the perfect hcp lattice sites. Figure 13 shows an hcp lattice, and the lattice vectors a, b, and c in the Cartesian coordinate directions. With these lattice vectors there are four particles per unit cell, placed at positions given in Table I.

These unit cells are repeated throughout the calculational volume to yield an hcp structure with one set of close-packed planes normal to the z-axis. For a perfect hcp structure, which corresponds to a close-packing arrangement of spheres, the relationships between the lattice vector magnitudes and the volume per particle are[2]

$$b = a\sqrt{3} \quad , \quad c = a\sqrt{8/3} \quad ,$$

and (150)

$$\Omega_0 = \frac{\sqrt{3}}{4} a^2 c = \frac{a^3}{\sqrt{2}} \quad .$$

TABLE I

PARTICLE POSITIONS WITHIN AN hcp UNIT CELL

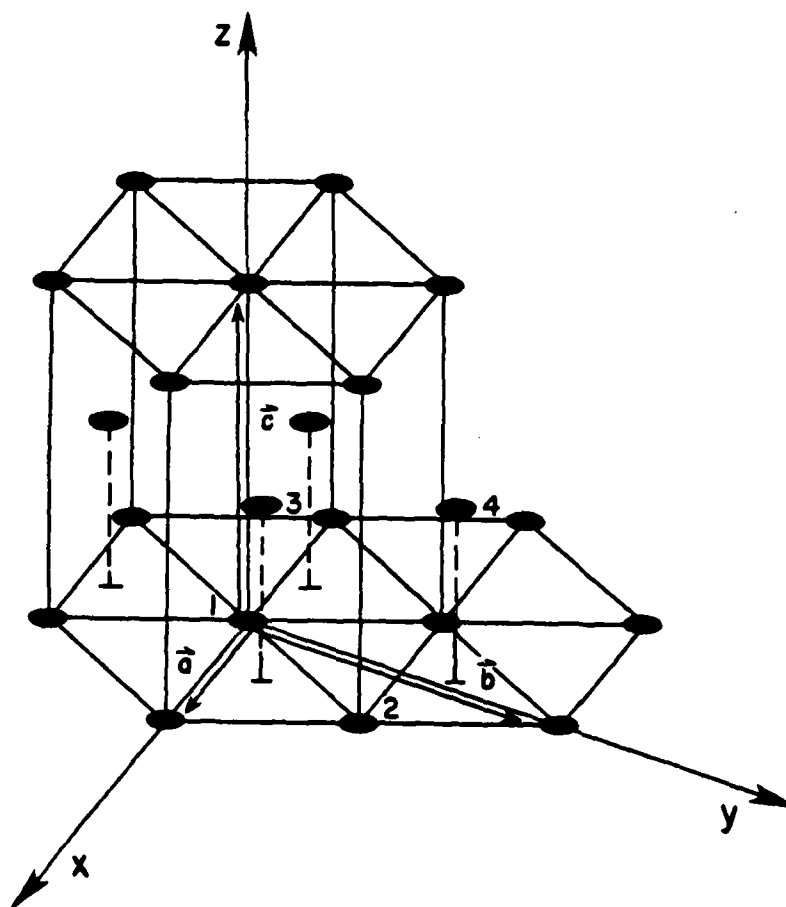| Particle	x	y	z
1	0	0	0
2	1/2 a	1/2 b	0
3	1/2 a	1/6 b	1/2 c
4	0	2/3 b	1/2 c

Fig. 13.
The hexagonal close-packed structure with lattice
vectors $\vec{a}$, $\vec{b}$, and $\vec{c}$ indicated. The four particles in
a unit cell are numbered.

The radial distances to the shells of particles relative to the origin placed at one of the lattice sites and the number of particles within a shell are shown for a perfect hcp lattice in Fig. 14. The bcc positions are also shown on this figure, along with a plot of the effective pair potential.

An hcp crystal produced by the molecular dynamics program is shown in Fig. 15. In this figure the near neighbors within each close-packed plane normal to the z-axis have been connected by lines for clarity. The dashed and dotted vertical lines indicate the relative positions of the planes. Figure 16 shows two such planes as viewed looking down the z-axis. Here we have noted the traditional A, B, C designations for the relative positioning of the planes. For an hcp structure, the close-packed planes are stacked in an ABAB··· arrangement. For a face-centered cubic (fcc) structure the stacking is ABCABCABC····.

3. bcc Initial Positions. The lattice positions of a body-centered cubic structure with an a' lattice constant (cube-edge dimension) are determined easily. The distance between a particle and its nearest neighbor is R_1 and

$$R_1 = \frac{\sqrt{3}}{2} a' \quad . \tag{151}$$

There are two particles per unit cell so that the volume per particle is

$$\Omega_0 = \frac{a'^3}{2} = \frac{4}{3\sqrt{3}} R_1^3 \quad . \tag{152}$$

The position vectors $\vec{R}(N)$ to all points in the lattice may then be specified[2] by
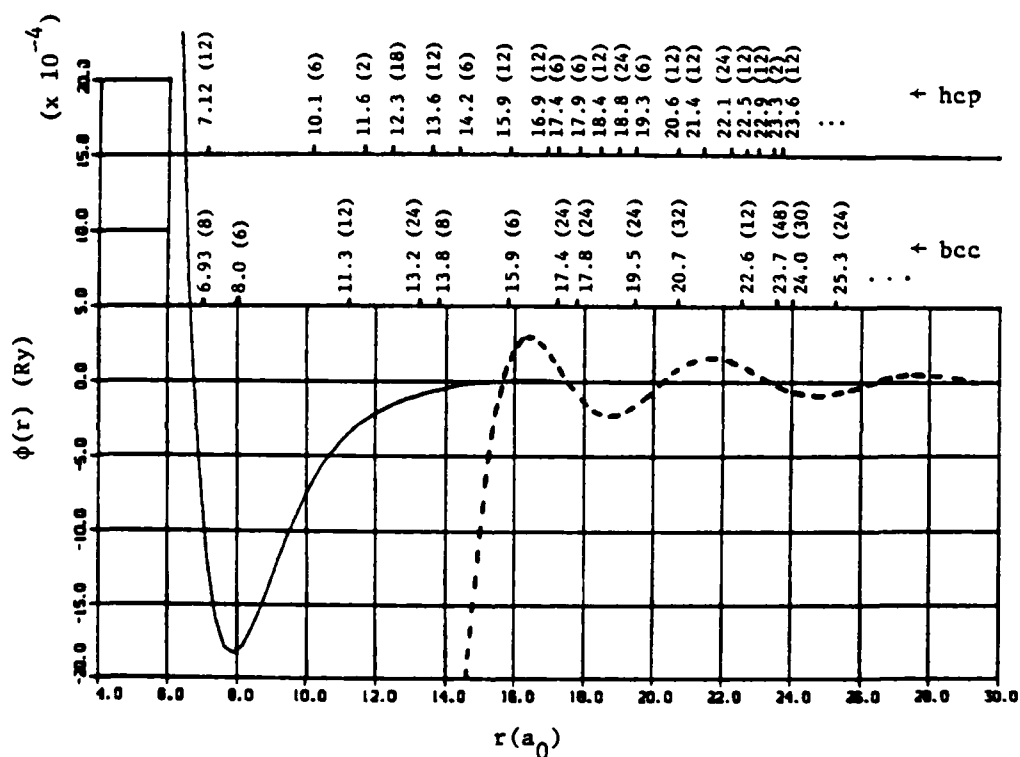
Fig. 14.
Radial positions of particle shells for the hcp
and bcc crystal structures appropriate to a volume
per particle of 256 a_0^3. The number in parentheses
is the number of particles in each shell. The
total ion-ion interaction potential of Fig. 9 is
also plotted.
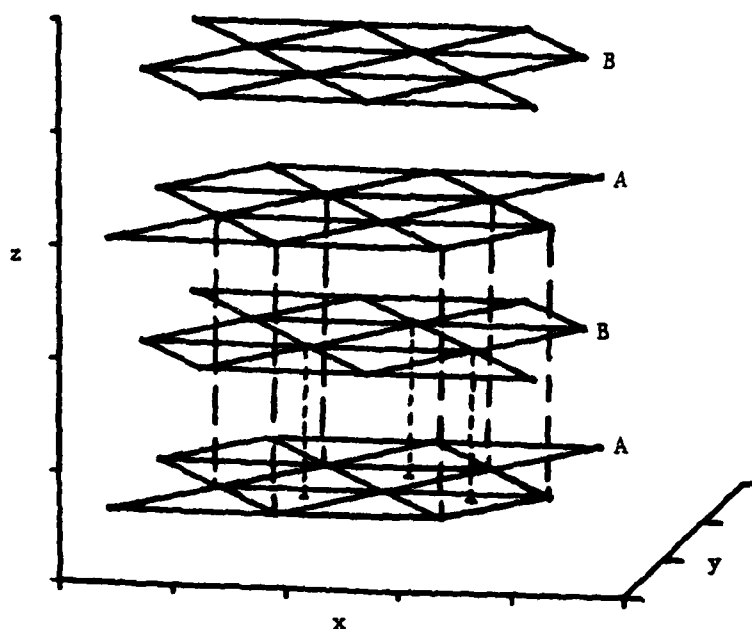
Fig. 15.
The hexagonal close-packed structure as set up by the
molecular dynamics program. Solid lines are drawn
between nearest neighbors in each close-packed plane
normal to the z-direction for clarity. The dashed
lines indicate the relative positions of the planes
marked by A and B.
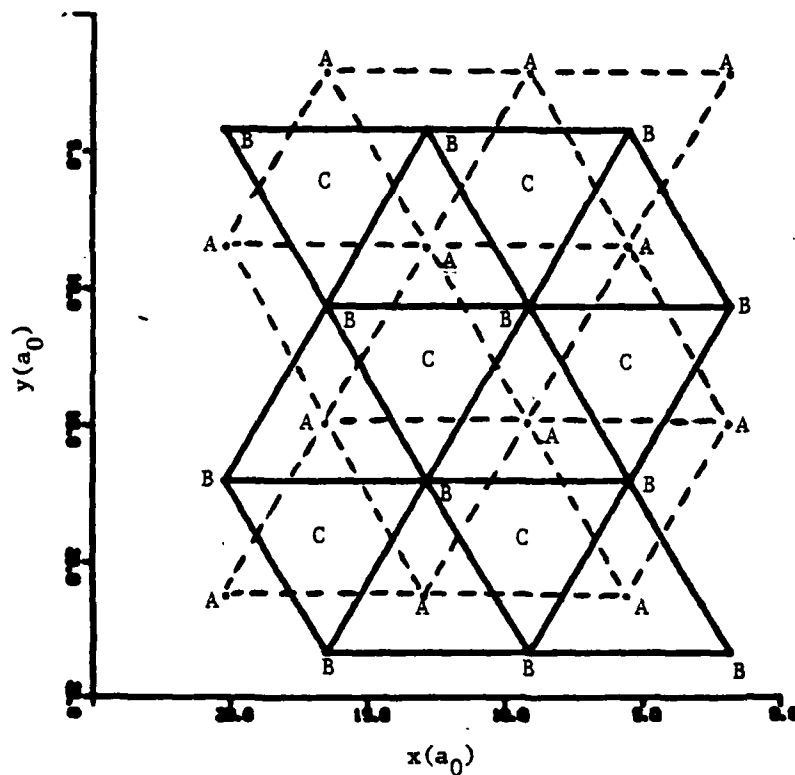
Fig. 16.
Close-packed hcp planes viewed down the z-axis. The
dashed lines indicate an A-plane in Fig. 15. The solid
lines indicate a B-plane. For an hcp structure, planes
which occupy the C positions do not occur.

$$\vec{R}(N) = \frac{R_1}{\sqrt{3}} (N_1 \hat{x} + N_2 \hat{y} + N_3 \hat{z}) \quad , \tag{153}$$

where N_1, N_2, N_3 are integers and are constrained to be either all even or all odd. This constraint is given equivalently by requiring that $(N_1 + N_2)$. $(N_2 + N_3)$, and $(N_1 + N_3)$ be all even. The distance to each particle is given by

$$|\vec{R}(N)| = \frac{R_1}{\sqrt{3}} (N_1^2 + N_2^2 + N_3^2)^{1/2} \quad . \tag{154}$$

Using these relations we easily generate the points in a perfect bcc lattice with a computer program and we have used this method to study perfect lattice calculations of the total crystal potential, as described in Sec. IV.C.

However, for the molecular dynamics calculations we choose to use a different but equivalent method. We want to create a bcc structure that is oriented to resemble as closely as possible the hcp structure that we are studying. We will create a bcc system with (110) close-packed planes normal to the z-direction because our hcp close-packed planes are normal to the z-direction.[*]

This may be accomplished by setting up a face-centered tetragonal (fct) lattice with lattice vector magnitudes given by

$$a = c = \sqrt{2} \, b = \sqrt{2} \, a' \quad , \tag{155}$$

where a' is the desired bcc lattice constant. This structure is shown schematically in Fig. 17. The dashed lines outline the cubic box.

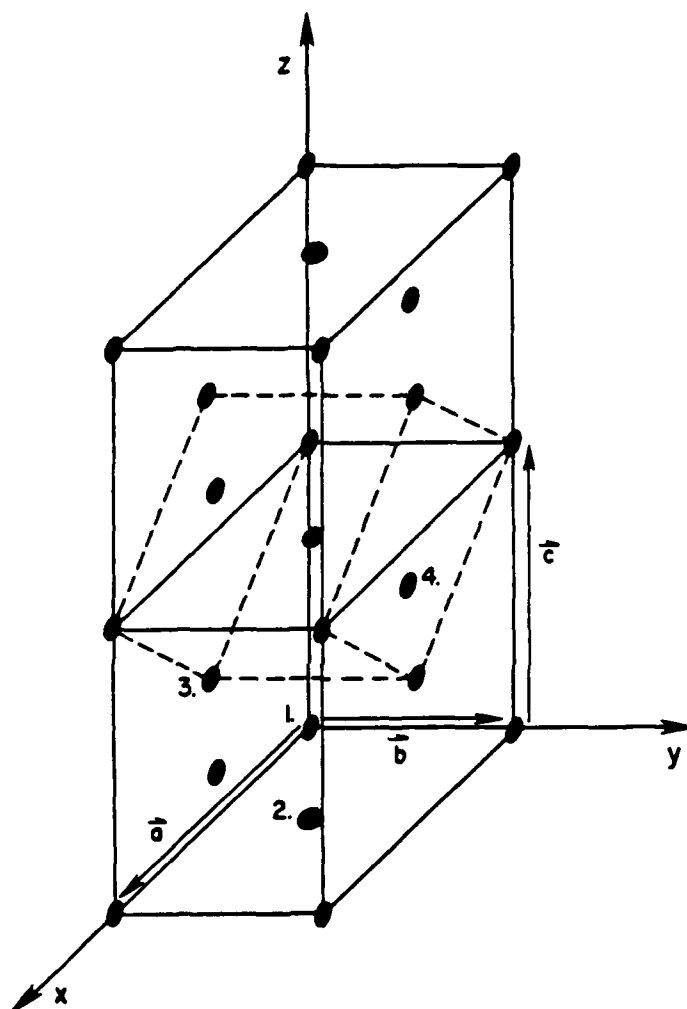[*]Based on a procedure by Brad Lee Holian, Los Alamos National Laboratory.

Fig. 17.
A face-centered tetragonal structure with a = c =
√2 b appropriate to produce a body-centered cubic
(bcc) structure with (110) planes normal to the
z-direction. The four points in a unit cell are
numbered. The dashed lines indicate the bcc struc-
ture.

The bcc (110) planes are the faces of the fct structure normal to the z-axis.

This crystal structure has four particles per unit cell with positions given by Table II and indicated in Fig. 17.

Figure 18 shows the bcc lattice as set up by the molecular dynamics program. In this figure a body-centered cube is outlined and lines are drawn through the cube diagonal and body-centered particle to indicate the (110) plane. Figure 19 is a drawing of the same lattice with lines drawn connecting the nearest neighbors within a close-packed plane. The numbers 1 and 2 designate relative positions of one plane with respect to another. Figure 20 shows a "1" plane and a "2" plane as viewed looking down the z-axis. These last two figures may be compared with Figs. 15 and 16 for the hcp lattice. We note here, in passing, that a slight compression of the planes in Fig. 20 in the y-direction to form hexagonal planes and a relative shift between planes 1 and 2 in the x-direction will create a hexagonal close-packed structure (or fcc structure, depending on the stacking). The radial distances to the shells and the number of particles in each shell for a bcc lattice are shown relative to hcp structure and the effective pair potential in Fig. 14.

TABLE II

PARTICLE POSITIONS WITHIN THE fct UNIT CELL

Particle	x	y	z
1	0	0	0
2	1/2 a	1/2 b	0
3	1/2 a	0	1/2 c
4	0	/2 b	1/2 c
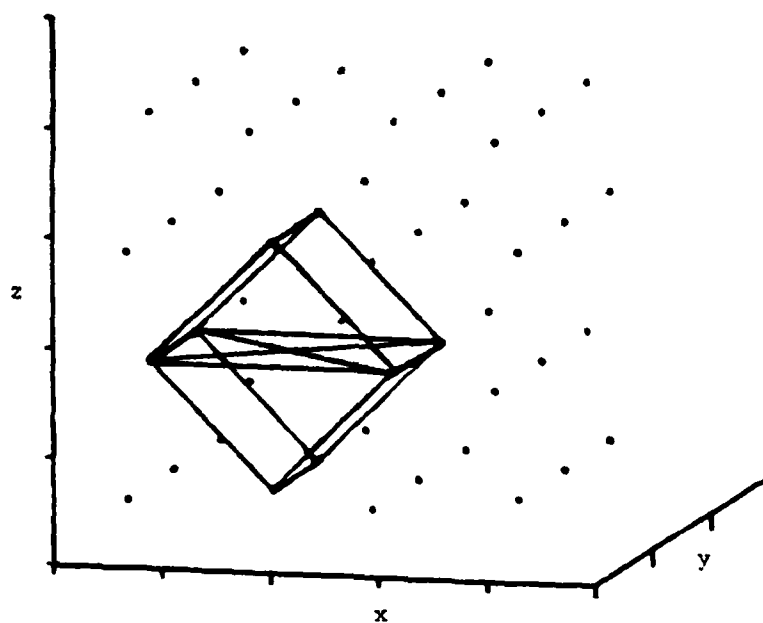
Fig. 18.
The body-centered cubic structure as set up by the
molecular dynamics program. The lines outline the
basic cube and indicate the close-packed plane
through the cube diagonal and body-centered particle.
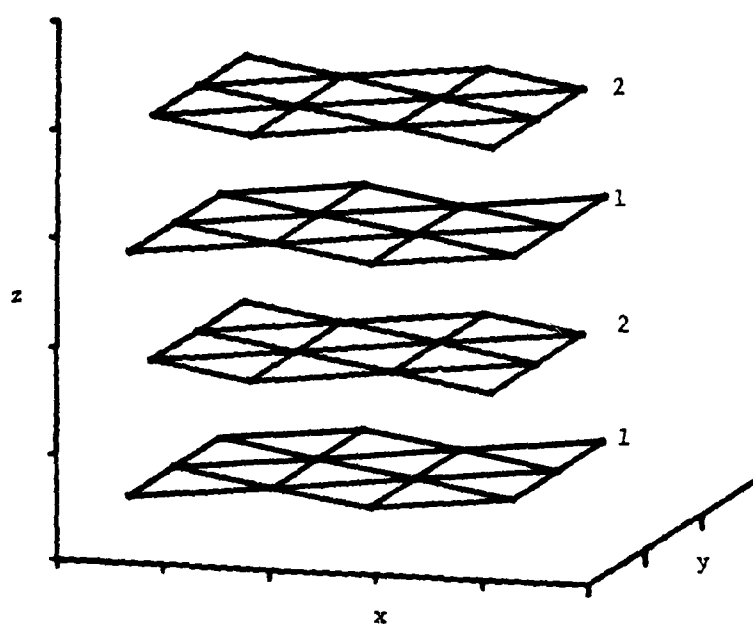
Fig. 19.
The same body-centered cubic structure as in Fig. 18
but with lines drawn between the nearest neighbors
within a close-packed plane for comparison with the
hcp structure of Fig. 15.

MICROCOPY RESOLUTION TEST CHART

NATIONAL BUREAU OF STANDARDS 1963 A

$x(a_0)$
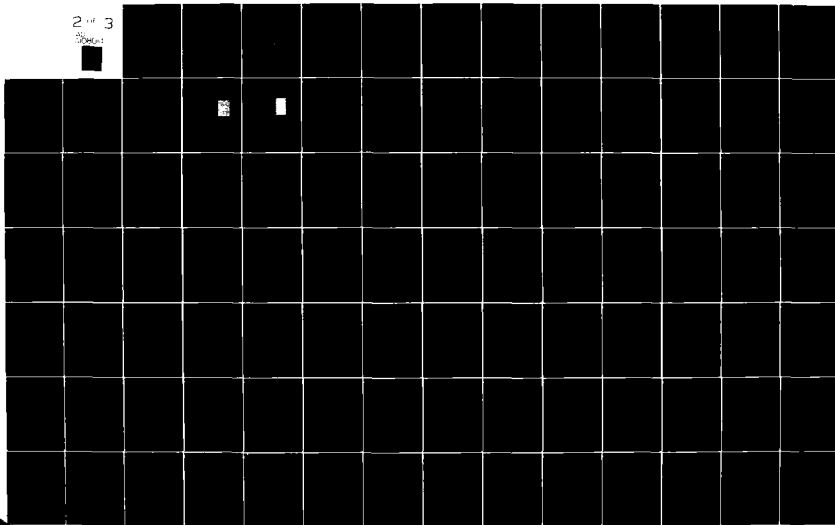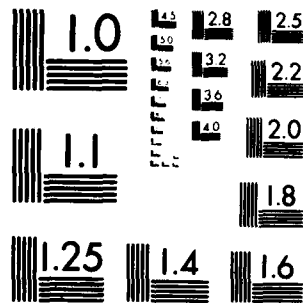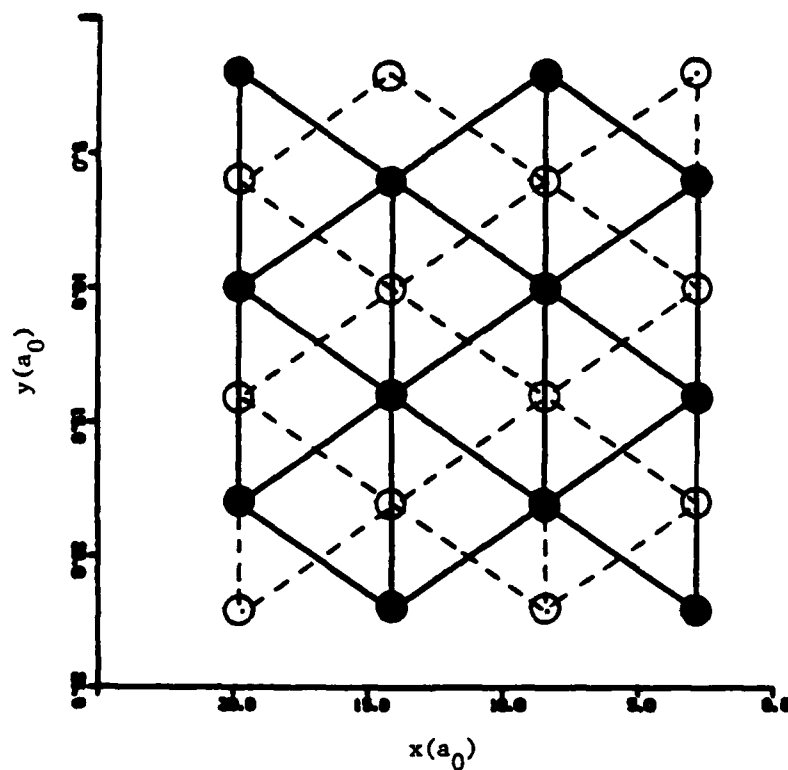
Fig. 20.
Close-packed planes of a bcc lattice viewed down the
z-axis. The dashed lines and open circles indicate
planes marked 1 in Fig. 19. The solid lines and solid
circles indicate planes marked 2.

C.   Determination of Run Parameters

In this section we determine run parameters for use as input to the molecular dynamic calculations. These parameters are the time step Δt of Eqs. (90)-(92), the maximum range of the potential RMAX (see Fig. 1), and the system size. There is no standard procedure for choosing these parameters and generally each must be investigated to minimize the effects on the calculations. We discuss how we have determined each of these parameters for use in our calculations.

1. Determination of the Time Step. The time step must be kept small enough that errors of order $(\Delta t)^3$ inherent in the central difference scheme described in Sec. II.B are negligible. Another way of thinking is that we must not let the particles in the system move very far before stopping and recalculat'.g the forces on them. Also, we must not have Δt so small that the calculations require an inordinate amount of computer time.

To evaluate Δt, we investigate the environment that a single particle in our system experiences. We do this by performing a "cell model" calculation where one particle is allowed to move in the force field of all the others which are constrained to their perfect lattice positions. Doing this, we can map the potential surface for a particle in this system.

We set up a bcc lattice with near neighbor distance R_1 of 6.93 a_0, which is appropriate to an atomic volume for sodium of 256 a_0^3. A plot of the potential surface for a particle moving in the (001) (or xy) plane in the +x and +y directions is shown in Fig. 21. This cell model potential well is quite harmonic and symmetric, as shown in Fig. 22, where the potential of a particle moving along three crystal directions
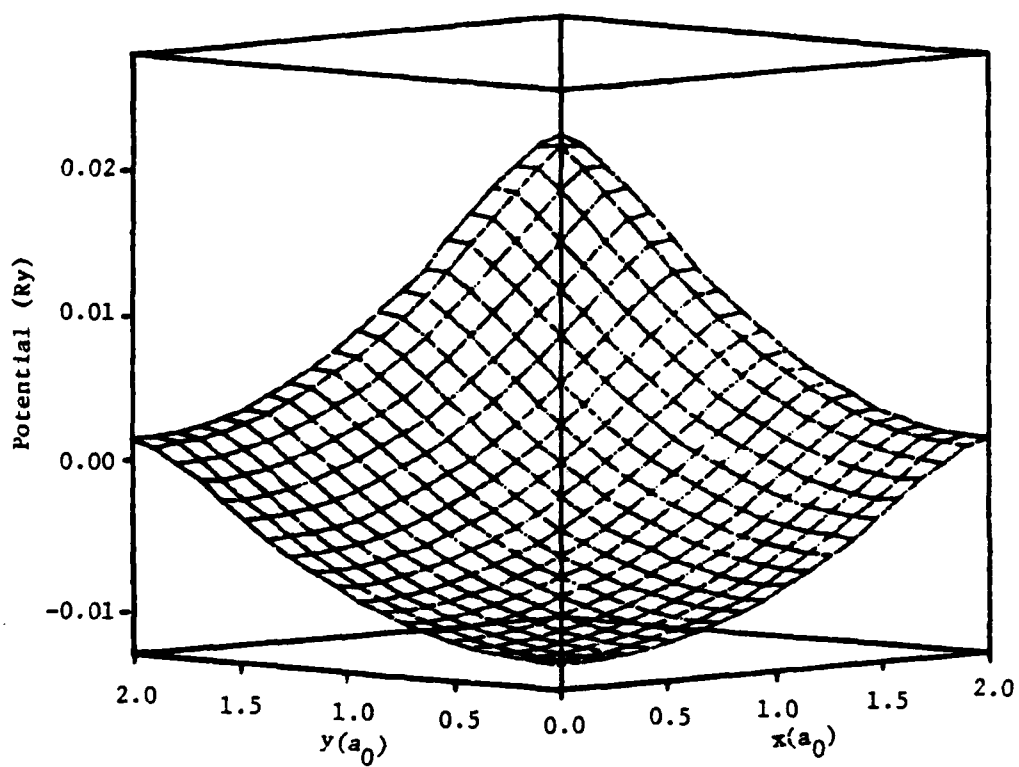
Fig. 21.
The cell model potential surface for a particle moving in the (100) plane in the +x,+y quadrant.
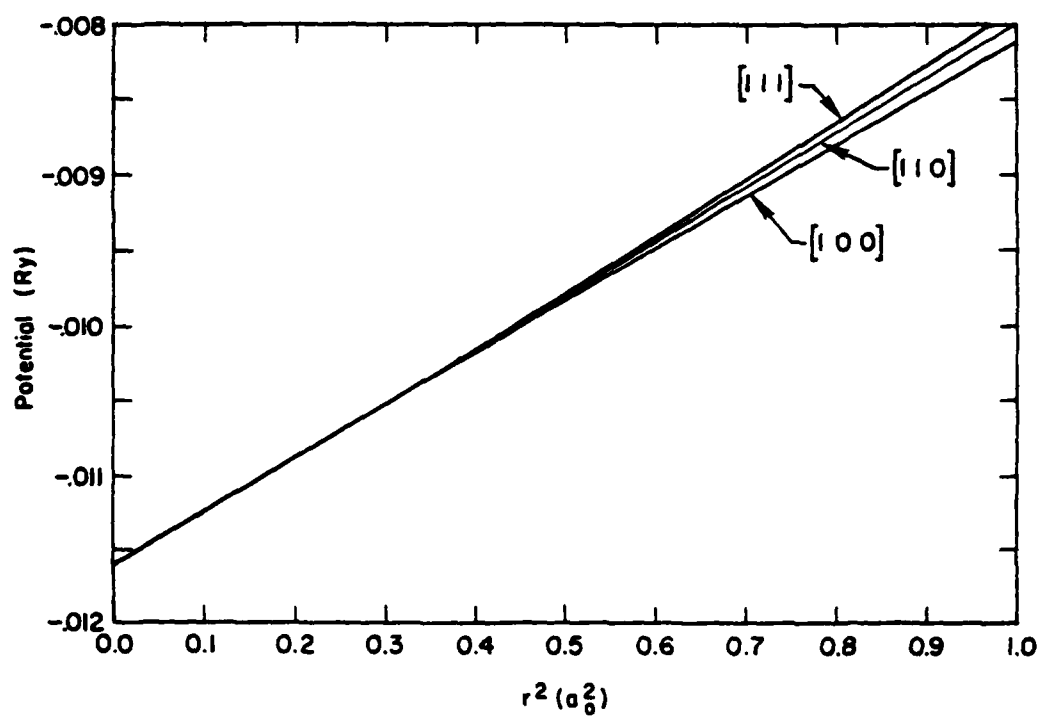
Fig. 22.
The potential for a particle in the cell model moving from the origin
in the [111], [110], and [100] directions plotted vs r^2.

is plotted versus the square of its distance from its perfect lattice site. The directions were chosen to indicate the most and least drastic paths for the particle. The three directions shown are (1) the [111] direction which is toward the body center (the nearest neighbor), (2) the [110] direction which is across a cube face diagonal, and (3) the [100] direction which is down a cube side.

The curves are linear in r^2 out to at least an atomic unit and we, therefore, represent the potential in this region by a harmonic potential of the form

$$\phi(r) = \frac{1}{2} kr^2 + C \quad . \tag{156}$$

We calculate the slope of the line for the [111] direction (the largest slope of the three) and find that

$$k \cong 0.0072 \ Ry/a_0^2 \quad ,$$

which allows us to calculate the period of a harmonic oscillation in this potential as

$$T = 2\pi \sqrt{\frac{m}{k}} \cong 74 \ T\emptyset \quad , \tag{157}$$

where $T\emptyset$ is the time unit evaluated in Sec. IV.A. We now use a convention which is based on experience and says that a conservative time step estimate should allow a particle to move 1/60th of its period per time step. Using this estimate would yield a Δt of about 1.0 $T\emptyset$. We will use this number for our calculations.

2. Determination of RMAX. We choose the range of the potential RMAX (see Fig. 1) with two thoughts in mind. We want the effect of all particles farther away from a given particle than RMAX to be negligible

and we want to minimize the effect of particles moving from outside to inside the RMAX range. Noting the small magnitude of the oscillations in the potential and force functions of Figs. 9 and 10, we intuitively feel that an RMAX greater than 16 a_0 would be suitable. To get a better indication of the effect of RMAX on the calculations, we will calculate the perfect crystal total potential per particle for the bcc lattice for different values of RMAX.

The total crystal potential per particle is given by Eq. (106) as

$$\Phi = \frac{1}{2N} \sum_{i=1}^{N} \sum_{j=1}^{N'} \phi(r_{ij}) \quad , \tag{158}$$

where

$$r_{ij} = |\vec{r}_i - \vec{r}_j| \quad . \tag{159}$$

To calculate this for a perfect crystal, we arbitrarily place one particle at the origin (particle i) so that

$$\Phi = \frac{1}{N} \sum_{i=1}^{N} \left[\frac{1}{2} \sum_{j=1}^{N'} \phi(r_{ij}) \right] \quad . \tag{160}$$

The sum over i is N because the result for all particles in a perfect lattice is identical. We take the sum on j to be over all the other particles. The result is

$$\Phi = \frac{1}{2} \sum_{j=2}^{N} \phi(r_{ij}) \quad . \tag{161}$$

To calculate the crystal potential, it is inappropriate to extend the discrete sums to infinity. Additionally, the values for the

molecular dynamics system will be summed discretely using Eq. (106) and
will be cut off at RMAX, where RMAX must be kept to a reasonable value
so that the length of the calculations does not become prohibitive.
We will, therefore, separate the discrete sum into a discrete part
(subscript d) out to RMAX and a continuous part (subscript c) from RMAX
to infinity, so that

$$\Phi = \Phi_d + \Phi_c \quad , \tag{162}$$

where the discrete part is given by

$$\Phi_d = \frac{1}{2} \sum_{j=2}^{r_{ij} \leqslant RMAX} \phi(r_{ij}) \quad . \tag{163}$$

We calculate the continuous part by assuming that the density
approaches a uniform distribution at large r. For a uniform density
with one particle assigned to each volume per particle, Ω_0, the system
potential is given by

$$\Phi = \frac{2\pi}{\Omega_0} \int_0^\infty dr \ r^2 \phi(r) \quad . \tag{164}$$

The continuous part in Eq. (162) is given by

$$\Phi_c = \frac{2\pi}{\Omega_0} \int_{RMAX}^\infty dr \ r^2 \phi(r) \quad . \tag{165}$$

The total number of particles within a sphere of radius r is
plotted in Fig. 23 for the hcp and bcc crystal structures and the uni-
form density distribution as given by $(4\pi/3\Omega_0)r^3$. Also shown in this
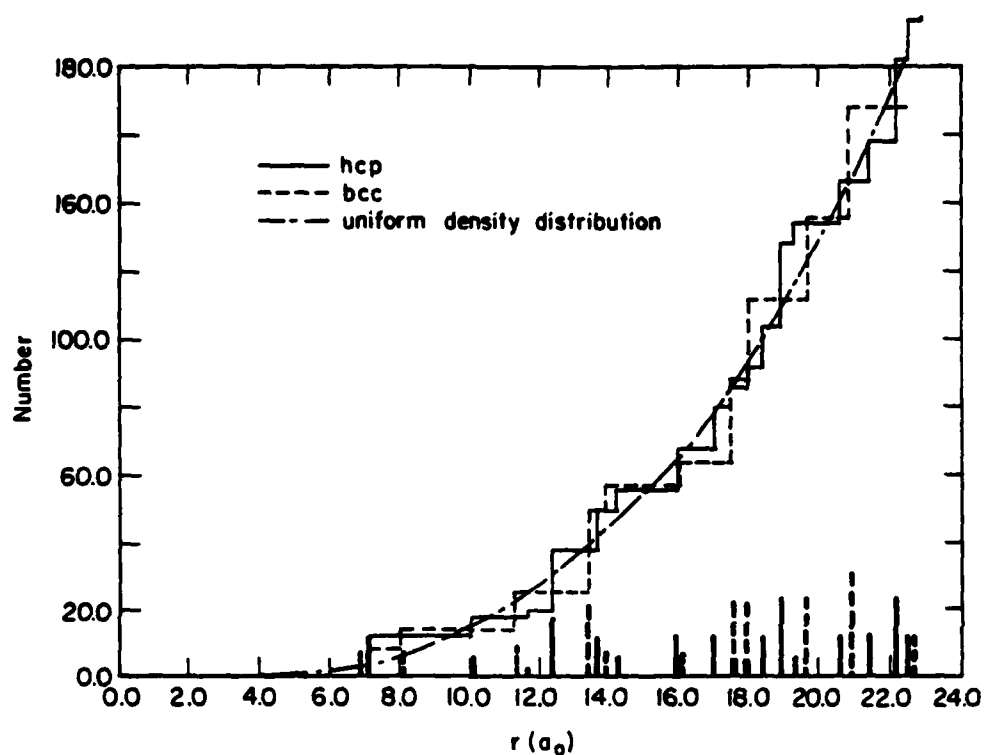
Fig. 23.
Number of particles within a given radius vs radius for the hcp
and bcc crystal structures and for a uniform density distribu-
tion. The vertical lines on the r-axis indicate the positions
of the crystal structure shells and the height of these lines
indicates the number of particles in each shell.

figure are the positions and number of particles in each shell of the crystal structures.

To calculate the continuous contributions to the potential, we will use the large r limit for the potential. As discussed in Sec. III.B.5, in this limit the potential goes as

$$\frac{\cos 2k_f r}{(2k_f r)^3} \; .$$

We calculate this term to be

$$\phi(r)\Big|_{\text{large } r} = \phi_A(r) = \frac{-18 \; \pi z^2 w_{2kf}^2}{\epsilon_f} \; \frac{\cos 2k_f r}{(2k_f r)^3} \tag{166}$$

where ϵ_f is the electron kinetic energy at the Fermi sphere and w_{2k_f} is the magnitude of $w_{Bq}/\epsilon(q)$ evaluated at $q = 2k_f$. For an atomic volume of $256 \; a_0^3$, which yields a Fermi wavenumber of $0.4872 \; a_0^{-1}$, the value for w_{2k_f} is 0.0067. We call $\phi_A(r)$ the asymptotic form of the potential function. This asymptotic form is plotted in Fig. 24. The dashed line in this figure is the actual potential function [$\phi(r)$ of Eq. (77)].

Using the asymptotic form, we calculate the continuous part of the crystal potential to be

$$\phi_c = \left(\frac{2\pi}{3\Omega_0 k_f^3}\right)\left(\frac{-18\pi z^2 w_{2kf}^2}{\epsilon_f}\right)\left[-\text{Ci}(2k_f \cdot \text{RMAX})\right] \; , \tag{167}$$

where Ci is the cosine integral as defined in Ref. 22.

We calculate the total crystal potential using Eqs. (162), (163), and (167). The results are plotted in Fig. 25. Large jumps are noted in the

Fig. 24.
The asymptotic form of the potential, $\phi_A(r)$, as given by Eq. (166).
The dashed line is the actual potential, $\phi(r)$.
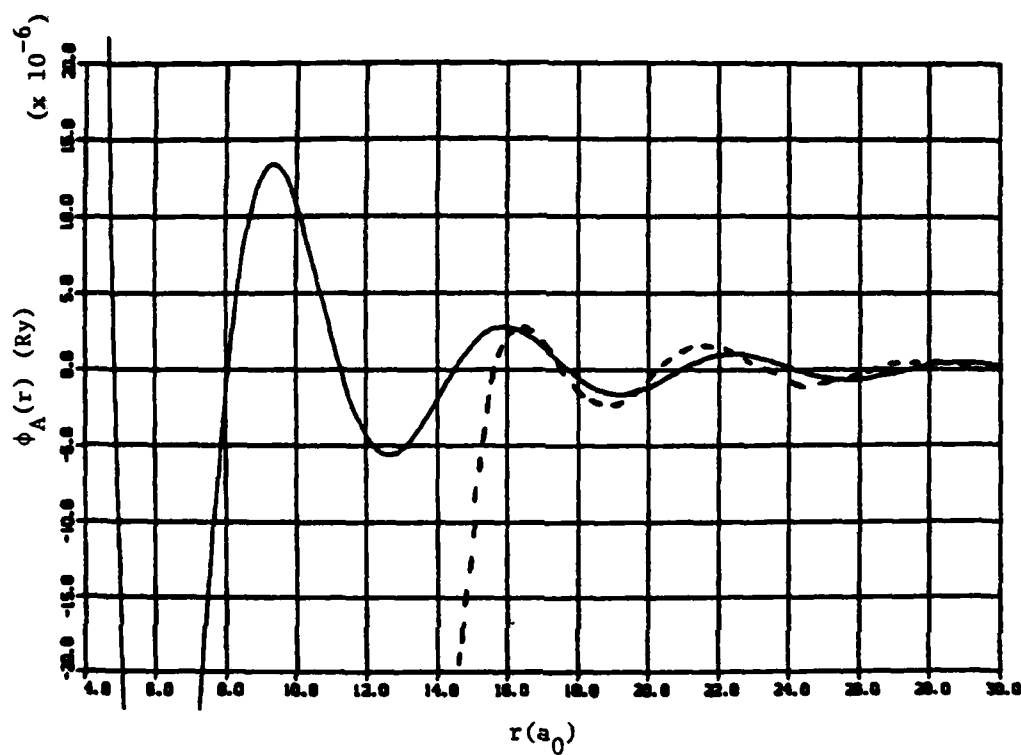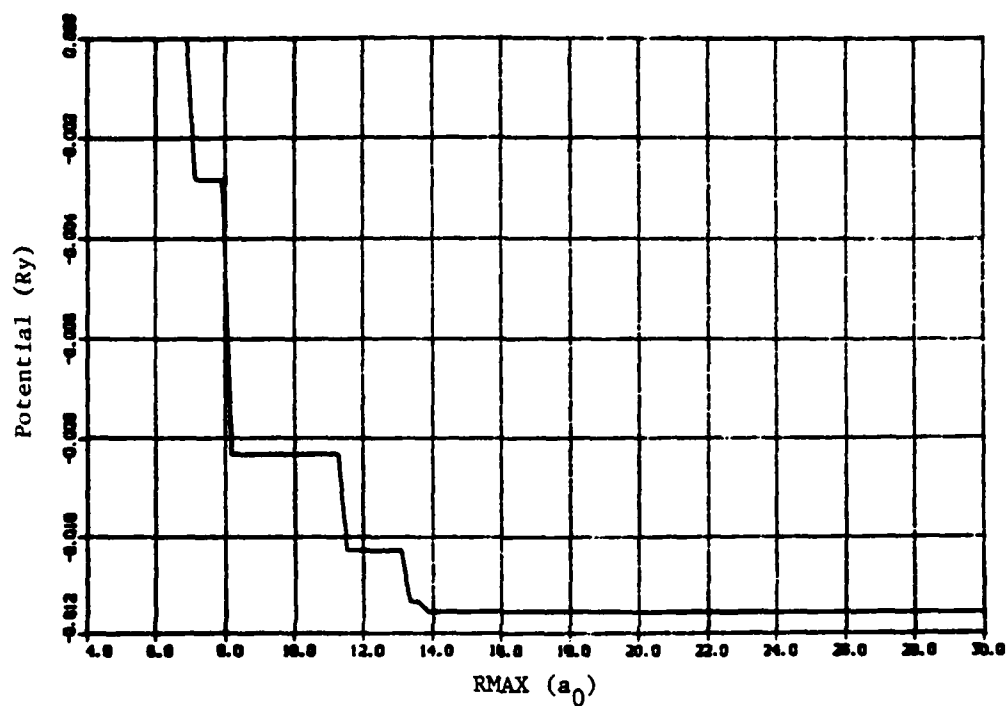
Fig. 25.
Crystal potential per particle vs the range of the potential, RMAX, for a bcc structure with volume per particle of 256 a_0^3.

value as shells of atoms in the structure are included in regions where the magnitude of the potential function is appreciable. The results shown in this figure indicate that a choice of RMAX greater than 16 a_0 is suitable because the magnitude of the potential is small and the effect of particles outside RMAX can be suitably accounted for by the continuous contribution Φ_c. There is one more point to consider before investigating the magnitude of this contribution.

As mentioned at the beginning of this discussion, RMAX must also be chosen to minimize the effect of particles moving from outside to inside the RMAX range. This is done by choosing RMAX to coincide with one of the zeros of the force function. In this way, a particle sitting at RMAX would have seen zero force whether or not the potential was cut off there.

With the above discussion in mind, we have somewhat arbitrarily chosen RMAX to be at the zero of the force function after one positive hump and one negative hump (see Fig. 10). This occurs at RMAX = 21.65 a_0 for sodium with a volume per particle of 256 a_0^3. At this RMAX we calculate the following values for Φ, Φ_c, and their ratio.

$$\Phi \qquad -1.154 \times 10^{-2}$$

$$\Phi_c \qquad 1.1 \times 10^{-5}$$

$$\Phi_c/\Phi \qquad 9.5 \times 10^{-4}$$

The continuous contribution to the potential is less than 1% of its value. Because this value is independent of the details of the molecular dynamics system structure and is much smaller than the absolute accuracy of our calculations (see discussion at the end of Sec. V), we will neglect it for this study.

Because the potential and force functions depend on the atomic volume, the appropriate value for RMAX will also vary. Figure 26 is a plot of the RMAX value appropriate for each atomic volume in our range of interest. A linear fit of the points of this plot yields

$$\text{RMAX} = 0.008063 \, \Omega_0 + 19.59 \quad . \tag{168}$$

We use this value of RMAX for our molecular dynamics calculations.

3. Determination of System Size. The system size is determined in the molecular dynamics program by specifying the number of unit cells to be stacked in a given direction. L_x, L_y, and L_z are integers that specify the number of unit cells in each Cartesian direction, respectively. If a, b, and c are the magnitudes of the lattice vectors in these directions, then the lengths of the sides of the computational box are

$$
\begin{aligned}
xL &= L_x \cdot a \quad , \\
yL &= L_y \cdot b \quad , \text{ and} \\
zL &= L_z \cdot c \quad .
\end{aligned}
\tag{169}
$$

We are constrained by the minimum image convention, discussed in Sec. II.B.3, so that each box length must be at least twice the magnitude of the range of the potential, RMAX. We mentioned in Sec. IV.B.2 the possibility of the hexagonal close-packed planes normal to the z-axis being stacked either in the ABAB$\cdots$ (for hcp) or ABCABC$\cdots$ (for fcc) arrangement. Therefore, we would like to have a multiple-of-six number of close-packed planes in the z-direction so that neither of these possibilities is prohibited by the periodic boundary conditions.

With these constraints in mind, we choose for the hcp structure

$$L_x = 7 \quad , \; L_y = 4 \quad , \; L_z = 6 \quad , \tag{170}$$
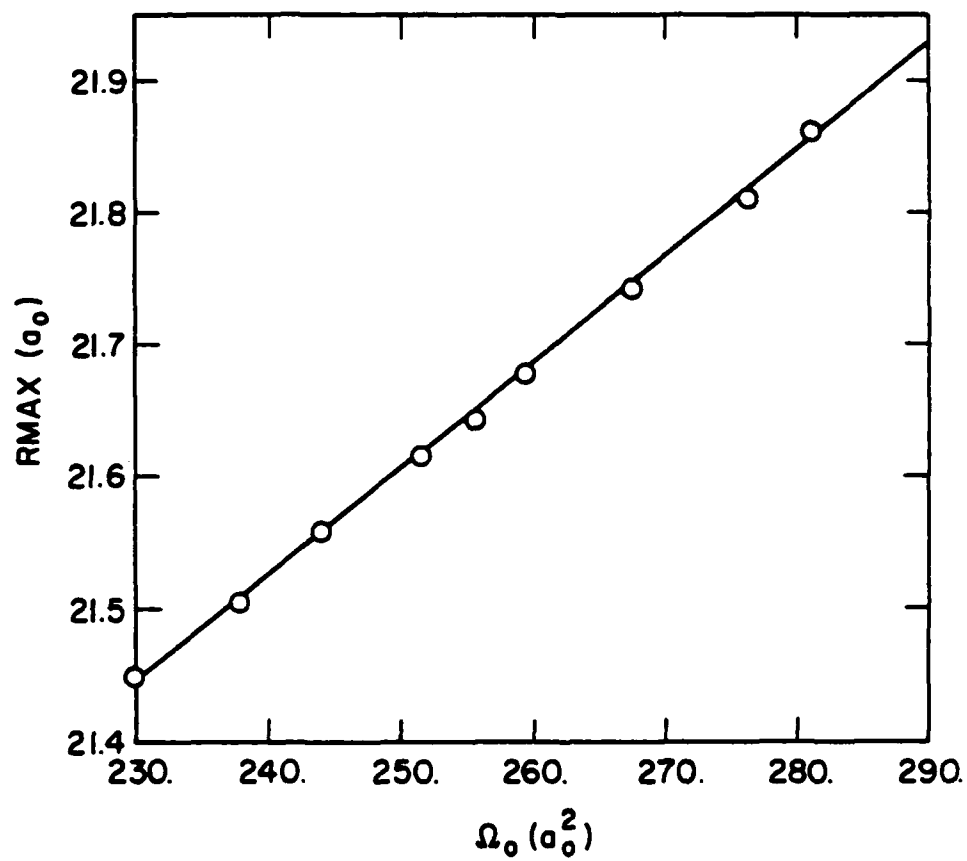
Fig. 26.
Values of RMAX plotted vs atomic volume.

and for the bcc structure (in reality a face-centered tetragonal as discussed in Sec. IV.B.3)

$$L_x = 4 \quad , \quad L_y = 7 \quad , \quad L_z = 6 \quad . \tag{171}$$

Because each of these has 4 atoms per unit cell, they contain $N = 672$ particles and have 12 close-packed planes normal to the z-axis. Figures 27 and 28 are schematics of these structures in their initial, perfect crystal configuration.

To investigate the system size dependence, we have calculated the temperature for bcc sodium for system sizes $N = 672$, 864, 1372, and 2048 at input temperatures of 50 and 300 K. The results of these calculations are shown in Fig. 29. It is obvious from these results that no definitive statement may be made regarding the N dependence other than it is small and within $\pm 1\%$ for these large systems. Therefore, we perform our calculations using the 672-particle systems described above.

D.   Example Calculations

To illustrate the molecular dynamics technique and the approach to equilibrium, we describe two calculations in detail. The calculations are of the bcc structure described in Sec. IV.B.3, performed at an atomic volume of 256 a_0^3 and with input temperatures of 50 K and 300 K, respectively.

These calculations were run for 300 cycles, which corresponds to a time of 150 time units or 1.05×10^{-12} seconds. The time histories of the system energies per particle are shown in Fig. 30. The solid lines are the total (potential plus kinetic) energy, the dashed lines are the potential energies, and the chain-dashed lines are the kinetic energies.

27a

27b

z(a_0)

z(a_0)

y(a_0)

y(a_0)
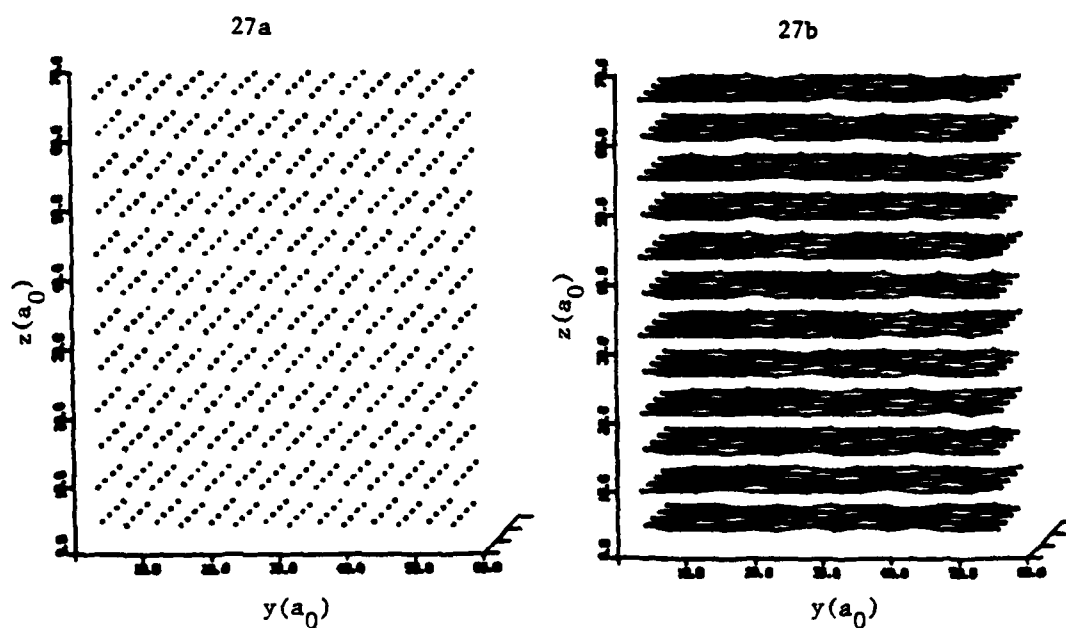
Fig. 27.
a. The body-centered cubic structure for a 672-particle system as set up by the molecular dynamics program.
b. The same structure but with nearest neighbors within a close-packed plane connected by lines.
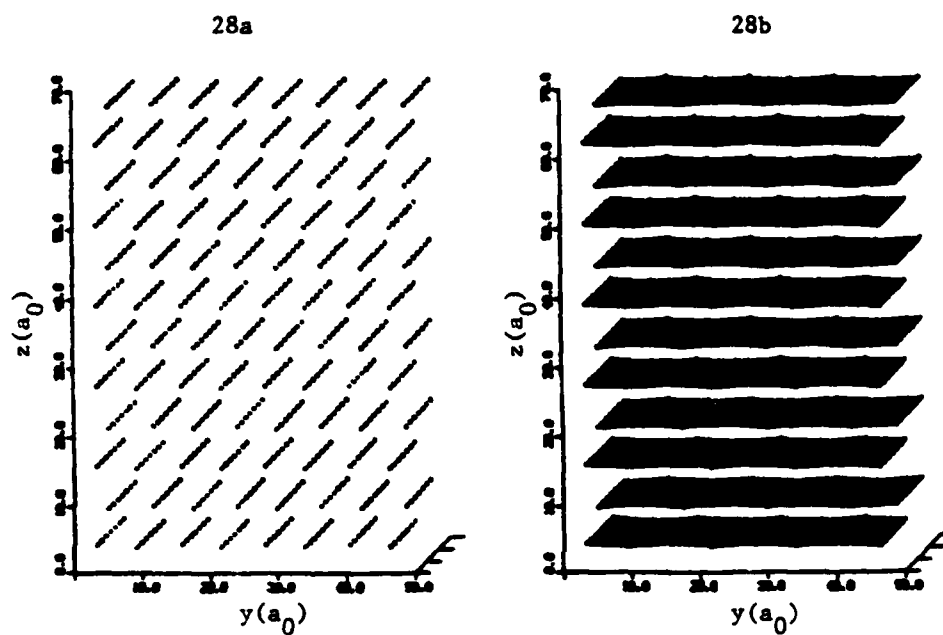
Fig. 28.
a. The hexagonal close-packed structure for a 672-particle system as set up by the molecular dynamics program.
b. The same structure but with nearest neighbors witnin a close-packed plane connected by lines.
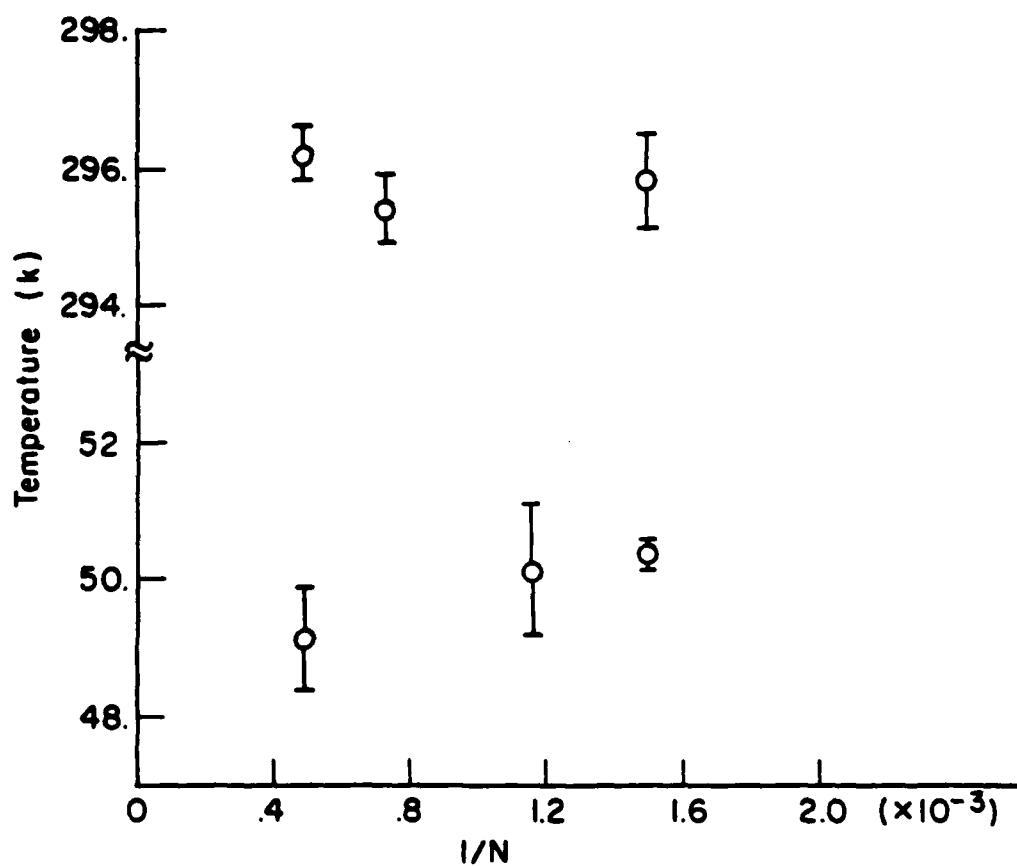
Fig. 29.
Calculated temperature vs 1/N where N is the number of particles
in the system. Values are plotted for input temperatures of
50 K and 300 K.
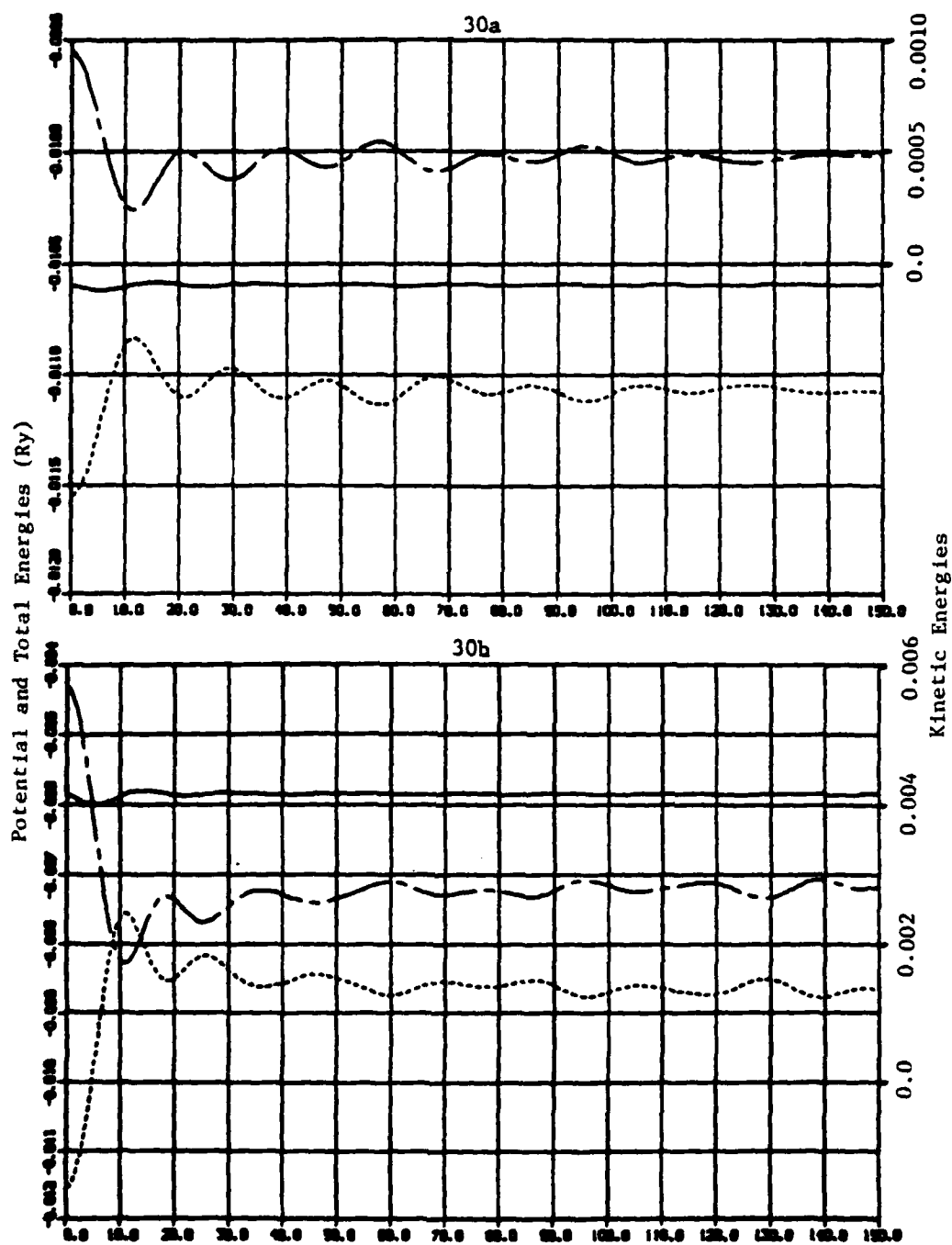
Fig. 30.
Time histories of the kinetic (chain-dashed), total (solid), and
potential (dashed) energies for a molecular dynamics calculation of
bcc sodium with atomic volume of 256 a_0^3 and input temperatures of
a) 50 K and b) 300 K.

It is obvious from these figures how the energies equilibrate from the
initial conditions where the particles are placed at perfect lattice
sites and assigned initial velocities as discussed in Sec. IV.B.1. As
the particles move from this initial, unphysical condition, part of the
energy is partitioned to potential energy and the system equilibrates
with the total energy remaining constant.

Once the system relaxes from the initial conditions and begins to
oscillate about the equilibrium values (this happens at about 45 time
units for these calculations), we begin our time average and average to
the end of the calculation.

The average of the kinetic energies yields the temperature by way
of Eq. (109). The average total energy is the structure-dependent en-
ergy of the system, E_s, which will be added to the volume-dependent
energy contributions, as discussed in Sec. V, to yield an equation-of-
state point, E_{TOT} (Ω_0, T), in volume and temperature space. Table III
gives the E_s and T values obtained from these calculations.

An indication of the thermal motion of the particles in a system
may be obtained by calculating their atomic distribution. It is given
by

$$4\pi r^2 \, d(r) \quad , \tag{172}$$

TABLE III

RESULTS OF THE EXAMPLE CALCULATIONS FOR bcc SODIUM
WITH INITIAL CONDITIONS OF 50 K and 300 K

$\Omega_0(a_0^3)$	T (K)	E_s (Ry)
256	50.17 ± 0.2	$-0.0105949 \pm 1. \times 10^{-7}$
256	293.38 ± 0.6	$-0.0058439 \pm 3. \times 10^{-7}$

where $d(r)$ is the actual particle density at a radius r from a reference particle. We calculate this distribution for each particle in the system and divide the total by the number of particles to obtain the average atomic distribution for the system. Figures 31a and 31b show the atomic distributions for the systems described above. The solid lines are the distributions at a given instant. The dashed lines are the distributions averaged over 100 time units, which indicate the perfect lattice positions about which the particles are oscillating (compare with Fig. 14). At 300 K it is difficult to distinguish the structure of the lattice.

A more qualitative indication of the thermal motion of the particles is seen from Figs. 32a and 32b which are plots of the positions of the particles at a given instant seen looking down the x-axis. In the perfect lattice position, each y,z lattice coordinate would show only one point. At 300 K there are indications that some particles may have moved out of their perfect lattice positions. We will investigate this more later when we discuss melting.

As mentioned in Sec. II.B.4, an indication of system equilibration is that the kinetic temperatures be isotropic. The kinetic temperatures are T_x, T_y, and T_z, and are calculated from the velocity distributions in the x-, y-, and z-directions, respectively [see Eq. (110)]. Figures 33a and 33b are time history plots of the system temperature (solid line) and the three kinetic temperatures for the example calculations. The temperature is seen to be isotropic within the fluctuations of the system temperature.

For a final topic regarding these two example calculations, we discuss a measure of how normal the velocity distribution is. Such a
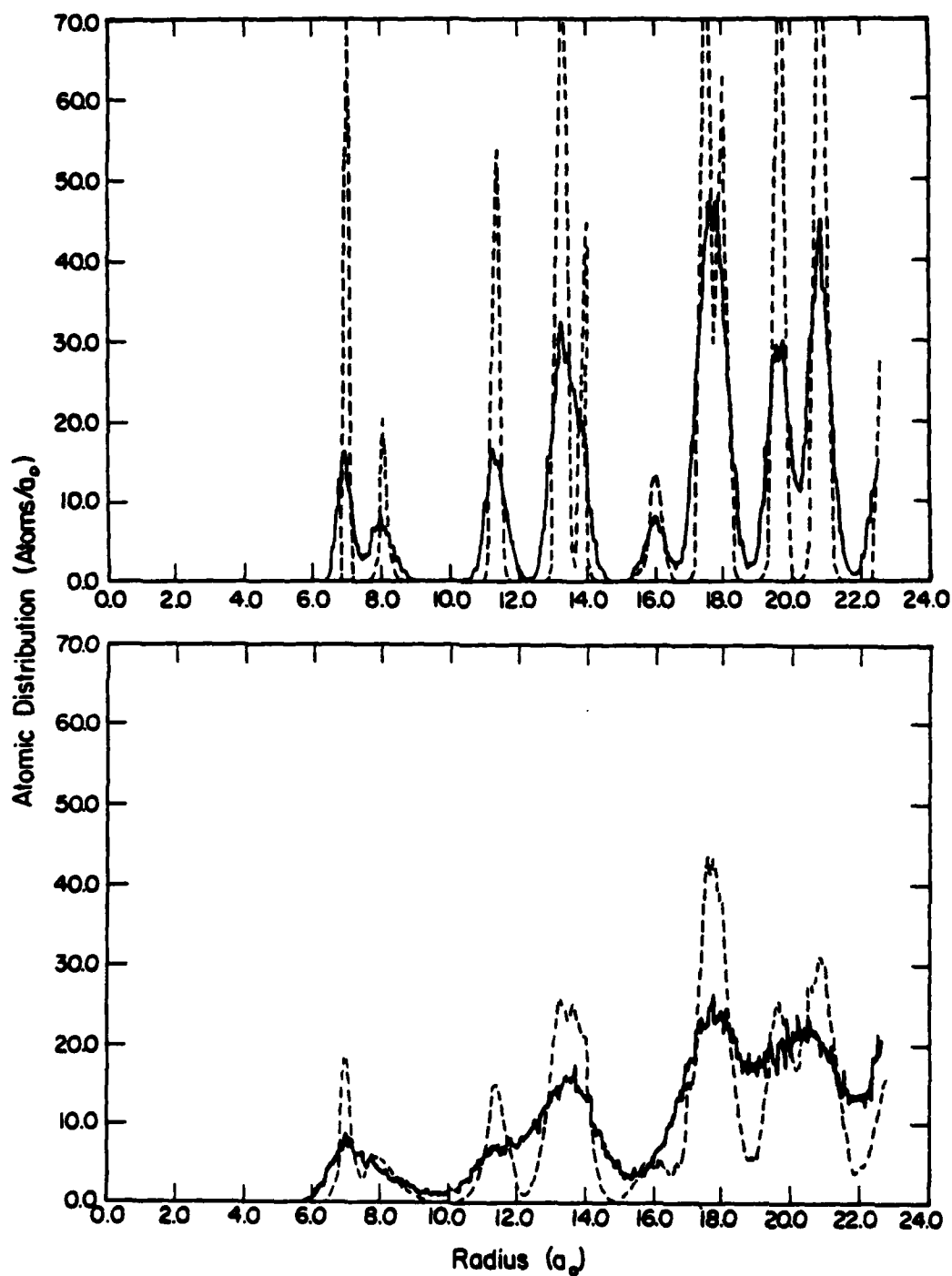
Fig. 31.
The atomic distributions for bcc sodium at an atomic volume of 256 a_0^3 and temperatures of a) 50 K and b) 300 K.

32a 32b
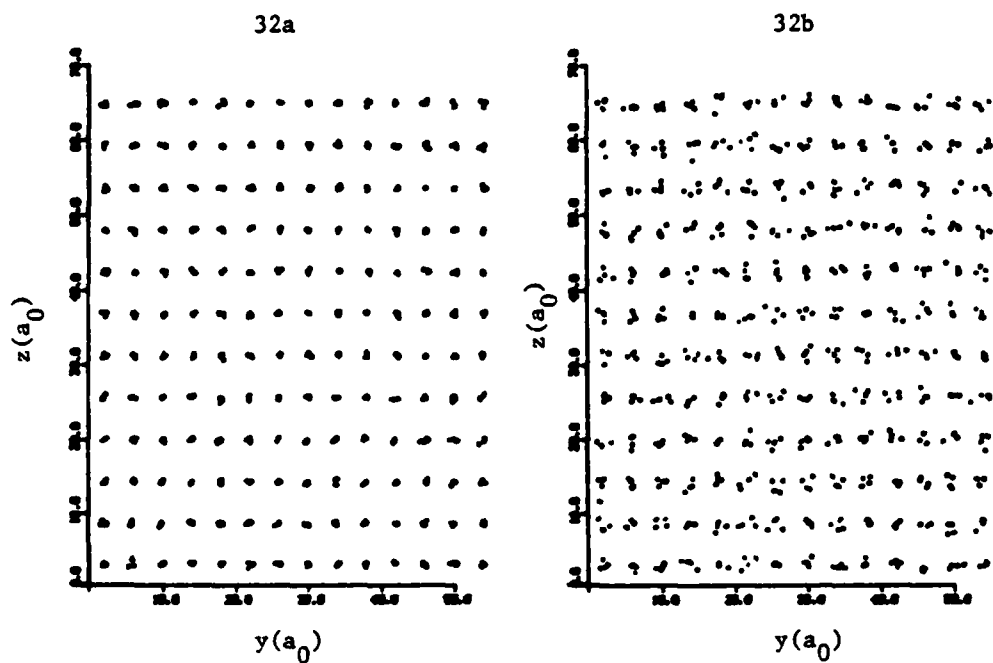
Fig. 32.
Particle positions for bcc sodium at an atomic volume of 256 a_0^3 and
temperatures of a) 50 K and b) 300 K.

33a
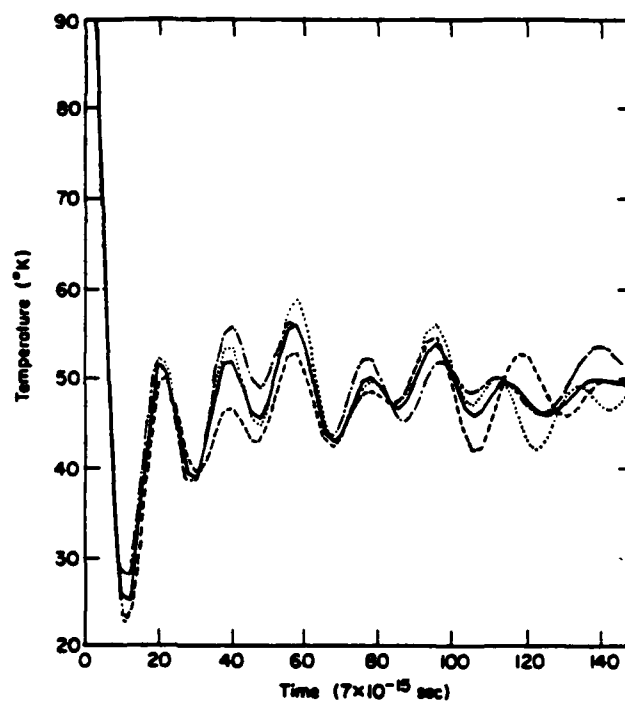
33b
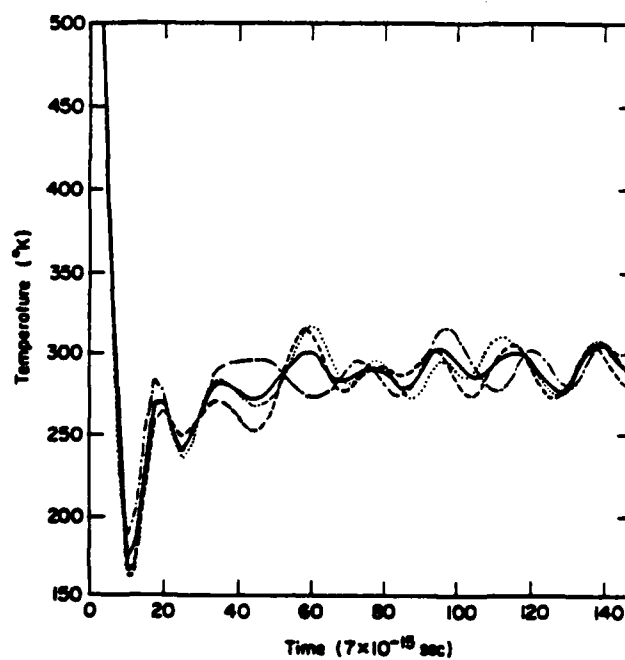
Fig. 33.
The temperature (solid line) and kinetic tempera-
tures (T_x, T_y, T_z) (dotted, chain-dotted, dashed lines)
for bcc sodium at atomic volume of 256 a_0^3 and tem-
peratures of a) 50 K and b) 300 K.

measure is the kurtosis [see discussion after Eq. (110)]. The $\underline{n}$th-order central moment of the N-particle distribution is given by

$$\mu_n = \frac{1}{N} \sum_{i=1}^{N} (x_i - \bar{x})^n \qquad (173)$$

where x_i is the value of x for the $\underline{i}$th particle and $\bar{x}$ is the mean. The kurtosis measures the "degree of peaking" of the distribution and may be defined in two different ways. The first kurtosis, denoted by β, is[19]

$$\beta = \frac{\mu_4}{\mu_2^2} . \qquad (174)$$

μ_2 is the second-order central moment and is the square of the standard deviation, $\sigma = (kT/m)^{\frac{1}{2}}$. The second definition of kurtosis we denote by C.[23]

$$C = \mu_4 - 3\mu_2^2 . \qquad (175)$$

We note that

$$\beta = 3 + \frac{C}{\sigma^4} = 3 + \frac{C}{(kT/m)^2} . \qquad (176)$$

β is equal to three for a normal distribution and this value for β is used as a standard to indicate how normal a distribution is.[19] C is zero for a normal distribution.

It is not possible to precisely predict the behavior of the kurtosis. However, we may derive an expected dependence from a simple model and then compare the calculated kurtosis with it to see if the results are consistent. As we discussed in Sec. II.B, the molecular dynamics system forms a microcanonical ensemble with the additional

constraint that the system momentum is conserved. Holian[*] has calculated the kurtosis for a microcanonical ensemble of a one-dimensional chain of hard rods. His calculation is presented in Appendix B. For large N, he predicts that the kurtosis, C, is

$$C = -\frac{6}{N}\left(\frac{kT}{m}\right)^2 \quad ,$$

so that we expect C to vary as T^2/N. Figure 34 is a time history plot of the measured kurtosis C times the factor $N/(kT/m)^2$ for the 50-K and 300-K example calculations. We see that C rapidly increases from its large, negative, initial value as the system equilibrates. The value for $CN/(kT/m)^2$ equilibrates, roughly, to between -100 and 0 for both cases.

With these numbers, we calculate β.

$$\beta = 3 + \frac{CN/(kT/m)^2}{N} = \begin{cases} 3.0 \\ 2.85 \end{cases} \quad . \tag{178}$$

The measured values of C are consistent with the results based on the simple model of Appendix B. The value for β of 2.85 (close to 3) indicates that the distribution may be adequately represented by a normal distribution.[19]

In this section we have discussed two example molecular dynamics calculations. We have found that the system we are using is adequately represented by a normal distribution of velocities and is reasonably isotropic. To determine the equation-of-state points that will become our data for studying the equation of state of sodium, we will follow

---

[*]Brad Lee Holian, Los Alamos National Laboratory.
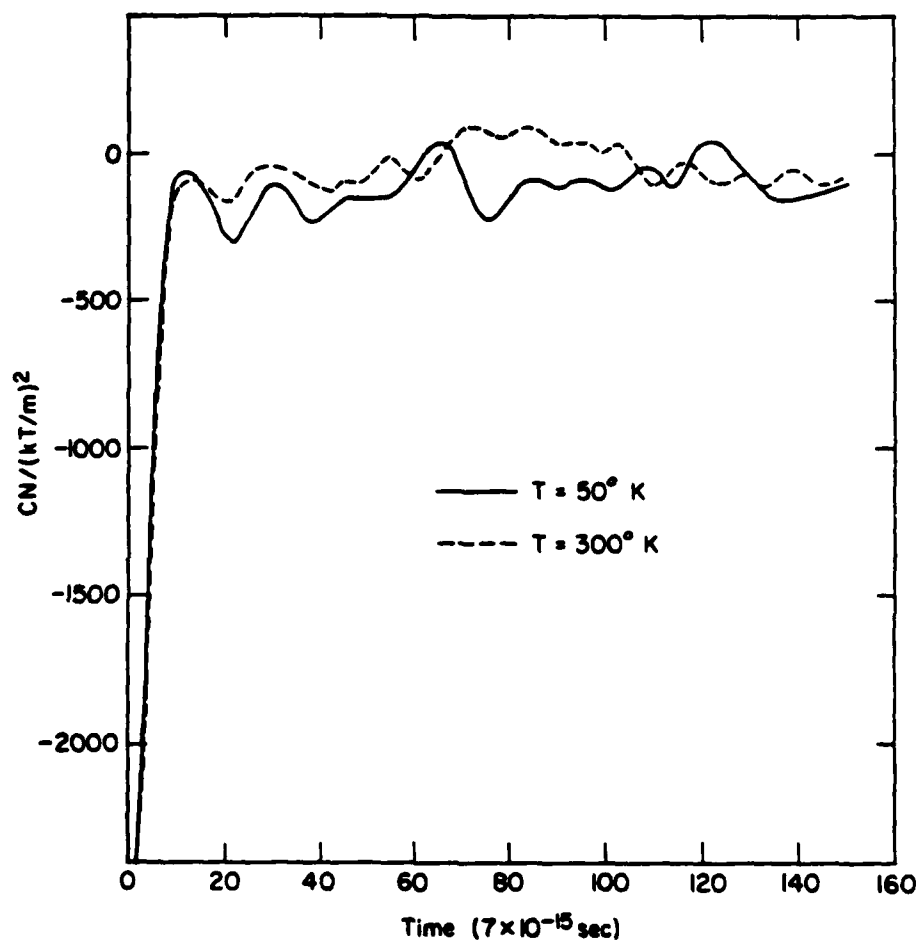
Fig. 34.
The kurtosis, C, times the factor $N/(kT/m^2)$ vs time for molecular dynamics calculations of bcc sodium at an atomic volume of 256 a_0^3 and temperatures of 50 K and 300 K.

the procedure outlined above. After allowing the system to relax from
the initial conditions, we take a time average of the calculated values
to yield an average system temperature and average structure-dependent
energy. This structure-dependent energy is added to the volume-depend-
ent terms, as described in Sec. V, to yield an equation-of-state point.

V. CALCULATION OF THE TOTAL SYSTEM ENERGY

We now determine the expression for the total system energy. In developing the effective ion-ion interaction potential of Sec. II.A, we neglected the terms that were dependent only on the volume of the system and not on the detailed ion arrangement. We will here evaluate these terms in a consistent manner so that they may be added to the energy calculated by the molecular dynamics program to yield the total system energy. We will call these terms "volume-dependent terms" (E_v) and the molecular dynamics energy the "structure-dependent terms" (E_s).

The total system energy, E_{TOT}, is given by

$$E_{TOT} = T_I + V_I + E_e = T_I + V , \tag{179}$$

where T_I is the kinetic energy of the ions, V_I is the ion-ion potential, and E_e is the total conduction electron energy. We write V_I[21] as the sum of the coulomb and exchange repulsion terms of Eqs. (75) and (76).

$$V_I = V_{ES} + V_R = \frac{1}{2} \sum_{ij}' \frac{z^2 e^2}{r_{ij}} + \frac{1}{2} \sum_{ij}' \alpha_B e^{-\gamma_B r_{ij}} . \tag{180}$$

The sums are over all ion positions, where r_{ij} is defined by

$$r_{ij} = |\vec{r}_j - \vec{r}_i| \tag{181}$$

and the factors of 1/2 in Eq. (180) take into account double counting.

To keep track of the volume-dependent terms in the total conduction electron energy, E_e, we evaluate the electron energy terms of Eq. (13) in a slightly different, but entirely equivalent manner. We rely on the local pseudopotential approximation to write [see Eqs. (34), (56), and (57)]

$$\langle \vec{k} | W | \vec{k} + \vec{q} \rangle = \frac{1}{\Omega} \int W(r) e^{-i\vec{q}\cdot\vec{r}} d^3 r = W_q = S_q w_q \quad . \tag{182}$$

We use the subscript 0 to denote $q = 0$ terms and we, therefore, write Eq. (13) for the electron energy in the $\underline{k}$th state as

$$E_k = \varepsilon_k + W_0 + {\sum_q}' W_q W_{-q} (\varepsilon_k - \varepsilon_{k+q})^{-1} \quad , \tag{183}$$

where the prime on the sum indicates that the $q = 0$ term is omitted. We have constructed the local pseudopotential, which consists of bare-ion, screening, and exchange and correlation terms given by Eq. (39) as

$$W = W_B + W_s + W_x = W_B + W_{sx} \quad , \tag{184}$$

where, by Eq. (71)

$$W_B = W_z + W_c \quad . \tag{185}$$

W_z is the coulomb part of the bare-ion potential and W_c is the core repulsion part.

To calculate the total conduction electron energy, we must sum E_k over all the occupied states and subtract off the electron-electron coulomb self-energy, E_{ee}, and the exchange and correlation energies, E_{xc}, which are double-counted in the sum $\sum_k E_k$.

The coulomb self-energy is given by Eq. (52) as

$$E_{ee} = \frac{\Omega}{2} \sum_q dq \, W_{s-q} = \frac{\Omega}{2} d_0 W_{s0} + \frac{\Omega}{2} {\sum}' dq \, W_{s-q} \quad , \tag{186}$$

where here we include the volume-dependent $q = 0$ term.

In dealing with the exchange and correlation effects, we have assumed that they may be approximated by a local one-electron potential[2] (see Sec. II.A.5). Wallace[2] discusses the approximation for exchange that depends only on the density of the conduction electrons. The total exchange energy of the conduction electrons in their ground state is assumed to be

$$\sum_k n_k \int \psi_k^*(\vec{r}) X(\vec{r}) \psi_k(\vec{r}) \, d\vec{r} \quad , \tag{187}$$

where $X(r)$ is the operator that represents exchange and correlation and is a function of the density only. He uses a variational calculation to relate the exchange potential W_x to X by

$$W_x = \frac{\partial(dX)}{\partial d} \quad , \tag{188}$$

where d is the conduction electron density. He evaluates the exchange and correlation double-counting correction[2] as

$$E_{xc} = -\Omega d_0 (X_0 - W_{x0}) + \frac{\Omega}{2} \sum_q{}' W_{x-q} \quad , \tag{189}$$

so that the total double-counting correction is

$$E_{ee} + E_{xc} = \frac{\Omega}{2} d_0 W_{s0} - \Omega d_0 (X_0 - W_{x0}) + \frac{\Omega}{2} \sum_q{}' d_q W_{sx-q} \quad . \tag{190}$$

We may now write the total conduction electron energy as

$$E_e = \sum_k n_k E_k - (E_e + E_{xc}) \quad . \tag{191}$$

The sum over the occupied states is

$$\sum_k n_k E_k = \sum_k n_k \varepsilon_k + NzW_0 + \frac{\Omega}{2}\sum_q{}' dq W_q \quad , \qquad (192)$$

where we have used the expression for the Fourier component of the density d_q of Eq. (45) and $d_0 = z/\Omega_0$. We arrive at the following expression for the total conduction electron energy:

$$E_e = \sum_k n_k \varepsilon_k + NzW_0 - \frac{\Omega}{2} d_0 W_{s0} + \Omega d_0 (X_0 - W_{x0}) + \frac{\Omega}{2}\sum_q{}' d_q (W_{-q} - W_{sx-q}) \quad . \tag{193}$$

At this point we must digress for a moment to discuss how the total adiabatic potential, $V = V_I + E_e$, is evaluated for a crystal structure. From Eqs. (179), (180), and (193), V is given by

$$V = \frac{1}{2}\sum_{ij}{}' \frac{z^2 e^2}{r_{ij}} + \frac{1}{2}\sum_{ij}{}' \alpha_B E^{-\gamma_B r_{ij}} + \sum_k n_k \varepsilon_k + NzW_0 - \frac{\Omega}{2} d_0 W_{s0}$$

$$+ \Omega d_0 (X_0 - W_{x0}) + \frac{\Omega}{2}\sum_q{}' dq(W_{-q} - W_{sx-q}) \quad . \tag{194}$$

The last term in this expression is evaluated using the relations of Sec. II.A to be

$$\frac{\Omega}{2}\sum_q{}' d_q (W_{-q} - W_{sx-q}) = N\sum_q{}' S_q S_{-q} F(q) = E_{bs} \quad . \tag{195}$$

This is the band structure energy of Eq. (30) with F(q) given by Eq. (79) so that the expression includes the screening, exchange, and correlation effects as discussed in Sec. II.A. Note that the first sum in Eq. (194) is divergent as are the W_{s0} term [see Eq. (53)] and the W_{z0}

part of W_0 [see Eq. (72)]. A standard evaluation of the first sum is to use the Ewald method[2] whereby the first sum in Eq. (194) is split into two sums, one in q space and one in real space. The divergent term in this sum cancels with the W_{s0} and W_{z0} terms[2] so that the expression for V is finite. The band structure energy is evaluated readily for a perfect crystal because the structure factors are delta functions about the reciprocal lattice vectors, Q, and

$$E_{bs} = N \sum_{Q} {}' F(Q) \quad , \tag{196}$$

which yields a finite result. Wallace[2] discussed this method in detail and used it to evaluate the total adiabatic potential for sodium and potassium.[21]

For our purpose here, however, we are calculating the terms for the adiabatic potential of Eq. (194) differently and we must ensure that we are properly accounting for all the terms. Having restructured the q-space sum for the band structure energy of Eq. (195) in terms of a real space sum of the effective interaction, $V_{IND}(r)$, over arbitrary ion positions[1,6] [see Eq. (31)], we note an obvious difficulty since the sum

$$\sum_{ij} {}' V_{IND}(r_{ij}) \tag{197}$$

is divergent because of the leading 1/r term at large r [see Eq. (139)] in $V_{IND}(r)$.

The difficulty arises because the q-space sum of Eq. (195), originating from the perturbation calculation [see Eq. (13)], explicitly

leaves out the divergent $q = 0$ term, yet we have reintroduced it by transforming to the sum in r space, which we take to infinity. To correct for this discrepancy, we allow the $q = 0$ term to be part of the q-space sum when we restructure

$$N \sum_q S_q S_{-q} F(q) \tag{198}$$

as

$$\frac{1}{2} \sum_{ij}' V_{IND}(r_{ij}) + \sum_q F(q) \quad, \tag{199}$$

where

$$V_{IND}(r) = \frac{2}{N} \sum_q F(q) e^{-i\vec{q}\cdot\vec{r}} \quad, \tag{200}$$

which are the same as Eqs. (31) and (32) with the primes missing from the q sums. E_{bs}, as defined here, does not have a finite value. Note that, with the help of Eq. (195),

$$N \sum_q S_q S_{-q} F(q) = N \sum_q' S_q S_{-q} F(q) + N S_q S_{-q} F(q)\big|_{q=0} = \frac{\Omega}{2} \sum_q d_q (W_{-q} - W_{sx-q})$$

$$= \frac{\Omega}{2} \sum_q' (W_{-q} - W_{sx-q}) + \frac{\Omega}{2} d_0 (W_0 - W_{sx0}) \quad, \tag{201}$$

so that we may write for the total adiabatic potential

$$V = \frac{1}{2}\sum_{ij}' \frac{z^2 e^2}{r_{ij}} + \frac{1}{2}\sum_{ij}' \alpha_B e^{-\gamma_B r_{ij}} + \sum_k n_k \varepsilon_k + NzW_0 - \frac{\Omega}{2} d_0 W_{s0}$$

$$+ \Omega d_0 (X_0 - W_{x0}) - \frac{\Omega}{2} d_0 (W_0 - W_{sx0}) + \frac{\Omega}{2}\sum_q d_q (W_{-q} - W_{sx-q}) \quad . \quad (202)$$

The last sum is now, in a consistent way, equal to

$$\frac{1}{2}\sum_{ij}' V_{IND}(r_{ij}) + \sum_q F(q) \quad . \tag{203}$$

The terms may be combined and arranged to yield

$$N^{-1}V = \frac{1}{2N}\sum_{ij}' \left[\frac{z^2 e^2}{r_{ij}} + \alpha_B e^{-\gamma_B r_{ij}} + V_{IND}(r_{ij}) \right] + \frac{1}{N}\sum_k n_k \varepsilon_k$$

$$+ z\left(\frac{W_0}{2} + X_0 - \frac{W_{x0}}{2}\right) + \frac{1}{N}\sum_q F(q) \quad . \tag{204}$$

This is the expression for the total system potential, which is added to the kinetic energy of the ions to yield the total system energy of Eq. (179).

$$E_{TOT} = T_I + V = T_I + V_I + E_e \quad . \tag{205}$$

The term in the square brackets of Eq. (204) is the effective ion-ion interaction, $\phi(r)$, of Eq. (77) and the $1/r$ coulomb term is canceled at large r by the leading $-1/r$ term in $V_{IND}(r)$, as discussed in Sec. III; therefore, all the terms in Eq. (204) are finite.

The ion kinetic energy is the time-averaged molecular dynamics kinetic energy, as discussed in Sec. II. The sum in the brackets of Eq. (204) is the time-averaged molecular dynamics potential energy.

The sum of the two is the total structure-dependent system energy, E_s, and is calculated by the molecular dynamics program as discussed in Sec. III.B.5. The remaining terms of Eq. (204) are the volume-dependent terms, E_v, which must be calculated separately. We will now evaluate these terms.

As in Sec. III.A.1, we find it convenient to write the volume-dependent terms as functions of r_s, the radius of the sphere whose volume is the average conduction electron volume,

$$\frac{4}{3} \pi r_s^3 = \frac{\Omega_0}{z} \quad . \tag{206}$$

We have evaluated $\frac{1}{N} \sum_k n_k \varepsilon_k$ in Sec. II.A.2 as an integral over the Fermi sphere to arrive at the average kinetic energy of the electrons times the valence

$$\frac{1}{N} \sum_k n_k \varepsilon_k = z \frac{3}{5} \varepsilon_f = z \frac{2.210}{r_s^2} \quad \text{Ry} \quad . \tag{207}$$

W_0 is given by Eq. (126), so that

$$\frac{zW_0}{2} = \frac{-z}{3} \varepsilon_f = \frac{-z(1.22772)}{r_s^2} \text{ Ry} \quad . \tag{208}$$

To evaluate $\frac{z}{2} W_{x0}$ we use Eq. (61) to write

$$\frac{z}{2} W_{x0} = \lim_{q \to 0} \frac{-4\pi e^2}{q^2} f(q) \, d_q \quad . \tag{209}$$

With Eq. (81)

$$f(q) = \frac{q^2}{2(q^2 + \xi k_f^2)} \tag{210}$$

and

$$d_0 = \frac{z}{\Omega_0} \quad , \tag{211}$$

we see that

$$\frac{zW_{x0}}{2} = \frac{-\pi z^2 e^2}{\Omega_0 \xi k_f^2} = -(0.407258) \; \frac{z}{\xi} \; \frac{1}{r_s} \; Ry \quad . \tag{212}$$

The remaining volume-dependent term is $\frac{1}{N} \sum_q F(q)$, which we convert to an integral, so that

$$\frac{1}{N} \sum_q F(q) = \frac{\Omega_0}{2\pi^2} \int_0^\infty q^2 F(q) \; dq \quad . \tag{213}$$

This integral is evaluated by numerical integration using the same procedure by which we evaluate the integral of Eq. (78), as described in Sec. III.B.5.

X_0 is the total exchange and correlation energy per electron for a uniform electron gas,[2]

$$X_0 = \epsilon_x + \epsilon_c \quad . \tag{214}$$

ϵ_x is the Hartree-Foch exchange energy and is calculated[11] to be the standard result

$$z\epsilon_x = -z \; \frac{0.916}{r_s} \; Ry \quad . \tag{215}$$

We approximate the correlation energy per electron, ε_c, using the Pines-Noziéres formula.[11] They interpolate between expressions that are valid in low-q and high-q regions in the same sense as the Hubbard interpolation formula discussed in Sec. II.A.5. The Pines-Noziéres formula yields

$$z\varepsilon_c = z(-0.115 + 0.031 \ln r_s) \quad . \tag{216}$$

All of these volume-dependent terms are evaluated separately and added to the molecular dynamics results. Values of the individual terms evaluated at an atomic volume of 256 a_0^3 are given in Table IV. Table V gives the total volume-dependent contribution to the system energy for several different volumes. This table also gives the results of the molecular dynamics calculation of the static (T = 0) potential energy per ion for bcc sodium. The sum of the two terms is given in the third column and is the total static potential of the system at the volume indicated. The values of this table are plotted in Fig. 35, where the delicate interaction between the structure- and volume-dependent terms is evident.

The volume-dependent terms are not determined absolutely beyond the second or third decimal place. However, we will be observing differences between structures at the same volume that are two or three orders of magnitude smaller. Therefore, we will calculate the values to the accuracy of Table V and recognize their validity when we have been treating the volume-dependent terms the same for each of the structures but not necessarily in an absolute sense.

We now have all the information necessary to calculate the total system energy. We will perform a molecular dynamics calculation at a

TABLE IV

CALCULATED VALUES OF THE VOLUME-DEPENDENT TERMS OF EQ. (214)
EVALUATED AT AN ATOMIC VOLUME OF 256 a_0^3, $r_s = 3.9390$

Term	Expression	Value (Ry)
$\frac{1}{N} \sum n_k \epsilon_k$	$z\left(\frac{2.210}{r_s^2}\right)$	0.14244
$z\epsilon_x$	$-z\left(\frac{0.916}{r_s}\right)$	-0.23255
$z\epsilon_c$	$-z(0.115 - 0.031 \ln r_s)$	-0.07250
$\frac{zW_0}{2}$	$-z\left(\frac{1.22772}{r_s^2}\right)$	-0.07913
$\frac{-zW_{x0}}{2}$	$+ \frac{z}{\xi}\left(\frac{0.407258}{r_s}\right)$	0.05703
$\frac{1}{N} \sum_q F(q)$	$\frac{\Omega_0}{2\pi^2} \int_0^\infty q^2 F(q) \, dq$ *	-0.27828
	Total	-0.46299

---

*After the original publication of this dissertation, a programming error was found in the subroutine which calculates this integral. Correction of this error results in a difference in the calculated volume-dependent terms, E_V, of about -0.02 Ry, causing the reported values to agree better with experiment. The new values have been included here, where necessary, or errata notes specified.

TABLE V

AT THE VOLUME INDICATED, COLUMN 2 IS THE SUM OF THE VOLUME-DEPENDENT TERMS OF EQ. (204), COLUMN 3 IS THE STATIC (T = 0) POTENTIAL PER ION FOR bcc SODIUM, AND COLUMN 4 IS THE TOTAL STATIC SYSTEM ENERGY

Ω_0 (a_0^3)	E_v (Ry)	E_s (Ry)	$E_v + E_s$ (Ry)
232	-0.466836	-0.0070983	-0.473934
240	-0.465522	-0.0087709	-0.474293
250	-0.463924	-0.0105869	-0.474511
256	-0.462989	-0.0115468	-0.474536
260	-0.462374	-0.0121400	-0.474514
270	-0.460868	-0.0134687	-0.474337
280	-0.459405	-0.0146061	-0.474011

given volume, Ω_0, and input temperature. Once the system has equilibrated, as discussed in Sec. IV.D, we will calculate the average temperature, T, potential energy per particle, and kinetic energy per particle. To the potential and kinetic energies, we will add the volume-dependent energy to obtain the total system enerty, $E_{TOT}(\Omega_0,T)$, as an equation-of-state point in volume and temperature space.

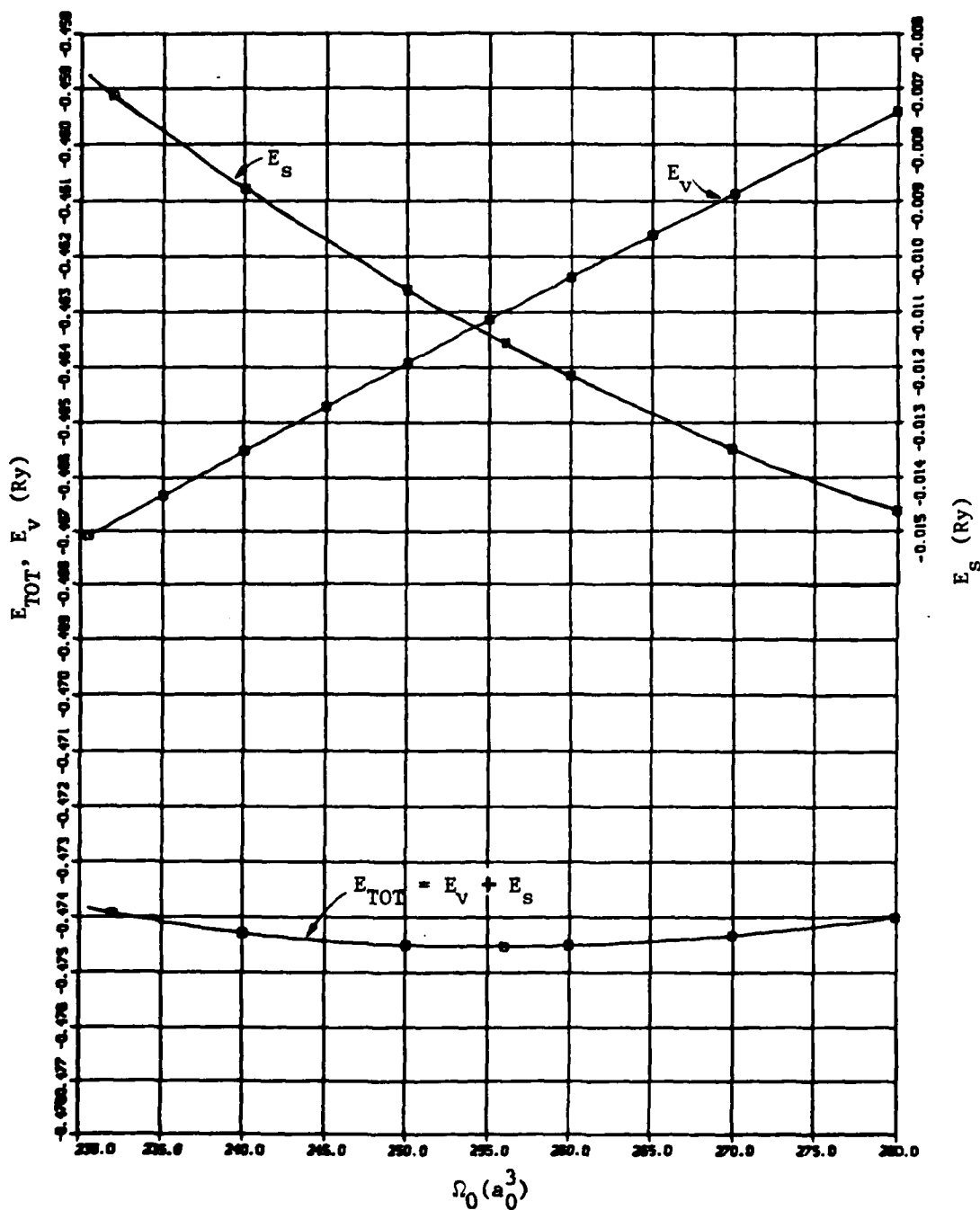Fig. 35.
The structure, E_s, and volume, E_V, terms and the total system energy, E_{TOT}, for bcc sodium at a temperature of zero Kelvin. The values for E_s have been shifted and can be read from the scale on the right.

VI. RESULTS

A. Equation-of-State Points for Solid Sodium

In this section we present the results of calculations of the total system energy, E_{TOT}, for solid sodium in the hcp and bcc phases.

1. Static Crystal Potential. We determined the static (zero temperature) system energy for sodium by calculating the crystal potential due to the ion-ion interaction potential, $\phi(r)$, using Eq. (106) and adding to it the volume-dependent terms as discussed in Sec. V. The results of this calculation for bcc sodium were presented in Table V and are plotted as the lower curve in Fig. 35. The results for both the bcc and hcp structures are plotted in Fig. 36 as a function of volume. We will call this energy the static crystal potential Φ_0.

We performed a least-squares fit to the calculated points in Fig. 36 to a cubic polynomial,

$$\Phi_0(\Omega_0) = p_1 + p_2\Omega_0 + p_3\Omega_0^2 + p_4\Omega_0^3 \quad . \tag{217}$$

The coefficients of this polynomial are given in Table VI.

TABLE VI

COEFFICIENTS OF THE CUBIC FIT OF THE CALCULATED STATIC CRYSTAL
POTENTIAL AS A FUNCTION OF ATOMIC VOLUME

Term	bcc	hcp
p_1 (Ry)	-0.310428 ± 0.011	-0.297263 ± 0.035
p_2 (Ry/a_0^3)	$(-1.676211 \pm 0.13) \times 10^{-3}$	$(-1.828394 \pm 0.42) \times 10^{-3}$
p_3 (Ry/a_0^6)	$(5.575895 \pm 0.51) \times 10^{-6}$	$(6.161591 \pm 1.6) \times 10^{-6}$
p_4 (Ry/a_0^9)	$(-5.985510 \pm 0.66) \times 10^{-9}$	$(-6.744432 \pm 2.1) \times 10^{-9}$

Φ_0 (Ry)

230.0 235.0 240.0 245.0 250.0 255.0 260.0 265.0 270.0 275.0 280.0
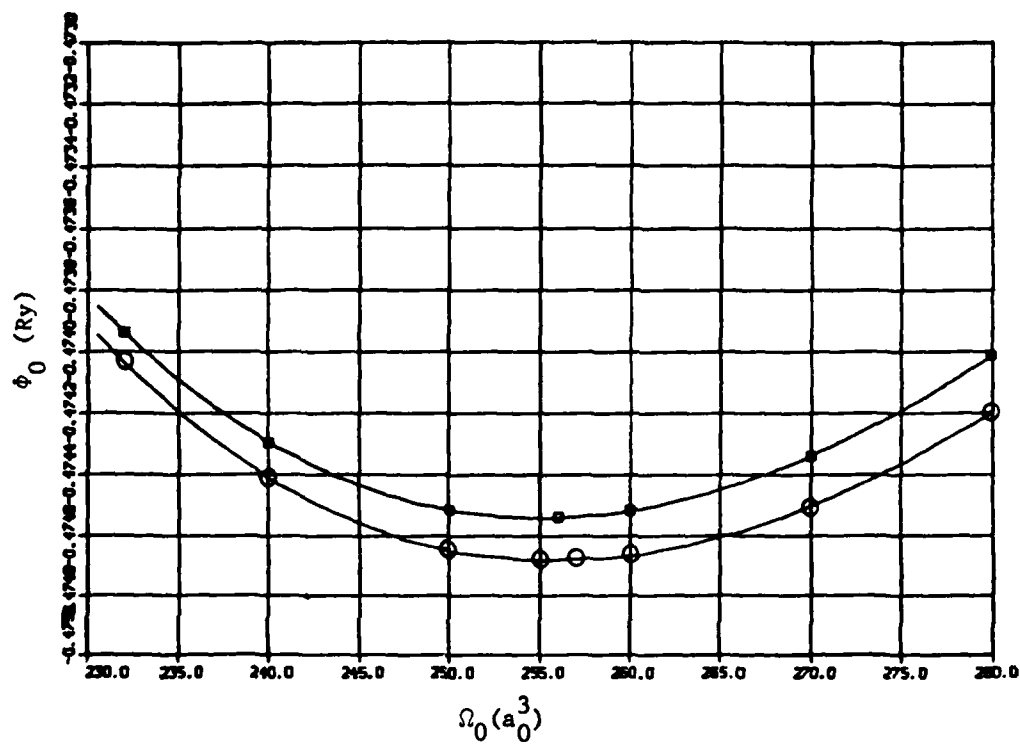
$\Omega_0(a_0^3)$

Fig. 36.

The total static crystal potential for hcp (circles) and bcc (squares) sodium.

For this classical system, at zero temperature, the Helmholtz free energy, F, is equal to the static crystal potential and we calculate the zero temperature pressure from

$$P_0 = -\left(\frac{\partial F}{\partial \Omega_0}\right)_{T=0} = -\frac{\partial \Phi_0}{\partial \Omega_0} \quad , \tag{218}$$

and the zero-temperature bulk modulus from

$$B_0 = \Omega_0\left(\frac{\partial^2 F}{\partial \Omega_0^2}\right)_{T=0} = \Omega_0 \frac{\partial^2 \Phi_0}{\partial \Omega_0^2} \quad . \tag{219}$$

We calculated the zero-temperature pressure and bulk modulus using the fits to Eq. (217). The results are plotted in Figs. 37a and b.

The measured zero-temperature and pressure static crystal bulk modulus for bcc sodium are reported by Wallace[21] as

$$\Phi_0 = -0.46 \text{ Ry} \quad ,$$

$$\Omega_0 = 255.5 \ a_0^3 \quad , \tag{220}$$

and $\qquad B_0 = 5.05 \times 10^{-4} \text{ Ry}/a_0^3 \quad .$

These are the values he used to fit the parameters α_B, β, and ρ in the pseudopotential, as discussed in Sec. III.A.2.

For bcc sodium our calculated Φ_0 is -0.475 Ry (see Fig. 36). We calculate the zero-pressure volume to be 255.1 a_0^3, which is 0.2% different from the observed value, and the bulk modulus to be 5.08 x 10^{-4} Ry/a_0^3, which is 0.5% different from the observed value.

As is apparent from Fig. 36, we calculate that the hcp structure is the stable phase for sodium at zero temperature. We calculate an energy
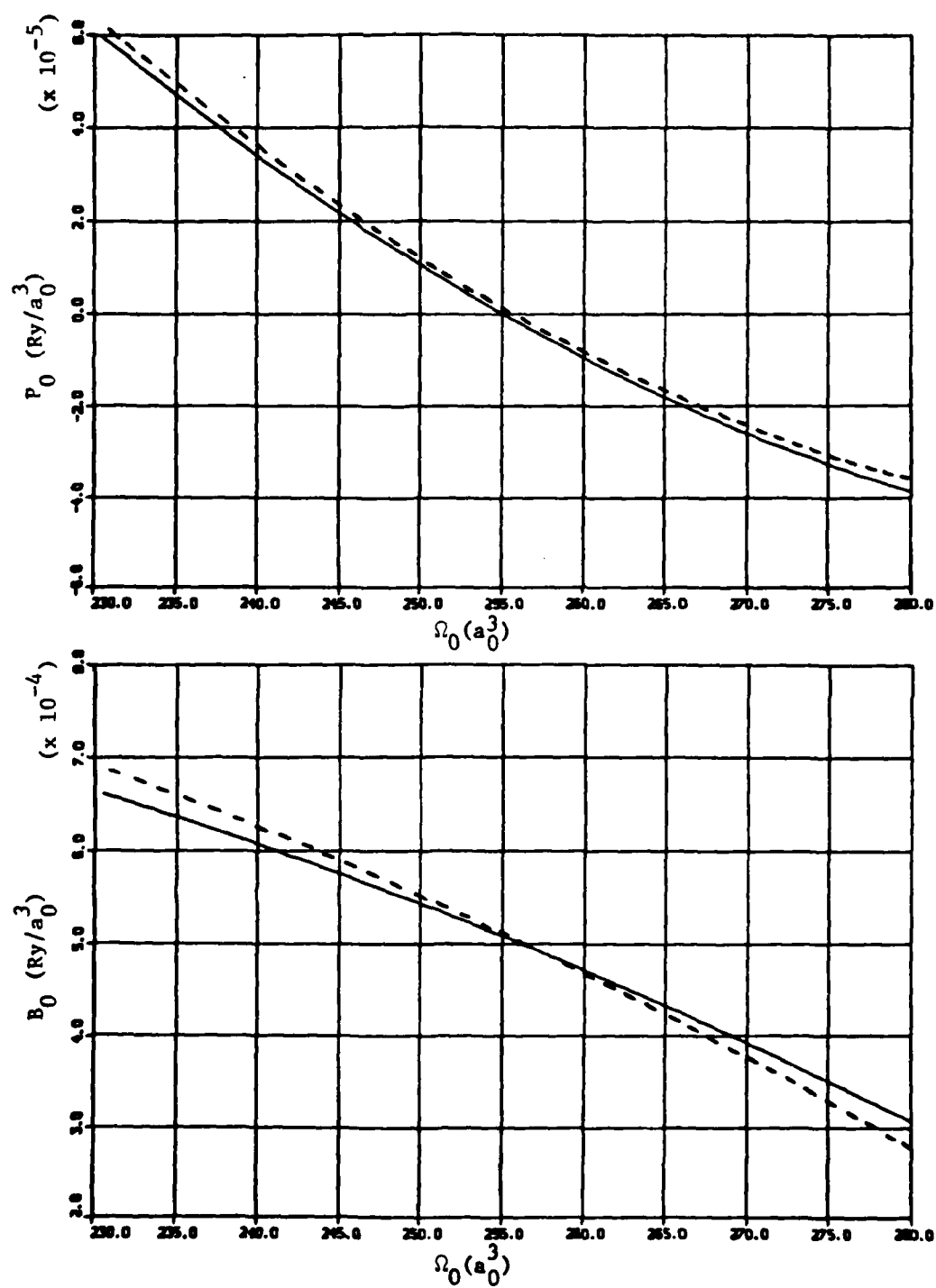
Fig. 37.
The zero temperature (a) pressure and (b) bulk modulus for the hcp
(dashed lines) and bcc (solid lines) of sodium as calculated from the
fits to Eq. (217).

difference of 14×10^{-5} Ry at an atomic volume of $256 \, a_0^3$. The experimental value reported by Straub and Wallace[24] is 3.15×10^{-5} Ry, and their calculated value is 6×10^{-5} where they have included the quantum mechanical zero-point energy of the sodium crystal structures.

With Φ_0 established, we proceed in the next section to calculate equation-of-state points at temperatures greater than zero.

2. Total System Energy. In this section we present the results of calculations of the total system energy, E_{TOT}, for bcc and hcp sodium at finite temperatures. The calculations proceed as discussed in Secs. IV and V. For each calculation the volume is predetermined as an input parameter, the temperature is calculated from the time average of the system kinetic energy, and the structure-dependent energy E_s is the time-averaged sum of the potential and kinetic energies. We add E_s to the volume-dependent term E_v to arrive at the total system energy $E_{TOT} = E = E_s + E_v$.

We know from harmonic theory that the system energy per particle must vary as

$$E = \Phi_0 + 3kT \quad , \qquad (221)$$

as T approaches zero. k is Boltzman's constant. We, therefore, write the energy as

$$E(\Omega_0, T) = \Phi_0(\Omega_0) + 3kT + f(\Omega_0, T) \quad , \qquad (222)$$

so that the function $f(\Omega_0, T)$ contains all contributions that are not harmonic. Our calculations thus become a direct measure of this function.

The results of the calculations of the total system energy at an atomic volume of $256 \, a_0^3$ are shown in Fig. 38. The solid straight lines
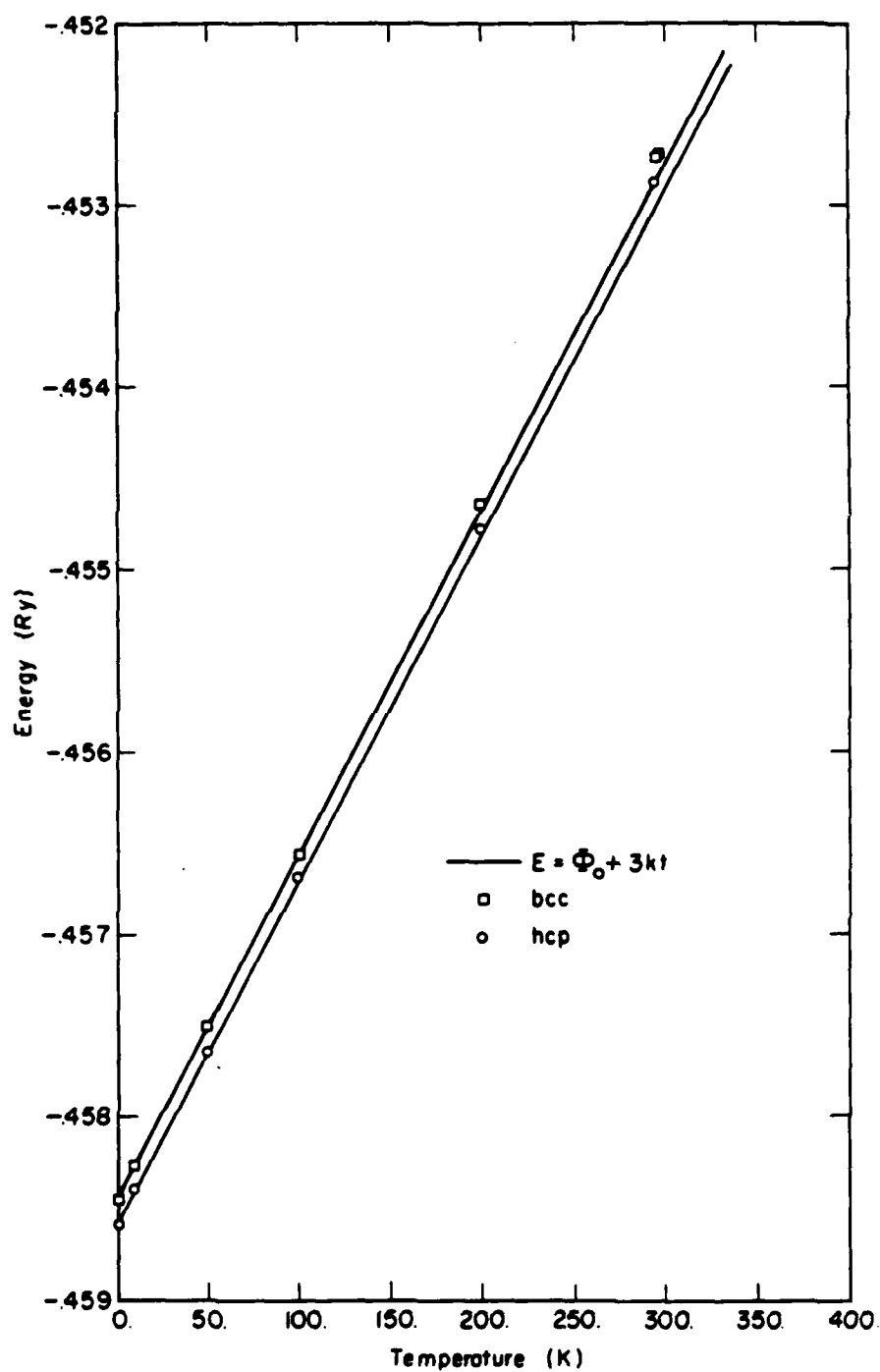
126

Fig. 38.
Total system energy vs temperature for hcp and bcc sodium
at an atomic volume of 256 a_0^3.

are drawn from Φ_0 for each structure at a slope of 3k. The error bars
on the calculations are less than the size of the circles and squares.
The deviation from harmonic behavior as temperature increases is obvious
from the figure.

We calculated the system energy $E(\Omega_0,T)$ for bcc and hcp sodium at
four different volumes--232, 250, 256, and 270 a_0^3--and at temperatures
between 0 and 400 K. The results of these calculations are tabulated in
Appendix C.

From the calculated values of $E(\Omega_0,T)$, $\Phi_0(v)$, and T, we calculate
the function

$$f(\Omega_0,T) = E(\Omega_0,T) - \Phi_0(\Omega_0) - 3kT \qquad (223)$$

directly. The results of this calculation are plotted in Fig. 39. The
error bars assigned to the values are the calculated standard deviations
of the means of the statistical time averages. The major portion of the
error in the calculated point is due to the statistical fluctuations of
the temperature.

We fit the data at each atomic volume with a T^2 form, which is all
the accuracy of the calculation justifies. The function $f(\Omega_0,T)$ then
takes the form

$$f(\Omega_0,T) = C(\Omega_0)T^2 \quad . \qquad (224)$$

The values of $C(\Omega_0)$ determined by a least-squares fitting procedure are
given in Table VII. These values may be compared with the value of the
T^2 coefficient to the free energy of sodium estimated from heat capacity
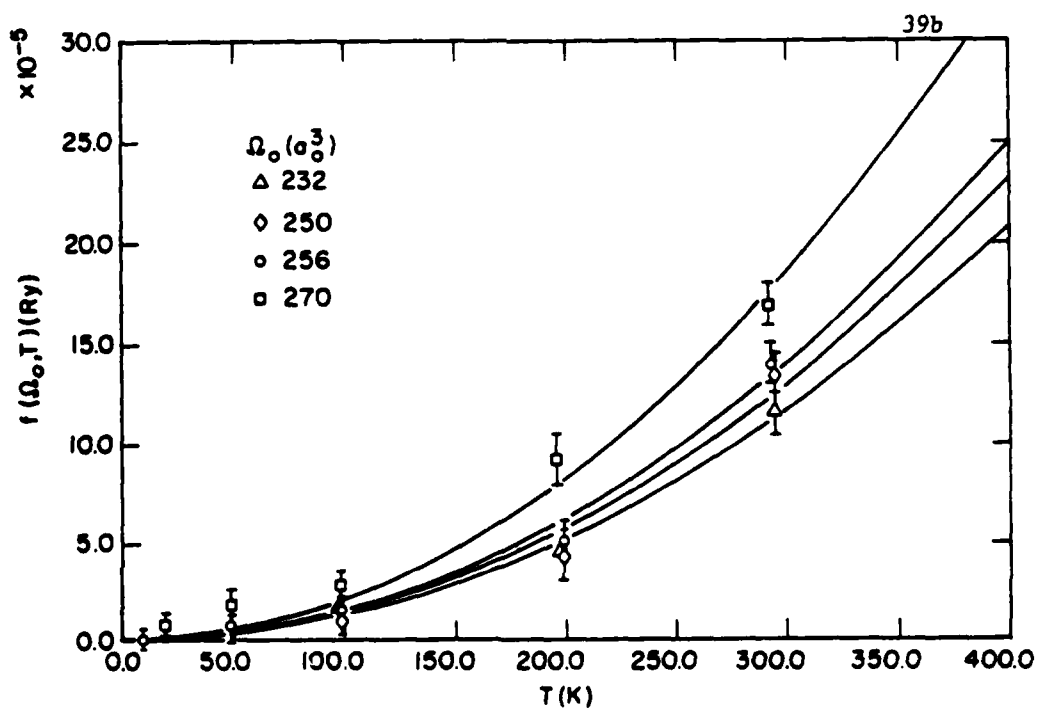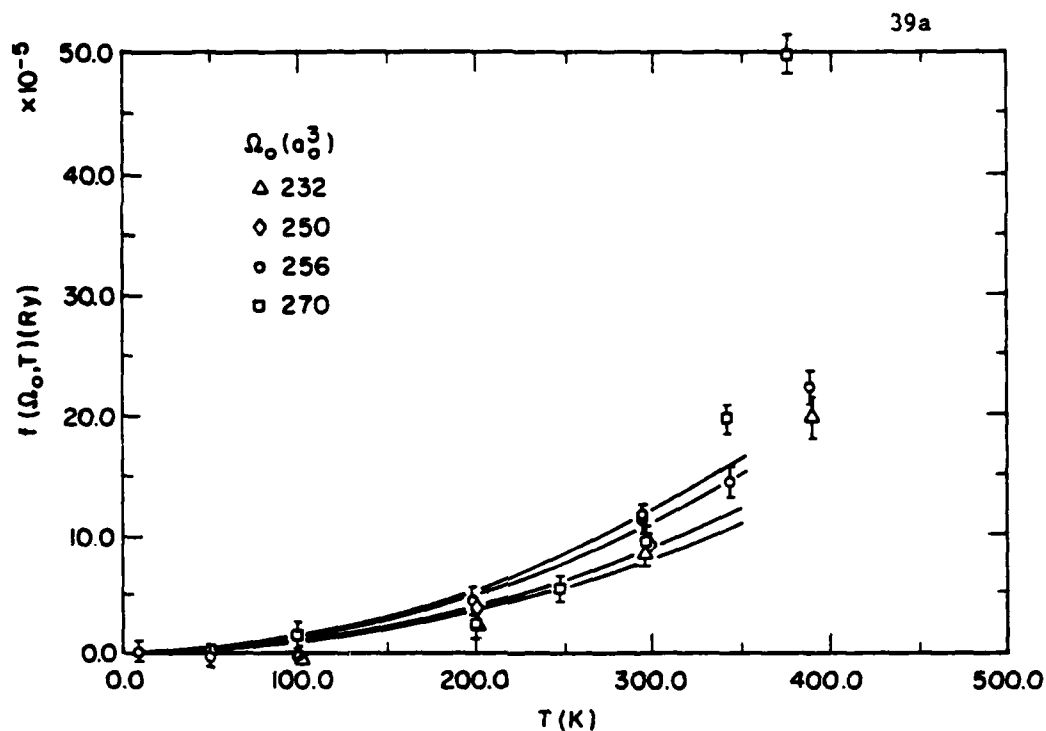measurements and reported by Wallace[2] as 8×10^{-10}.

Fig. 39.
The function $f(\Omega_0,T)$ defined by Eq. (223) plotted vs temperature
for (a) bcc and (b) hcp sodium.

TABLE VII

VALUES OF THE COEFFICIENT $C(\Omega_0)$

Ω_0 (a_0^3)	bcc $(\times 10^{-9} \ Ry/k^2)$	hcp $(\times 10^{-9} \ Ry/k^2)$
232	0.908 ± 0.64	1.301 ± 0.23
250	1.012 ± 0.52	1.475 ± 0.50
256	1.250 ± 0.10	1.563 ± 0.25
270	1.350 ± 0.51	2.057 ± 0.33

These values are plotted in Fig. 40 along with a linear least-squares fit to the data. The values for the fit

$$C(\Omega_0) = C_1 + C_2 \Omega_0 \tag{225}$$

are given in Table VIII.

The calculated values of $f(\Omega_0,T)$ for the bcc structure above 350 K in Fig. 39a were not used for the fits described above. The significant deviation of the 270 a_0^3 point indicates that something other than anharmonic effects are taking place. We checked this point and found that some particles were diffusing from their lattice sites so that partial melting had taken place. We will discuss melting in the following sections.

TABLE VIII

VALUES FOR THE COEFFICIENTS C_1 (Ry/k^2) AND C_2 $(Ry/k^2 a_0^3)$ OF EQ. (225)

	bcc	hcp
C_1	$(-1.958 \pm 3.4) \times 10^{-9}$	$(-3.247 \pm 5.7) \times 10^{-9}$
C_2	$(1.225 \pm 1.3) \times 10^{-11}$	$(1.923 \pm 2.2) \times 10^{-11}$

40a

$x \ 10^{-10}$

$C(\Omega_0) \ (Ry/k^2)$

$\Omega_0 (a_0^3)$

NBS FITTED DATA

40b

$x \ 10^{-10}$

$C(\Omega_0) \ (Ry/k^2)$

$\Omega_0 (a_0^3)$
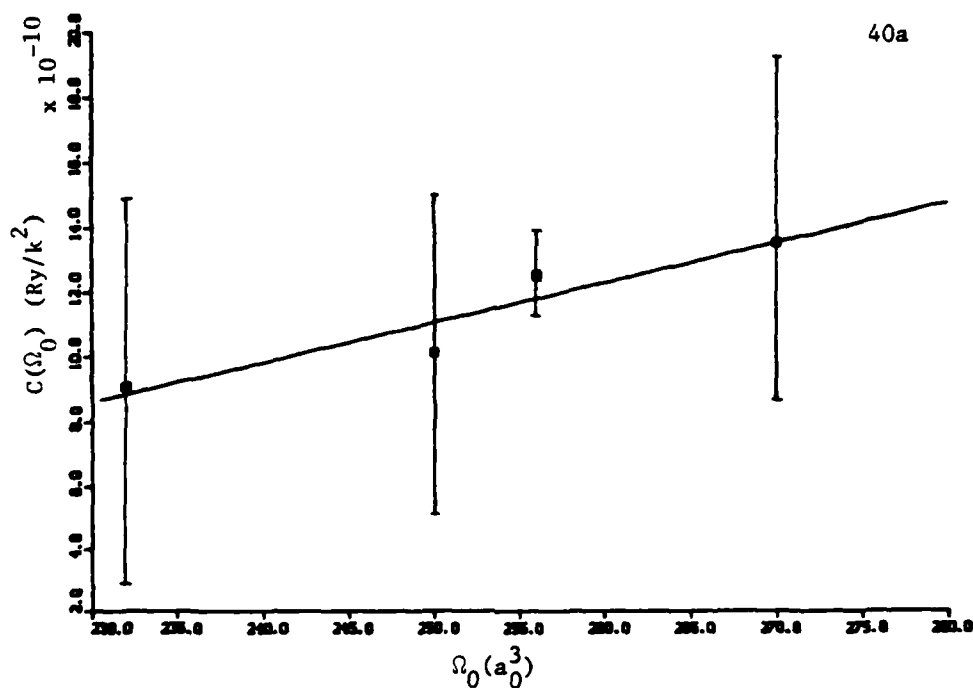
Fig. 40.
Values of $C(\Omega_0)$ vs atomic volume for (a) bcc and (b) hcp sodium.
The straight lines are linear least-squares fits to the points.

In this section we have reported the results of the calculation of the total system energy of solid sodium in the bcc and hcp structures. It is given by

$$E(\Omega_0, T) = \Phi_0(\Omega_0) + 3kT + C(\Omega_0)T^2 \quad , \tag{226}$$
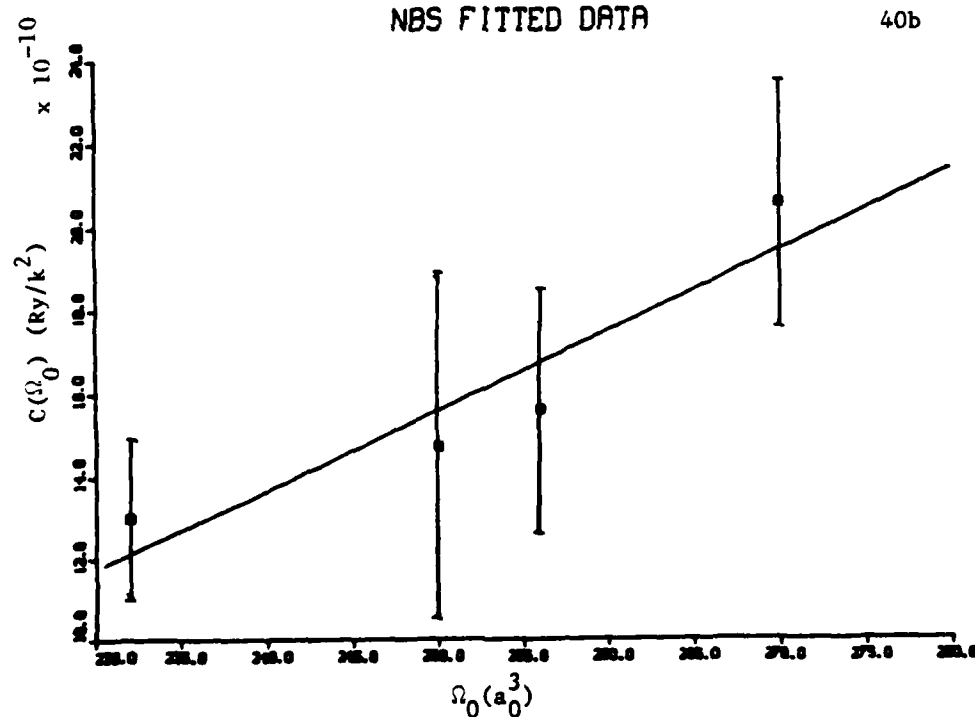
which is valid within the errors of our calculations for atomic volumes from 230 to 279 a_0^3 and temperatures from 0 to 300 K.

B. The Liquid Phase

We can cause the molecular dynamic system to melt by beginning a calculation at a temperature high enough that the particles have enough velocity to move from their crystal lattice positions and diffuse through the system. We did this for bcc sodium at an atomic volume 256 a_0^3 by choosing an input temperature of 700 K. The temperature history of this calculation is shown in Fig. 41a. If the system were harmonic the temperature would begin to oscillate about 700 K because the initial energy would be partitioned equally between the potential and kinetic energies (see discussion in Sec. IV.B.1). Due to the anharmonicity of the system, the initial temperature is about 620 K (see Fig. 41a). As diffusion occurs, the potential energy of the system is increased by particles moving out of their low-potential energy lattice positions. This occurs at the expense of the kinetic energy because the total energy in a molecular dynamics calculation is conserved. The potential, kinetic, and total energies are shown versus time in Fig. 41b. Thus the temperature of the system is lowered and the equation-of-state point moves horizontally to the left in an E,T plot, as indicated by the arrow at point 1 in Fig. 42.

We then use this calculation as a starting point to calculate equation-of-state points at other temperatures. We do this by artificially
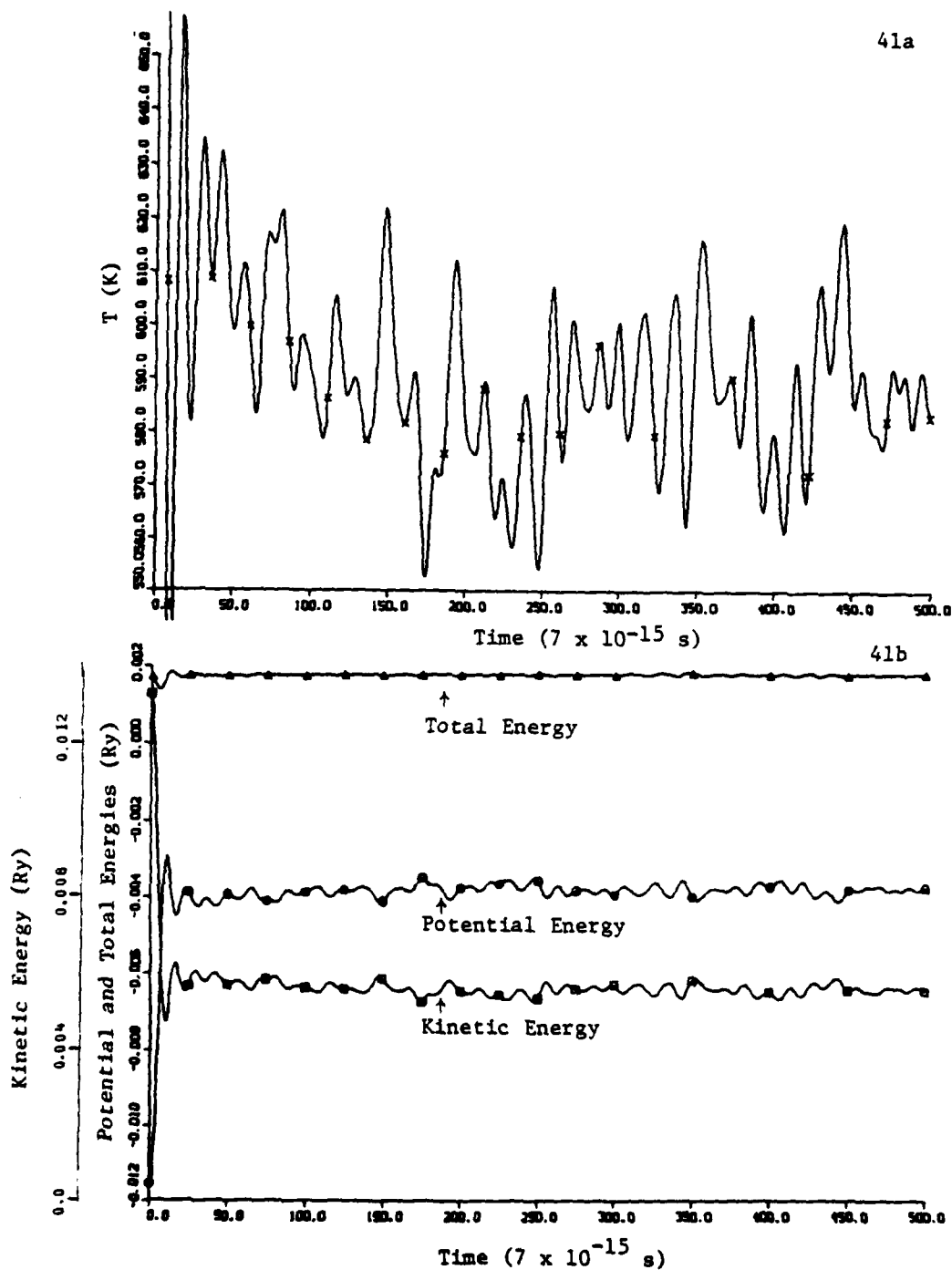
Fig. 41.
Time history of the (a) temperature and (b) potential, kinetic, and total energies for a calculation of bcc sodium at an atomic volume of 256 a_0^3 with input temperatures of 700 K.

(ERRATA: Add -0.016089 Ry to values)
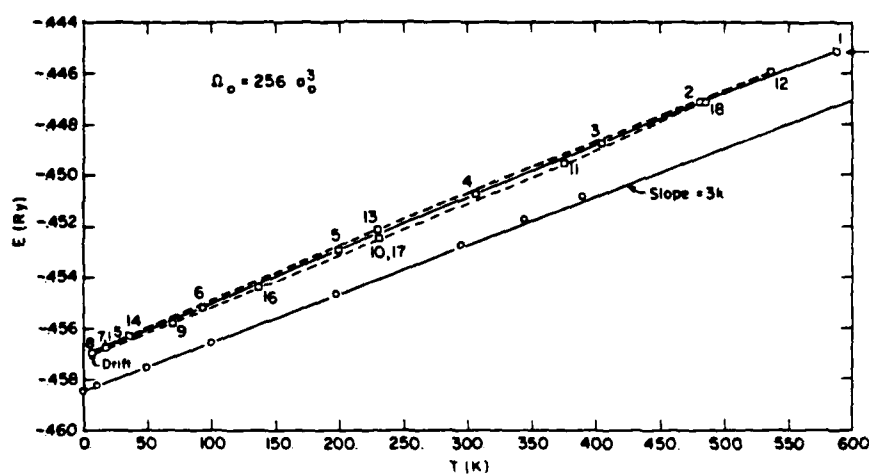
Fig. 42.
Equation-of-state points for solid and liquid sodium
at an atomic volume of 256 a_0^3. The numbers indicate
the order of the calculation as the liquid state formed
by calculation number 1 was cooled and reheated to pro-
duce the hysteresis shown.

multiplying the velocity of each particle by a factor close to 1.0 to slowly decrease or increase the temperature of the system. Then when the system has reached the temperature at which we want the equation-of-state point, we set this factor equal to 1.0 and allow the system to equilibrate and take time averages just as we did for the equation-of-state points arrived at in Sec. VI.A.

In this manner we investigated the equation of state for liquid sodium at an atomic volume of 256 a_0^3. The results are the square points shown in Fig. 42. The circles are the calculated bcc solid points which are plotted here for comparison. The calculations were performed in the order indicated by the numbers on the points. The system came down the solid curve, up the lower dashed curve, down the upper dashed curve, and back up the lower dashed curve. The hysteresis that is evident in this figure is due to the system "freezing out" available lower-energy configurations as the temperature is lowered.

The interesting point here is that the liquid phase defines its equation-of-state curve back to low temperatures where it has formed a metastable, glassy system. Within the confines of the periodic system and for the short times (in a physical sense) of a molecular dynamics calculation, this glassy state is stable enough to calculate equation-of-state points as we did for solid bcc and hcp sodium. We recognize, of course, that at low temperatures the bcc phase of sodium is also a metastable state with respect to the hcp phase.

This glassy state is most unstable at low temperatures. We allowed the system initially at 5 K to equilibrate for 1200 cycles. During this time it increased its temperature to 9 K by adjusting to a lower

potential energy configuration and moved along the line marked "DRIFT" in Fig. 42. Twelve hundred cycles is a rather long molecular dynamics calculation, but represents a very short real time (4×10^{-12} s). We will calculate the equation of state of liquid sodium by starting at a low-temperature, glassy state as the initial configuration, raising the temperature, and allowing the system to equilibrate, just as we did for the solid systems.

Because the glassy system drifts noticeably at low temperatures, we must estimate the static potential of this state. We do this by calculating the metastable equilibrium at a low, but finite, temperature (approximately 30 K). At this temperature we expect that the system is essentially harmonic in that the system energy will be equally partitioned between kinetic and potential (so that $\Delta PE = KE$ in Fig. 43). We then estimate the static potential for the glassy state as

$$\Phi_0 = PE - KE \quad . \tag{227}$$

We changed the volume of the glassy state by changing the periodic box dimensions and scaling the particle positions in the same ratio so that each particle retained the same relative position within the box. We then estimated the static potential using Eq. (227). The results are plotted in Fig. 44.

We fit the calculated points with a cubic polynomial,

$$\Phi_0(\Omega_0) = p_1 + p_2\Omega_0 + p_3\Omega_0^2 + p_4\Omega_0^3 \quad , \tag{228}$$
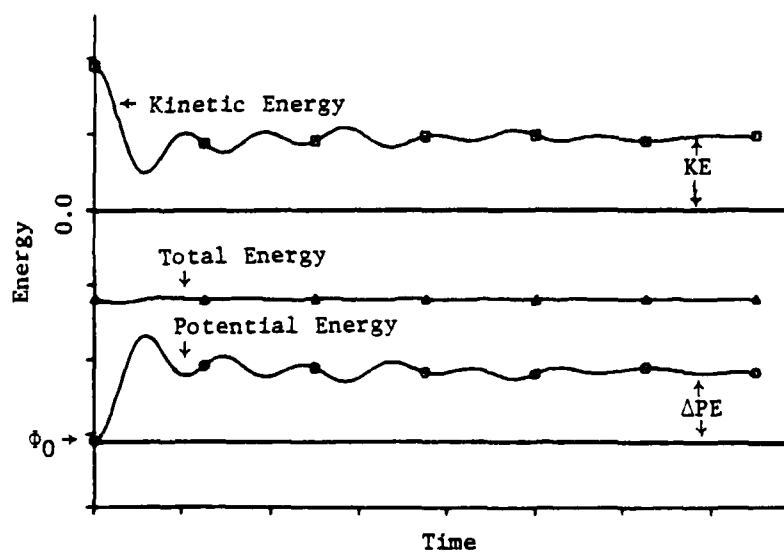
where the coefficients have the following values.

Fig. 43.
Time histories of the kinetic, potential, and total
energies of a molecular dynamics calculation. If the
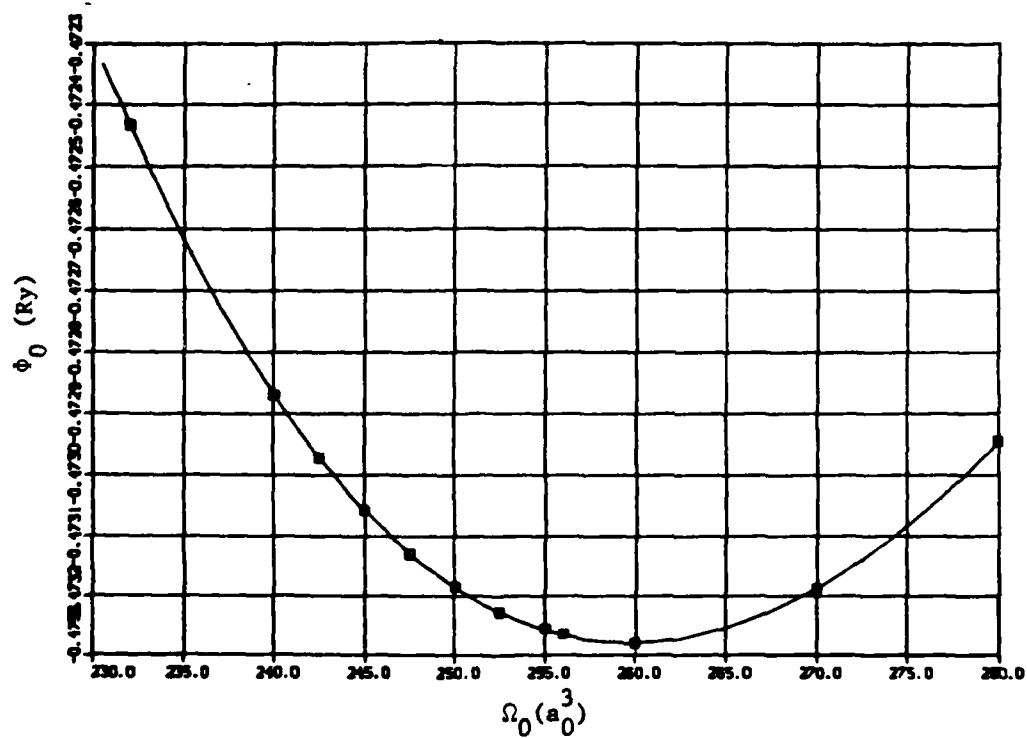system is harmonic, $\Delta PE = KE$.

Fig. 44.
The estimated static potential for the glassy state of sodium
plotted vs atomic volume.

$$P_1 = -0.304076 \pm 0.0056$$

$$P_2 = (-1.712226 \pm 0.065) \times 10^{-3}$$

$$P_3 = (5.660021 \pm 0.26) \times 10^{-6}$$

$$P_4 = (-6.067466 \pm 0.33) \times 10^{-9}$$

We calculated the finite temperature equation-of-state points for the liquid state of sodium at atomic volumes 232, 256, and 270 a_0^3. The results of these calculations are tabulated in Appendix C and plotted in Figs. 45a, b, and c, respectively. The equation-of-state points for bcc sodium at these volumes are included in these figures. The circles denote points that were calculated starting with the bcc configuration and the squares denote points that were calculated starting at the glassy state. The circled points on the liquid curve have melted from the bcc configuration.

We analyzed the equation-of-state points for the glassy state in much the same way we analyzed the solid equation-of-state points in Sec. VI.A. As before, we expect the temperature dependence of the energy to be of the form

$$E(\Omega_0, T) = \Phi_0(\Omega_0) + 3kT + f(\Omega_0, T) \quad . \tag{229}$$

However, Φ_0 is not well determined so we calculate

$$\Phi_0(\Omega_0) + f(\Omega_0, T) = E(\Omega_0, T) - 3kT \quad . \tag{230}$$

The resulting points are plotted versus temperature in Figs. 46 a, b, and c. We fit these points with a function of the form

$$\Phi_0(\Omega_0) + f(\Omega_0, T) = \Phi_0(\Omega_0) + C(\Omega_0)T^2 \quad . \tag{231}$$

with results shown in Table IX.
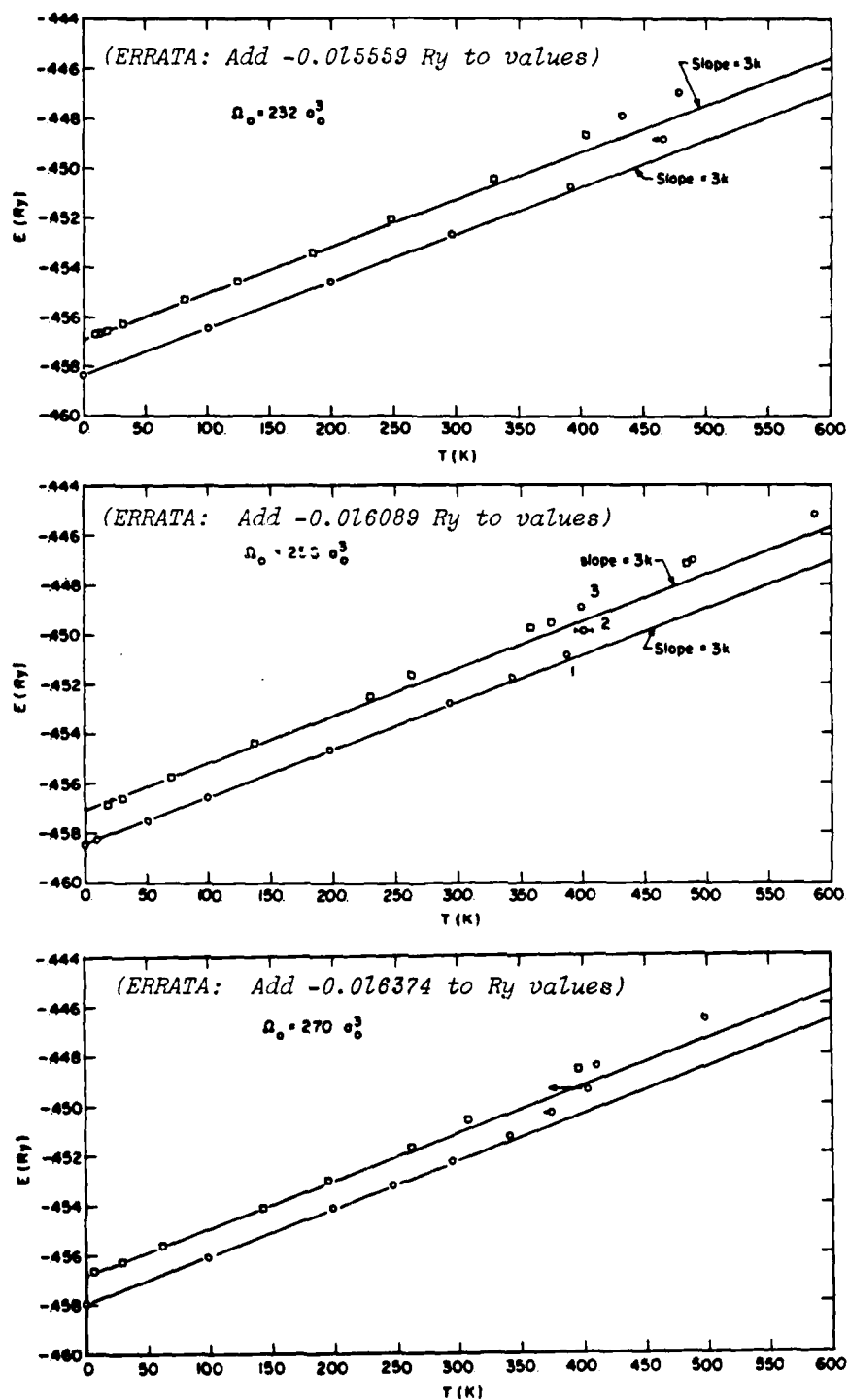
Fig. 45.
Equation-of-state points for bcc and liquid sodium. At
atomic volumes of (a) 232, (b) 256, and (c) 270 a_0^3. The
circles denote points started in the bcc configuration.
The squares denote points started in the glassy solid
configuration.

46a

(ERRATA: Add -0.015559 Ry to values)

T (K)

46b

(ERRATA: Add -0.016089 Ry to values)

T (K)
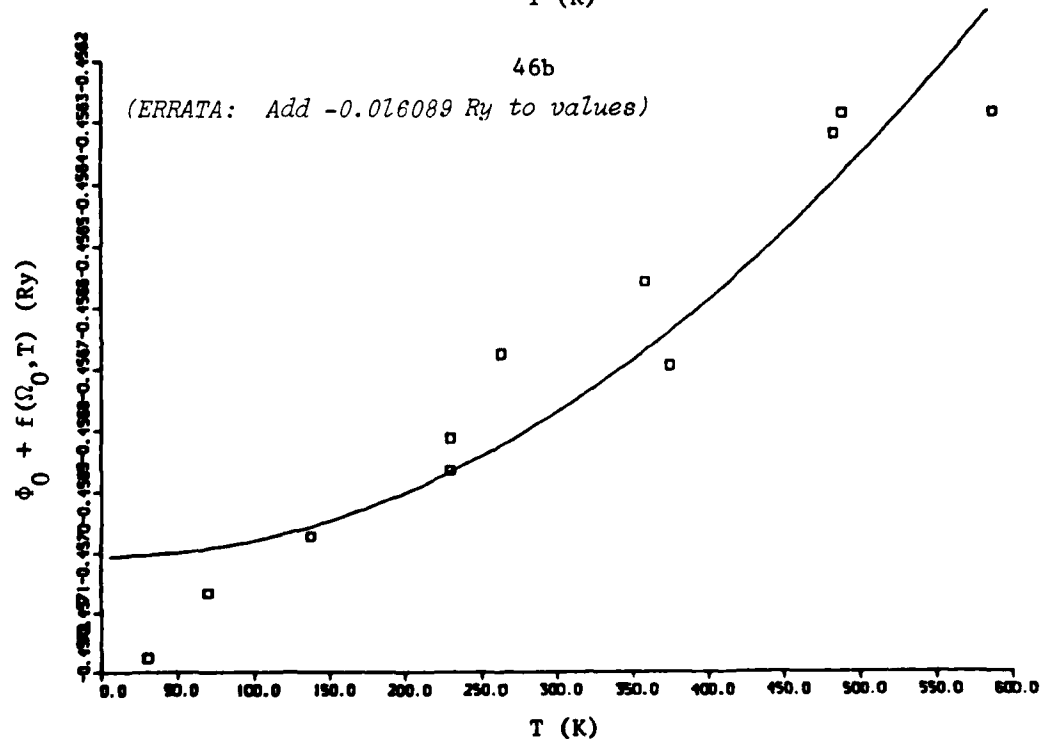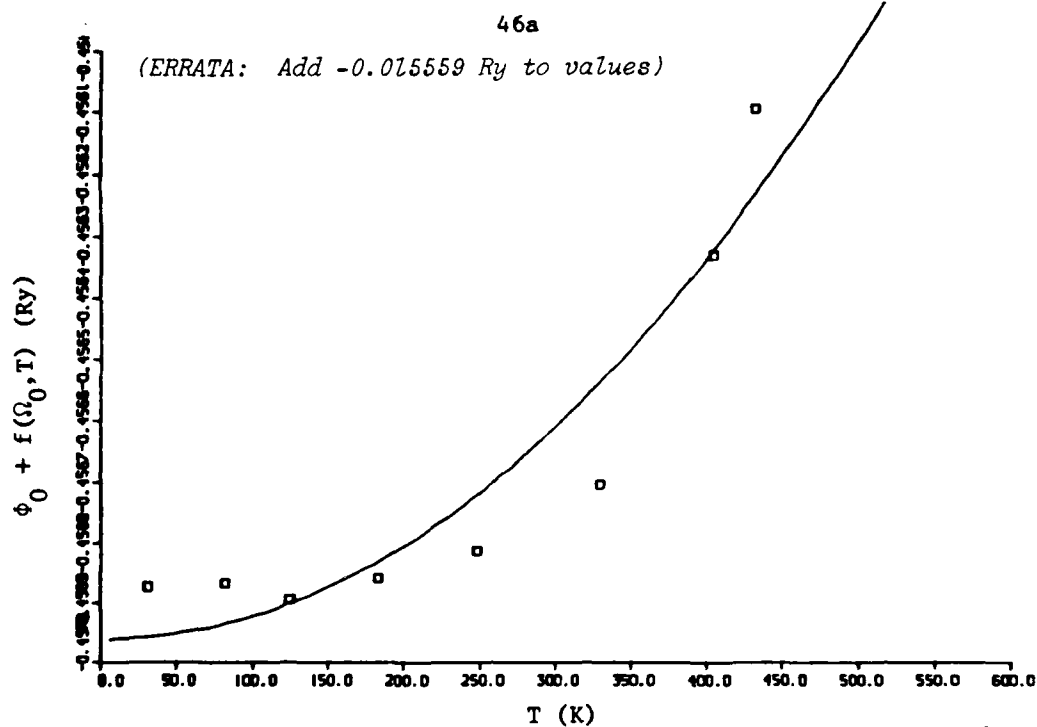
Fig. 46.

$\Phi_0 + f(\Omega_0,T)$ plotted vs temperature for the liquid state of sodium at (a) 232, (b) 256, and (c) 270 a_0^3.

46c

(ERRATA: Add -0.016374 Ry to values)
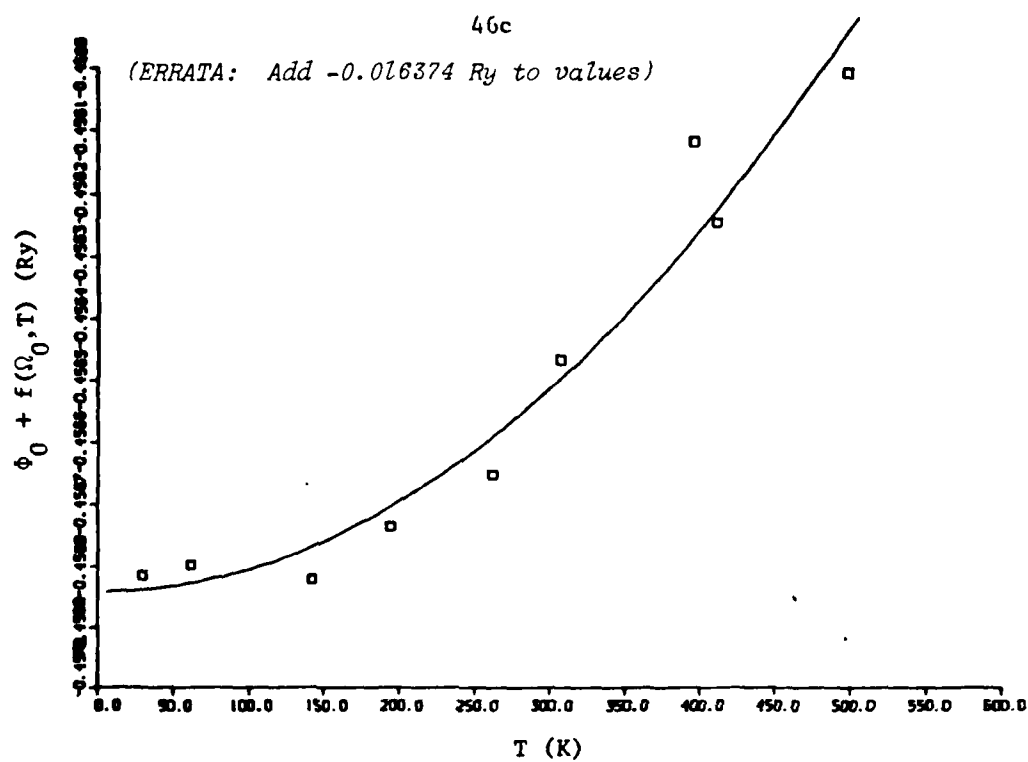
Fig. 46 (cont)

TABLE IX

COEFFICIENTS IN THE FIT TO $\phi_0(\Omega_0) + f(\Omega_0, T)$

$\Omega_0(a_0^3)$	$\phi_0(\Omega_0)$ (Ry)	$C(\Omega_0)$ (Ry/k^2)
232	$-0.472520 \pm 1.3 \times 10^{-4}$	$(3.915 \pm 1.4) \times 10^{-9}$
256	$-0.473094 \pm 1.2 \times 10^{-4}$	$(2.598 \pm 0.75) \times 10^{-9}$
270	$-0.473215 \pm 0.9 \times 10^{-4}$	$(3.630 \pm 0.72) \times 10^{-9}$

The values of $C(\Omega_0)$ in Table IX are plotted versus volume in Fig. 47. We fit these points with a straight line and arrived at

$$C(\Omega_0) = (0.657 \pm 11) \times 10^{-8} + (-0.126 \pm 4.3) \times 10^{-9}\, \Omega_0 \quad , \tag{232}$$

so that, in the same manner as for the solid bcc and hcp phases, we have specified the equation of state, $E(\Omega_0, T)$, for the glassy and liquid states of sodium over the volume and temperature ranges of our calculations.

C. Melting

We here discuss in more detail the dynamics of melting of our molecular dynamics system. We concentrate on the calculations performed at an atomic volume of 256 a_0^3 shown in Fig. 45b.

We may investigate whether or not a particular calculation has melted in four different ways.

First, as we have already mentioned, we notice which curve in E,T space it lies--the solid or the liquid curve. The point labeled 1 in Fig. 45b appears to be on the solid curve, 3 is on the liquid curve, and 2 is somewhere in between.

Second, we may evaluate the atomic distribution of particles as discussed in Sec. IV.D. The atomic distributions for points 1, 2, and 3 at

Fig. 47.
Values of the coefficient $C(\Omega_0)$ for the liquid state of sodium
plotted vs atomic volume.

one time are plotted as the solid lines in Figs. 48a, b, and c, respectively. From these plots no definitive statement may be made about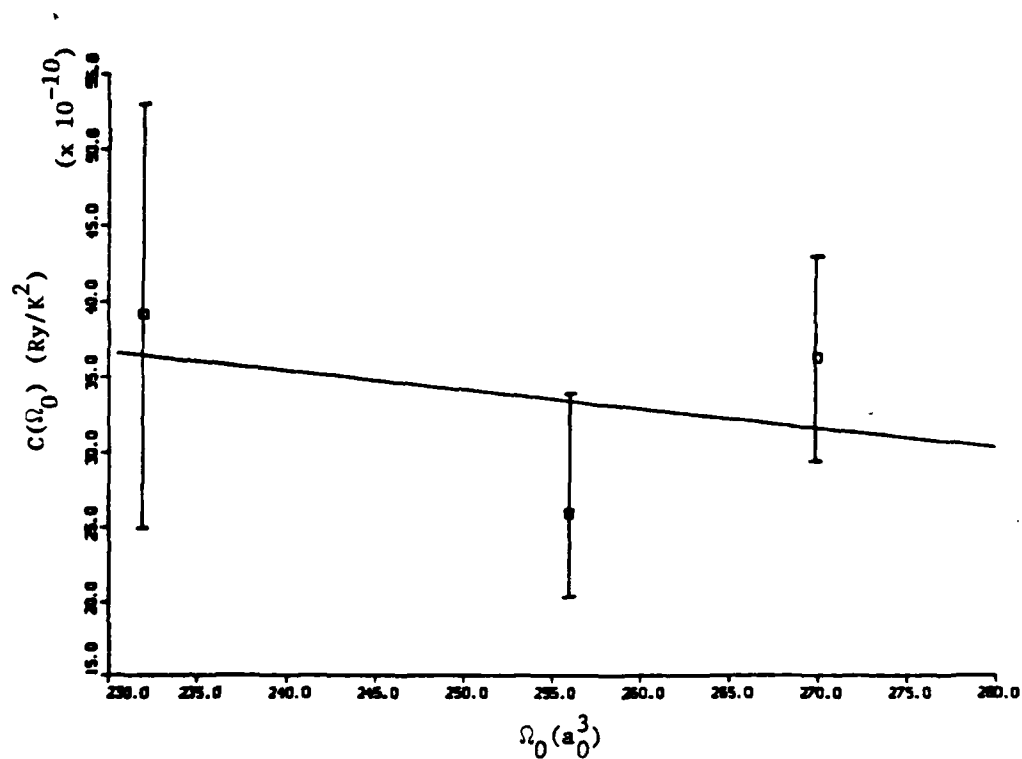 the state of the system. However, if the particle positions are averaged over time for point 1, as shown by the dashed curve in Fig. 48a, the crystal shell peaks are seen to appear, indicating that the particles are still oscillating about their lattice positions. When the same averaging is performed for point 3, the character of the distribution does not change. The same averaging for point 2 shows less peaking than 1 but more than 3. Therefore, we have another definitive difference between the liquid and solid equation-of-state points.

Thirdly, we may investigate the average distance that a particle is from its starting lattice position. We do this by calculating the mean-square displacement, $\overline{\Delta r^2}$, defined as

$$\overline{\Delta r^2} = <(r - r_0)^2> \quad , \tag{233}$$

where r_0 is the initial position of the particle and r is the current position. We then plot $\overline{\Delta r^2}$ versus time. This was done for calculations of points 1, 2, and 3 in Fig. 45b, with the results shown in Fig. 49. The mean-square displacement for point 1 has settled down to a constant value so that the average displacement of a particle from its original position remains constant. The calculated value for point 3, however, shows a reasonably constant slope, indicating that atomic diffusion is indeed occurring with particles moving away from their original lattice sites. The mean-square displacement for point 2 shows behavior in between these two extremes, indicating that partial melting is occurring.

Finally, we may look at plots of the positions of the particles in space. To help keep track of particles, we have chosen to connect nearest neighbor particles within each close-packed plane by lines.
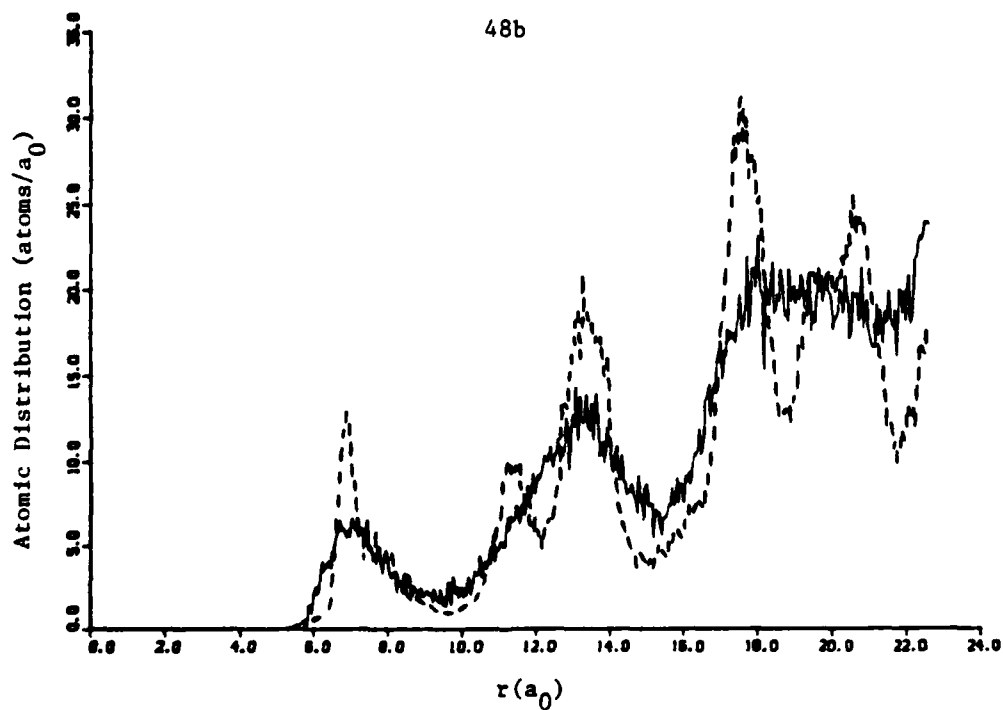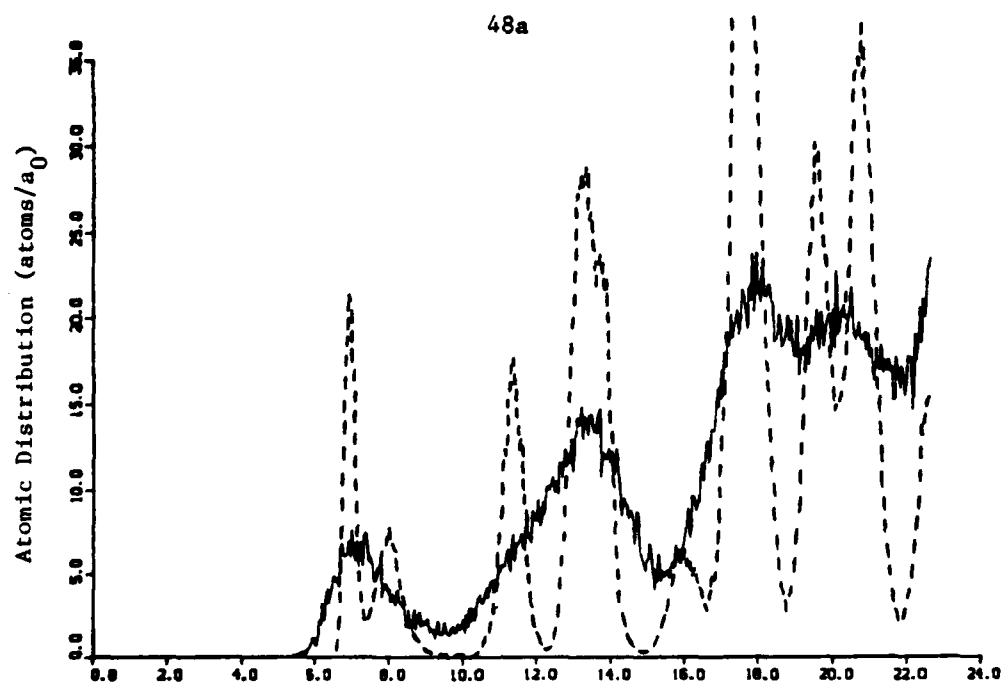
Fig. 48.
The solid lines are the atomic distributions at one instant and the dashed lines are the distributions of the particle positions averaged over 200 cycles for points (a) 1, (b) 2, and (c) 3 of Fig. 45b.

48c
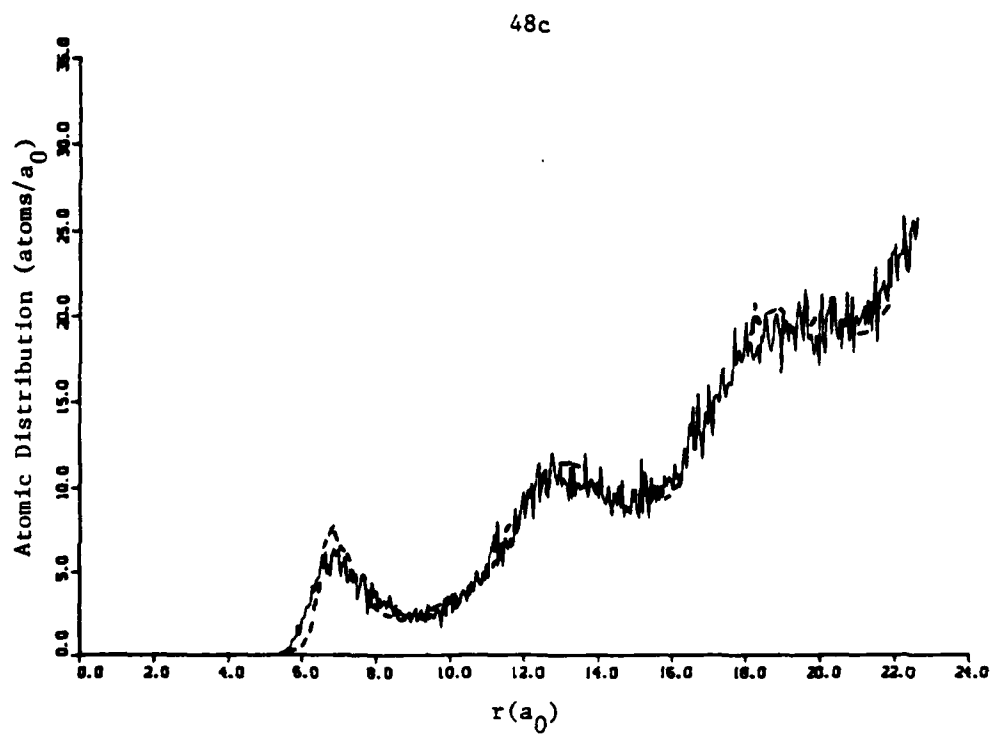
Fig. 48. (cont)
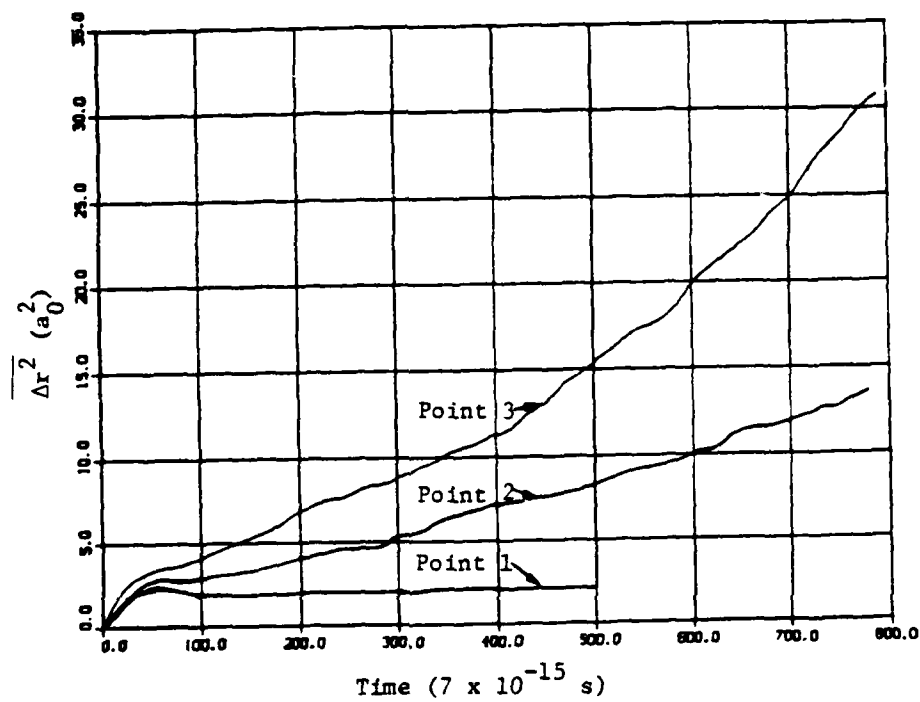
Fig. 49.
The mean square displacements vs time for the calculations
which produced points 1, 2, and 3 of Fig. 45b.

The initial configurations with these lines drawn have already been shown in Figs. 27 and 28. When a particle gets more than 8.0 a_0 from its near neighbor, the lines are no longer drawn. Figures 50a, b, and c show these plots for points 1, 2, and 3 of Fig. 45b. It is obvious that, for the most part, the particles of the calculation of point 1 maintain their positions within the crystal structure, while point 3 particles are diffusing through the system. For point 2 there seem to be regions where diffusion is occurring and regions where it is not.

From the four techniques mentioned above, we can state that point 3 has melted and point 1 has not. Point 2 is in some intermediate state. As the error bars on this point in Fig. 45b indicate, it did not reach a definite equilibrium state after a rather long molecular dynamics calculation. The time history of the temperature of this calculation is shown in Fig. 51. We notice here a long wavelength oscillation of the average temperature is present, as indicated by the dashed line. This calculation has not reached equilibrium. Point 3, however, has reached equilibrium on the liquid curve at about 400 K and we should be able to identify this as an upper limit to the melting temperature of sodium. We may make no such statement about a lower limit because point 1 may be metastable in the solid phase.

We investigated the melting of sodium at atomic volumes of 232 a_0^3 and 270 a_0^3 in the same manner as was done for the 256 a_0^3 calculations described above. The calculated points marked with arrows in Figs. 45a and c indicate calculations for which the diffusion and thus the decrease in temperature was proceeding too slowly to warrant allowing the calculations to proceed to equilibrium. From the calculated points we may,

50a

50b
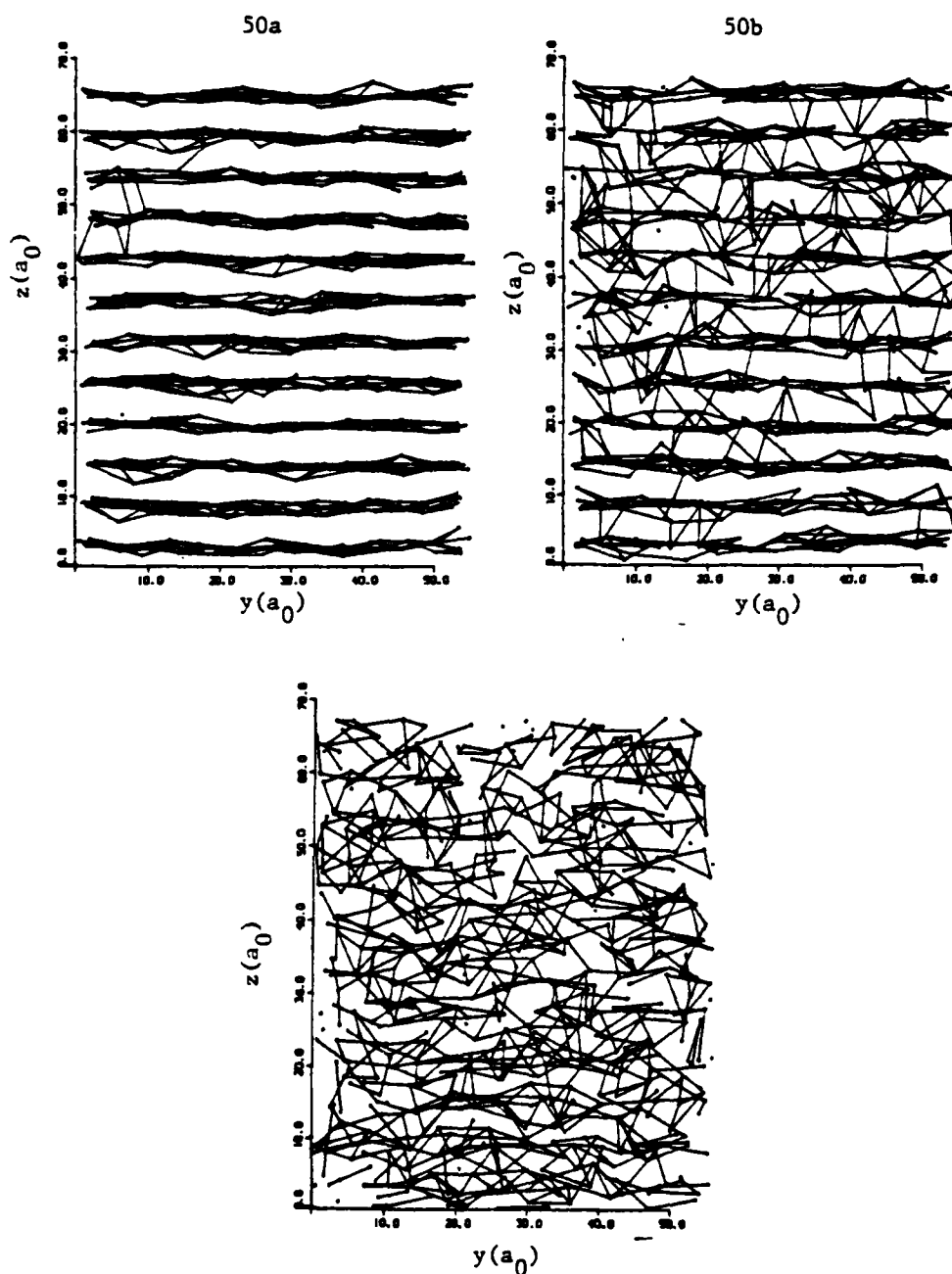
Fig. 50.
Positions of the particles in the molecular dynamics system viewed
looking down the x-axis. Lines have been drawn between near
neighbors within a close-packed plane at the initial configura-
tion. a, b, and c show the positions for the calculations which
produced points 1, 2, and 3 of Fig. 45b, respectively.
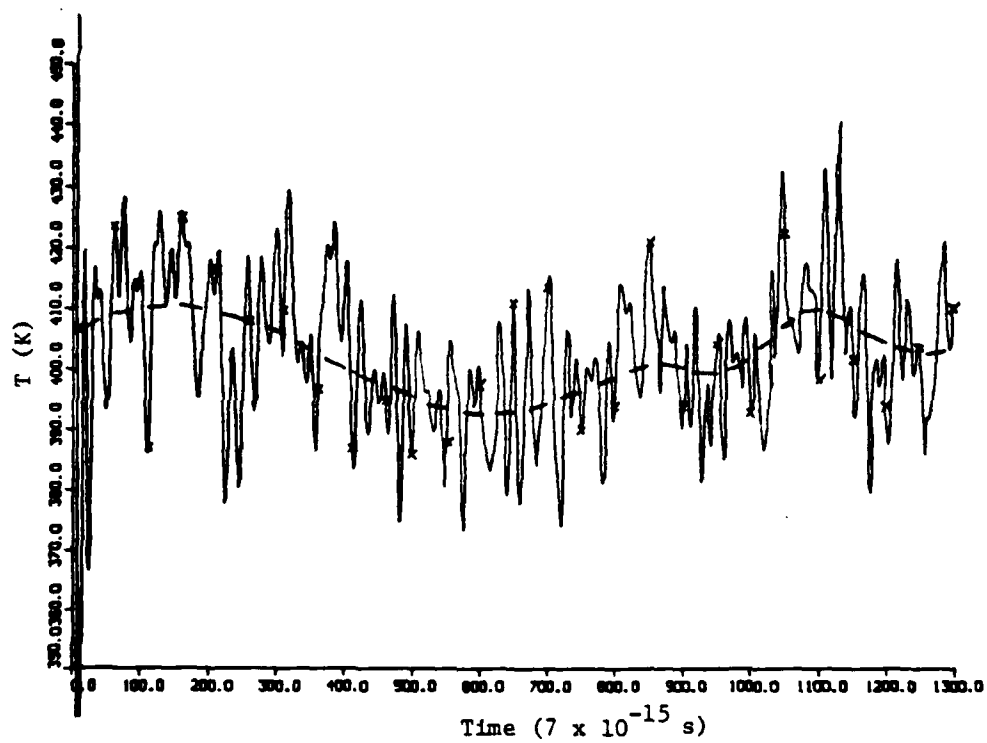
Fig. 51.
Time history of the temperature of the calculation which produced
point 2 in Fig. 45b.

however, place upper limits on the melting temperatures as 430 K for the $232 \, a_0^3$ case and 370 K for the $270 \, a_0^3$ case.

We compare our results with experimental data on sodium to indicate how realistic our molecular dynamics system is. The estimated upper limit to the melting temperatures of 400 K is consistent with the observed melting temperature of 370 K.

Gingrich and Heaton[25] reported the experimental atomic distribution for sodium at 373 K. It is shown as the dashed curve of Fig. 52, where it is compared with our calculated curve for liquid sodium at 400 K.

From the upper curve of Fig. 49 we calculate the self-diffusion coefficient for liquid sodium, which is defined as

$$D = \frac{\overline{\Delta r^2}}{6t} \, , \tag{234}$$

so that D is one-sixth the slope of the curve. We calculate this slope to be $0.056 \, a_0^2/T\emptyset$, which yields a self-diffusion coefficient of $D = 3.7 \times 10^{-5} \, cm^2/s$. The experimental value reported by Faber[26] is $4.2 \times 10^{-5} \, cm^2/s$.

We also compare the difference between the solid and liquid curves at constant temperature with the latent heat of fusion for sodium which is $31.7 \, cal/g = 2.32 \times 10^{-3} \, Ry/ion$. The difference between the solid and liquid curves at 400 K for the $256 \, a_0^3$ atomic volume case is 1.7×10^{-3} Ry/ion.

The above results indicate that the molecular dynamics system is reproducing the essential characteristics of solid and liquid sodium.

D. Dynamic Phase Change

In this section we investigate the bcc-to-hcp phase change. We have already mentioned that the constraint of the fixed boundary
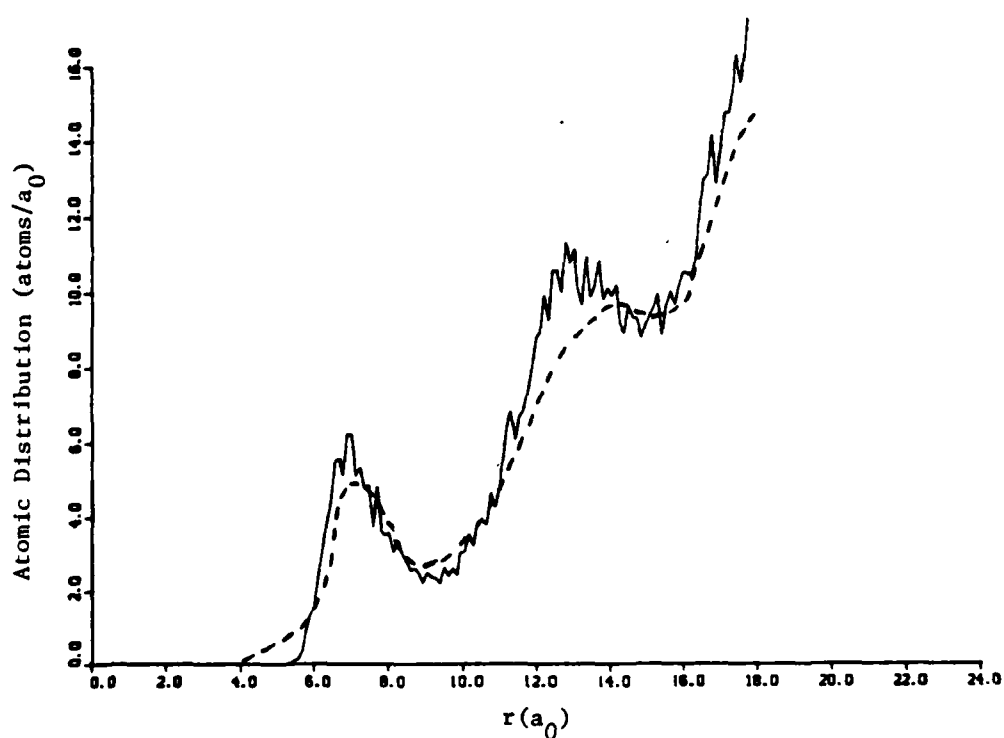
Fig. 52.
The solid line is the calculated atomic distribution of sodium at
400 K. The dashed line is the experimental curve from Ref. 25
at 373 K.

conditions may cause a system to be metastable. This is why we may per-
form calculations on bcc sodium at low temperatures even though the hcp
system is the preferred phase. Both the bcc and hcp 672-particle systems
occupy the same volume but the shape of the system boxes is different, as
described in Sec. IV.B. At the end of Sec. IV.B we mentioned that a com-
pression in the y-direction of the bcc close-packed plane, to form a
hexagonal structure and a corresponding increase in the x- and z-direc-
tions of appropriate magnitude to maintain constant volume, may allow the
hcp form to "fit" in the correctly shaped box.

We made this change of shape on a bcc system at a temperature of
50 K. The calculation was allowed to equilibrate for 150 time units, as
shown in the time history plots of the potential, kinetic, and total
energies of Fig. 53. The atomic distribution of the system at this time
was that shown in Fig. 54a, and the arrangement of particles is shown in
Fig. 55a. For this figure we have connected the nearest neighbors with
lines for clarity. (For a perfect bcc structure without thermal motion,
all the lines would be either horizontal or vertical in Fig. 55a).

By changing the shape of the box, we created a body-centered tetrag-
onal system, thus increasing the potential energy discontinuously and
doing work on the system. The jump in potential and total energies is
evident in Fig. 53 and the body-centered tetragonal atomic distribution
and particle positions are shown in Figs. 54b and 55b.

The system was allowed to equilibrate on its own. The change of
shape had the effect of pushing the system over a potential energy bar-
rier and allowing the particles to find their hcp configuration. This
is attained by the close-packed planes shifting relative to one another,
which is characteristic of martensitic phase transitions. This shifting
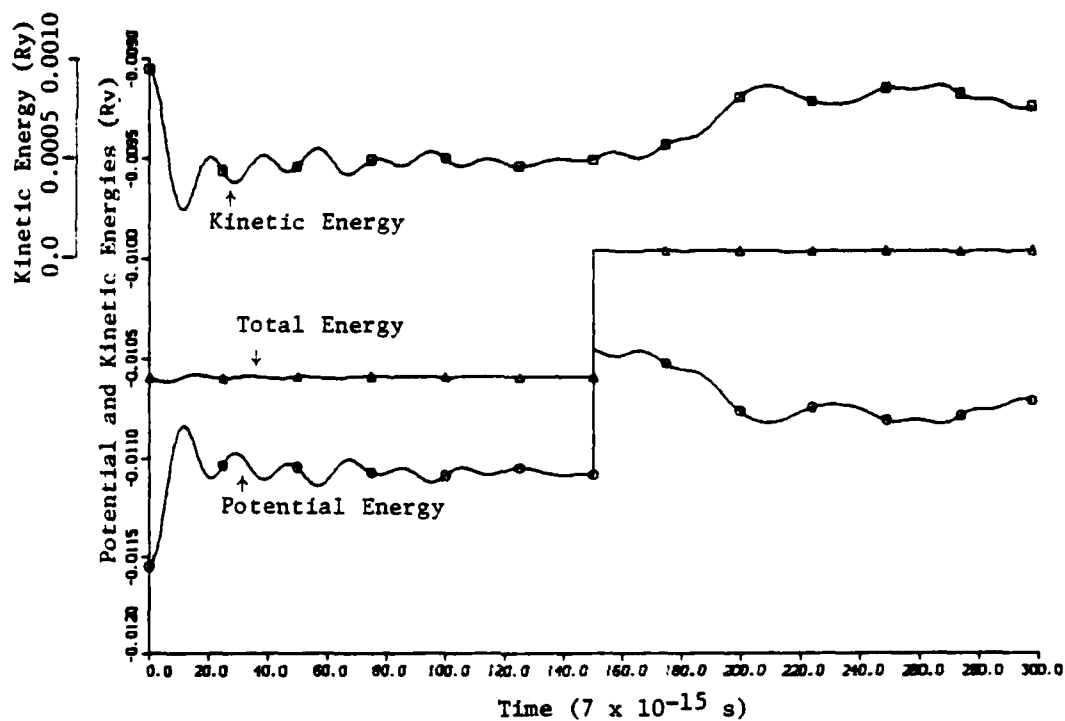
Fig. 53.
Time history plots of the potential, kinetic, and total energies of
the molecular dynamics calculation for which a shape change of the
periodic box was performed at 150 time units.

54a

54b

$r(a_0)$
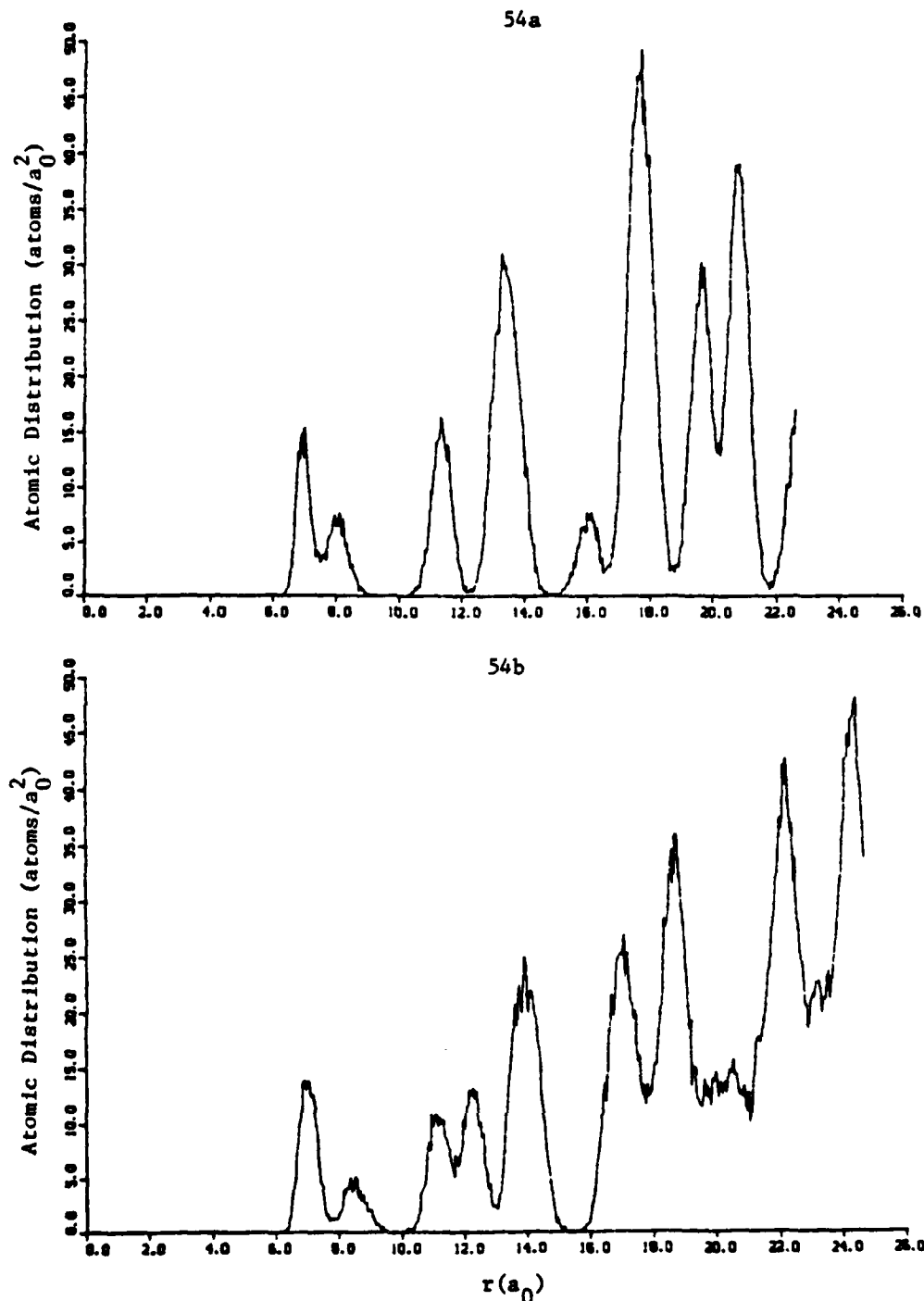
Fig. 54.
The atomic distributions for the dynamic phase change calculation
for (a) the bcc system before the change of shape of the periodic
box, (b) the body-centered tetragonal unstable system immediately
after the shape change, (c) the increased temperature hcp system
after the spontaneous phase change, and (d) the cooled hcp system.
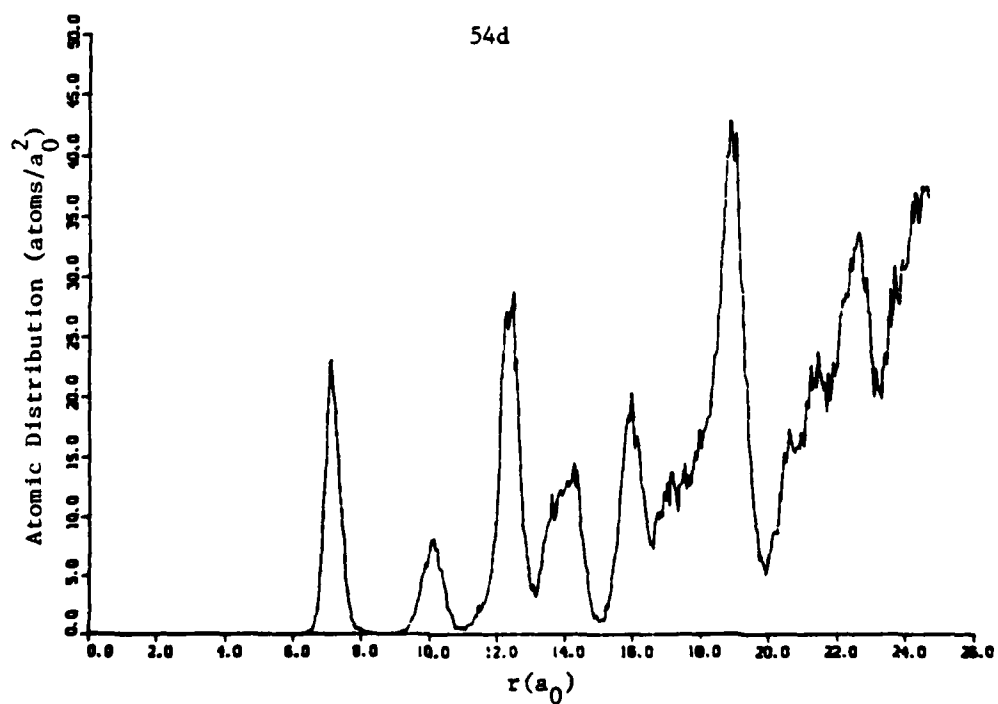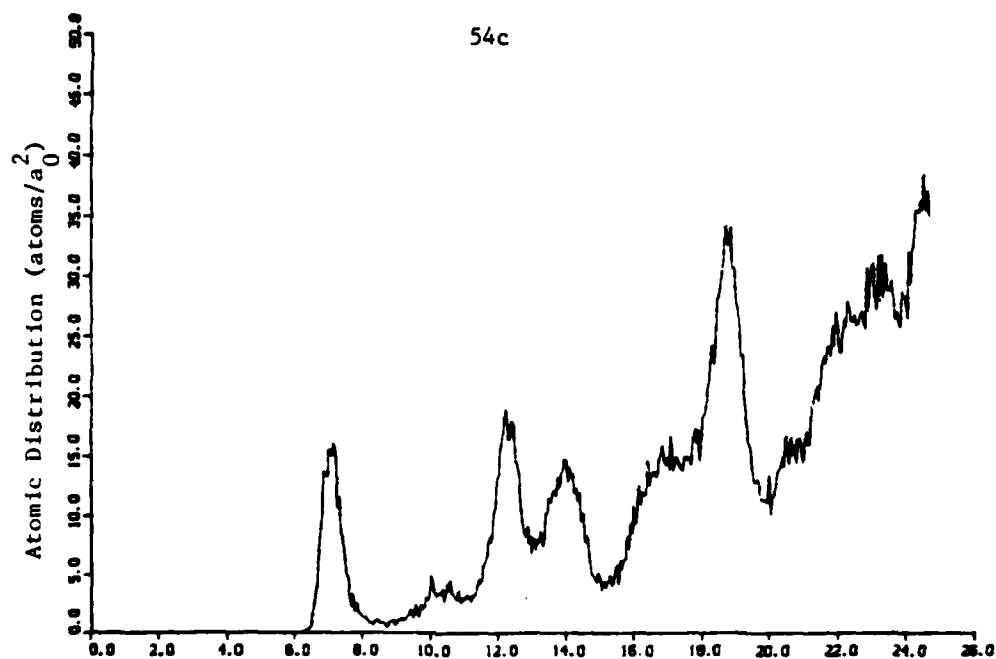
Fig. 54. (cont)
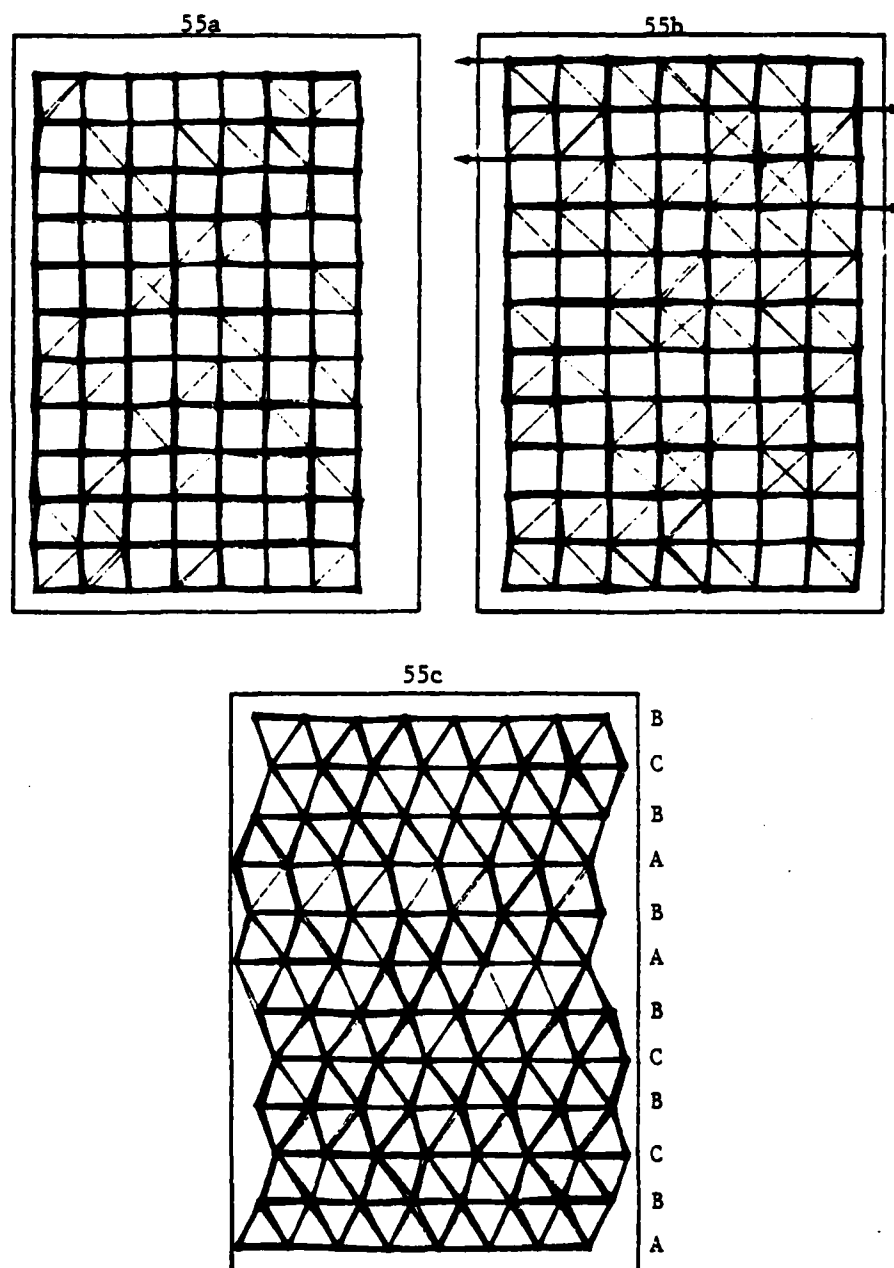
Fig. 55.
The molecular dynamics system viewed down the y-direction with nearest neighbors connected by lines for (a) the bcc system before the shape change, (b) the body-centered tetragonal system immediately after the shape change, and (c) the cooled hcp structure with the relative plane positions indicated by A, B, or C. Outlining the figures does not represent the periodic boundaries and is included for reference only.

is indicated by the arrows in Fig. 55b. As the planes shift, the potential energy is lowered and this is accompanied by a corresponding increase in the kinetic energy, thus raising the system temperature. The system reaches equilibrium as shown in Fig. 53. The atomic distribution for this elevated temperature system is shown in Fig. 54c. We then cooled the system back to about 50 K. The atomic distribution of Fig. 54d shows the peaks characteristic of the hcp structure. The particle positions are shown in Fig. 55c, where the hexagonal structure is apparent. An investigation of the stacking of the planes showed that the system did not equilibrate to a perfect hcp structure, which is an ABABAB··· arrangement of close-packed planes (as discussed in Sec. IV.B), but there are stacking faults as indicated by the ABC labeling of the planes of Fig. 55c. Such stacking faults are prevalent in nature.

We performed a computer experiment on a similar system where we heated the system close to melting and cooled it down. We found that the system would return to the hcp structure, but with stacking faults in different places.

It is difficult to make any quantitative statements about this demonstration. However, it does indicate that a change of shape of the periodic box is necessary to observe a phase change of the type demonstrated here. A shape change is one of the properties that characterizes a martensitic phase change in nature. A change of shape might not be necessary if the system size were very large or if free volume existed which would ease the constraining effects of the periodic boundaries.

VII. DISCUSSION AND CONCLUSIONS

In this paper we have demonstrated that the molecular dynamics technique, coupled with an interaction potential that adequately describes the ion-ion interaction, can be used to study the macroscopic properties of a simple metal. This technique is unique in that it provides a direct calculation of the anharmonic terms in the total system energy. We calculated and presented these terms as a function of volume and temperature for the solid hcp and bcc phases and the glassy solid and liquid state of sodium.

We also calculated and discussed the melting of sodium and were able to reproduce the experimental heat of fusion and put an upper limit on the melt temperature. We showed, by comparison with the experimental atomic distribution and diffusion coefficients, that our calculations adequately represent the dynamic properties of sodium.

As a final demonstration of the capabilities of this technique, we presented the results of a calculation that reproduces the bcc-hcp martensitic phase transition in sodium as a dynamic process. Although this transition was artificially induced by a change of shape of the calculational volume, it demonstrates that such studies are feasible and indicates that such shape changes, which occur in nature, will be a necessary part of future studies.

The possibilities of future work using this technique are many. Although we have the ability to determine the system energy using molecular dynamics, we must look elsewhere to determine the system entropy. This may be done by performing calculations in regions where the theories are known to work. For example, a quasi-harmonic theory may be used to

determine the entropies at low temperatures for the solid. Ideal
gas or hard-sphere theories may be used at high temperatures for the
liquid. Once the entropy is known, the molecular dynamics results may
be used to integrate for the free energies and thus the thermodynamic
properties will be completely specified. With this done, the phase
change and melt regions may be determined from a comparison of free
energies.

The technique should also prove valuable because it may be
extended to higher density and temperature regions. Such theoretical
determination of the equation-of-state and dynamic properties is applic-
able to many areas of current interest such as the study of shock-induced
conditions. The fact that the interaction potential is volume dependent
means that regions of varying densities, which exist (for example) during
the shocking of a material, may be realistically treated.

However, this pseudopotential theory as presented here is limited to
simple metals and compressions of about 50% by the nearly-free-electron
behavior and the theoretical constraint that the ion cores do not overlap.
The extension of the theory to handle systems with more complicated
electronic structures is being done (see, for example, Refs. 1, 2, 6,
and 7) and there is no compelling reason why the theory could not be
developed and this technique applied even after the ion cores overlap
and ionization occurs. We would then be able to calculate the properties
of materials at very high temperatures and pressures that are not easily
accessible to experiment.

APPENDIX A

CALCULATED VALUES OF THE EFFECTIVE ION-ION INTERACTION POTENTIAL AND FORCE FOR SODIUM AT AN ATOMIC VOLUME OF 256 a_0^3

(The potential and force are given by Eqs. (140) and (141) and are plotted in Figs. 9 and 10.)

Radius (a_0)	Potential (Ry)	Force (Ry/a_0)
4.02240E+00	9.20328E-02	1.04985E-01
4.28480E+00	6.79877E-02	7.95036E-02
4.54720E+00	4.97601E-02	6.03136E-02
4.80960E+00	3.59352E-02	4.57175E-02
5.07200E+00	2.54712E-02	3.45297E-02
5.33440E+00	1.75902E-02	2.59104E-02
5.59680E+00	1.17020E-02	1.92537E-02
5.85920E+00	7.35309E-03	1.41142E-02
6.12160E+00	4.19149E-03	1.01589E-02
6.38400E+00	1.94089E-03	7.13260E-03
6.64640E+00	3.04486E-04	4.83011E-03
6.90880E+00	-6.48514E-04	3.12003E-03
7.17120E+00	-1.29252E-03	1.85471E-03
7.43360E+00	-1.65277E-03	9.43054E-04
7.69600E+00	-1.81128E-03	3.05064E-04
7.95840E+00	-1.83111E-03	-1.23702E-04
8.22080E+00	-1.76011E-03	-3.95032E-04
8.48320E+00	-1.63394E-03	-5.50325E-04
8.74560E+00	-1.47856E-03	-6.22384E-04
9.00800E+00	-1.31232E-03	-6.36882E-04
9.27040E+00	-1.14761E-03	-6.13612E-04
9.53280E+00	-9.92284E-04	-5.67488E-04
9.79520E+00	-8.50833E-04	-5.09468E-04
1.00576E+01	-7.25276E-04	-4.47327E-04
1.03200E+01	-6.15967E-04	-3.86316E-04
1.05824E+01	-5.22138E-04	-3.29722E-04
1.08448E+01	-4.42371E-04	-2.79345E-04
1.11072E+01	-3.74927E-04	-2.35902E-04
1.13696E+01	-3.17975E-04	-1.99358E-04
1.16320E+01	-2.69757E-04	-1.69189E-04
1.18944E+01	-2.28698E-04	-1.44589E-04
1.21568E+01	-1.93461E-04	-1.24622E-04
1.24192E+01	-1.62962E-04	-1.08342E-04
1.26816E+01	-1.36354E-04	-9.48769E-05
1.29440E+01	-1.13000E-04	-8.34663E-05
1.32064E+01	-9.24368E-05	-7.35037E-05
1.34688E+01	-7.43424E-05	-6.45273E-05
1.37312E+01	-5.85057E-05	-5.62188E-05
1.39936E+01	-4.47862E-05	-4.83843E-05

Radius (a_0)	Potential (Ry)	Force (Ry/a_0)
1,42560E+01	-3.30775E-05	-4.09333E-05
1,45184E+01	-2.32816E-05	-3.38566E-05
1,47808E+01	-1.52863E-05	-2.72007E-05
1,50432E+01	-8.96650E-06	-2.10429E-05
1,53056E+01	-4.18232E-06	-1.54702E-05
1,55680E+01	-7.77224E-07	-1.05621E-05
1,58304E+01	1.42748E-06	-6.37928E-06
1,60928E+01	2.62846E-06	-2.95819E-06
1,63552E+01	3.03467E-06	-3.05335E-07
1,66176E+01	2.85028E-06	1.60352E-06
1,68800E+01	2.26252E-06	2.82192E-36
1,71424E+01	1.43578E-06	3.42963E-06
1,74048E+01	5.11839E-07	3.52433E-06
1,76672E+01	-3.86726E-07	3.21486E-06
1,79296E+01	-1.16232E-06	2.61285E-06
1,81920E+01	-1.73136E-06	1.82735E-06
1,84544E+01	-2.10731E-06	9.56685E-07
1,87168E+01	-2.23876E-06	1.02103E-07
1,89792E+01	-2.16199E-06	-6.72809E-07
1,92416E+01	-1.90541E-06	-1.30932E-06
1,95040E+01	-1.52315E-06	-1.77254E-06
1,97664E+01	-9.97614E-07	-2.04664E-06
2,00288E+01	-4.38748E-07	-2.13204E-06
2,02912E+01	1.18785E-07	-2.04231E-06
2,05536E+01	6.25982E-07	-1.80234E-06
2,08160E+01	1.04784E-06	-1.44587E-06
2,10784E+01	1.36541E-06	-1.01240E-06
2,13408E+01	1.56945E-06	-5.43035E-07
2,16032E+01	1.65664E-06	-7.64196E-08
2,18656E+01	1.62595E-06	3.53964E-07
2,21280E+01	1.48370E-06	7.21347E-07
2,23904E+01	1.24894E-06	1.00571E-06
2,26528E+01	9.51177E-07	1.19407E-06
2,29152E+01	6.23348E-07	1.28107E-06
2,31776E+01	2.92965E-07	1.26948E-06
2,34400E+01	-2.18462E-08	1.16984E-06
2,37024E+01	-3.06815E-07	9.98186E-07
2,39648E+01	-5.46034E-07	7.73581E-07
2,42272E+01	-7.23000E-07	5.16241E-07
2,44896E+01	-8.24288E-07	2.46397E-07
2,47520E+01	-8.48443E-07	-1.64891E-08
2,50144E+01	-8.04912E-07	-2.54348E-07
2,52768E+01	-7.09694E-07	-4.51820E-07
2,55392E+01	-5.76483E-07	-5.98256E-07
2,58016E+01	-4.13598E-07	-6.88274E-07
2,60640E+01	-2.29254E-07	-7.81342E-07
2,63264E+01	-3.63264E-08	-7.00391E-07
2,65888E+01	1.46631E-07	-6.31177E-07
2,68512E+01	3.00769E-07	-5.21951E-07

Radius (a_0)	Potential (Ry)	Force (Ry/a_0)
2.71136E+01	4.15012E-07	-3.83230E-07
2.73760E+01	4.87809E-07	-2.27429E-07
2.76384E+01	5.24316E-07	-6.76757E-08
2.79008E+01	5.26992E-07	8.49530E-08
2.81632E+01	4.94019E-07	2.17997E-07
2.84256E+01	4.24552E-07	3.26769E-07
2.86880E+01	3.23034E-07	4.05171E-07
2.89504E+01	2.02433E-07	4.49697E-07
2.92128E+01	7.98172E-08	4.59044E-07
2.94752E+01	-3.39044E-08	4.34669E-07
2.97376E+01	-1.34055E-07	3.84898E-07
3.00000E+01	-2.21066E-07	3.04202E-07

APPENDIX B

CALCULATION OF THE KURTOSIS, C, FOR A MICROCANONICAL ENSEMBLE
OF A ONE-DIMENSIONAL CHAIN OF HARD RODS*
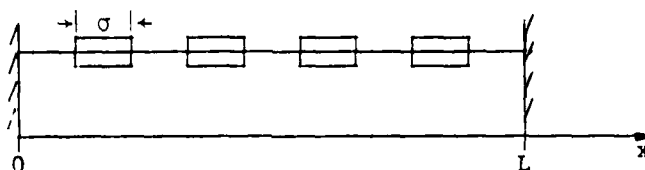
For a microcanonical ensemble the energy, number of rods, and volume
are constant.

E = energy

P = radius of the constant energy hypersphere in momentum

space = $(2mE)^{\frac{1}{2}}$

L = system length

N = number of rods

p_i = momentum of $\underline{i}$th particle

$V_N(p)$ = volume of an N-dimensional hypersphere of radius p

For this system we have

$$E = \frac{1}{2} Nkt = \frac{P^2}{2m} \quad ,$$

$$P = \sum_{i=1}^{N} p_i \quad ,$$

$$\bar{P} = \overline{\sum_{i=1}^{N} p_i} = 0 \quad \text{(center of mass fixed)}$$

$$P^n = \sum_{i=1}^{N} p_i^n \quad , \quad n = 1,2,\cdots \quad ,$$

*Based on a calculation by Brad Lee Holian, Los Alamos National Laboratory.

and

$$(2mE)^{\frac{1}{2}} \leqslant P \leqslant [2m(E + \Delta E)]^{1/2}$$

in the limit as

$$\frac{\Delta P}{P} = \frac{1}{2} \frac{\Delta E}{E} \to 0 \quad .$$

The partition function for the microcanonical ensemble is[29]

$$Z_N \frac{1}{N! h^N} \int^* dp_1 \int dp_2 \cdots \int dp_N \int dq_1 \int dq_2 \cdots \int dq_N \quad ,$$

where * implies that the momentum is constrained to be on the N-dimensional hypersphere of radius $P = (2mE)^{\frac{1}{2}}$, a constant energy surface.

$L - N\sigma$ is the length available to each particle, so that

$$Z_N = \frac{1}{N! h^N} \left(\int_0^{L-N\sigma} dq \right)^N \int^* dp_1 \cdots \int dp_N$$

$$= \frac{(L - N\sigma)^N}{N! h^N} \lim_{\frac{\Delta P}{P} \to 0} [V_N(P + \Delta P) - V_N(P)] \quad .$$

The average of the quantity P^n is given by

$$\overline{P^n} = \left(\frac{1}{Z_N} \right) \frac{(L - N\sigma)^N}{N! h^N} \int^* dp_1 \cdots \int dp_N \sum_{i=1}^{N} p_i^n \quad .$$

We now define

$$I_n(P) = \int^* dp_1 \cdots \int dp_N \sum_{i=1}^{N} p_i^n$$

so that

$$\overline{P^n} = \lim_{\frac{\Delta P}{P} \to 0} \frac{I_n(P + \Delta P) - I_n(P)}{V_n(P + \Delta P) - V_n(P)} \quad .$$

$I_n(P)$ is an N-dimensional hypersphere integral.

The volume, $V_N(P)$ is given by[30]

$$V_N(P) = \frac{\Pi^{N/2}}{\Gamma[(N/2) + 1]} P^N = V_N(1)P^N \quad .$$

For n odd

$$I_n(P) \approx 0 \quad ,$$

and for n even

$$I_n(P) = NV_N(1) \frac{\Gamma[(N/2) + 1]\Gamma[(N + 1)/2]}{\Gamma[(N + n)/2 + 1]\Gamma(1/2)} P^{N+n} \quad .$$

We now expand

$$(P + \Delta P)^{N+n} - P^{N+n} = P^{N+n}\left[\left(1 + \frac{\Delta P}{P}\right)^{N+n} - 1\right]$$

$$= P^{N+n}\left[1 + (N + n) \frac{\Delta P}{P} + \cdots - 1\right]$$

$$= P^{N+n}(N + n) \frac{\Delta P}{P} + \cdots$$

so that

$$I_n(P + \Delta P) - I_n(P) = NV_N(1) \frac{\Gamma[(N/2) + 1]\Gamma[(N + 1)/2]}{\Gamma[(N + n)/2 + 1]\Gamma(1/2)} (N + n)P^{N+n} \frac{\Delta P}{P} + \cdots \quad ,$$

and similarly

$$V_N(P + \Delta P) - V_N(P) = V_N(1)[(P + \Delta P)^N - P^N] = NV_N(1)P^N \frac{\Delta P}{P} + \cdots$$

so that

$$\overline{P^n} = \lim_{\frac{\Delta P}{P} \to 0} \frac{I_N(P + \Delta P) - I_N(P)}{V_N(P + \Delta P) - V_N(P)}$$

$$= P^n \frac{(N + n)\,\Gamma[(N/2) + 1]\,\Gamma[(N + 1)/2]}{\Gamma[(N + n)/2 + 1]\,\Gamma(1/2)} \quad,$$

and we see that

$$n = 0 \quad : \quad \overline{P^0} = N \quad,$$

$$n = 2 \quad : \quad \overline{P^2} = P^2 \quad, \text{ and}$$

$$n = 4 \quad : \quad \overline{P^4} = \frac{3P^4}{N + 2} \quad.$$

So, on using

$$\overline{V^n} = \frac{1}{N} \frac{\overline{P^n}}{m^n}$$

and

$$\frac{P^n}{Nm^n} = \frac{(2mE)^{n/2}}{Nm^n} = \frac{1}{N}\left(\frac{2E}{m}\right)^{n/2} = \frac{1}{N}\left(\frac{NkT}{m}\right)^{n/2} \quad,$$

we may calculate the kurtosis, C, in terms of the velocity moments.

$$C = \overline{V^4} - 3\overline{V^2}^2 \quad,$$

$$\overline{P^2} = P^2 \Rightarrow \overline{V^2} = \frac{kT}{m} \quad,$$

$$\overline{P^4} = \frac{3P^4}{n + 2} \Rightarrow \overline{V^4} = \frac{3N}{N + 2}\left(\frac{kT}{m}\right)^2 \quad,$$

so that

$$C = \frac{-6}{N + 2}\left(\frac{kT}{m}\right)^2 \quad,$$

or for large N

$$C \cong \frac{-6}{N}\left(\frac{kT}{m}\right)^2 \quad ,$$

which is the result used in the text in Sec. IV.D.

APPENDIX C

CALCULATED EQUATION-OF-STATE POINTS FOR hcp, bcc, AND LIQUID SODIUM

The equation-of-state points are tabulated according to the initial configuration of the system. For example, the high temperature bcc calculations are reported with the bcc results even though the system may have melted. All calculations for which the initial condition was the glassy state are reported as equation-of-state points for liquid sodium. The reported errors are the standard deviations of the means and represent the fluctuations of the system temperature and total energy at equilibrium.

	T (K)	Error (K)	Energy (Ry)	Error ($\times 10^{-6}$ Ry)
hcp Structure $\Omega_0 = 232$, $\Phi_0 = -0.458465$	98.83	0.4	-0.456570	0.4
	198.01	0.7	-0.454657	0.4
(ERRATA: Add -0.015559 Ry to energy values)	294.48	0.5	-0.452755	0.6
hcp Structure $\Omega_0 = 250$, $\Phi_0 = -0.458682$	99.63	0.3	-0.456778	0.2
	198.60	0.5	-0.454864	0.3
(ERRATA: Add -0.015960 Ry to energy values)	293.98	0.4	-0.452962	0.6
hcp Structure $\Omega_0 = 256$, $\Phi_0 = -0.458585$	10.03	0.04	-0.458394	0.06
	49.68	0.3	-0.457634	0.2
(ERRATA: Add -0.016089 Ry to energy values)	99.19	0.3	-0.456685	0.2
	198.11	0.5	-0.454771	0.2
	293.27	0.4	-0.452873	0.5

	T (K)	Error (K)	Energy (Ry)	Error (x 10^{-6} Ry)
hcp Structure $\Omega_0 = 270$, $\Phi_0 = 0.458131$	20.01	0.08	-0.457743	0.1
	49.31	0.3	-0.457176	0.2
(ERRATA: Add -0.016374 Ry to energy values)	98.73	0.3	-0.456227	0.2
	196.09	0.4	-0.454313	0.3
	291.93	0.4	-0.452416	0.5
bcc Structure $\Omega_0 = 232$, $\Phi_0 = -0.458447$	100.43	0.5	-0.456472	0.4
	199.62	0.8	-0.454558	0.6
(ERRATA: Add -0.15559 Ry to energy values)	296.41	0.8	-0.452656	0.6
	390.78	0.6	-0.450747	1.0
	432.10	0.5	-0.447884	0.6
	463.88		-0.448818	(not equilibrated)
	476.88		-0.446919	(not equilibrated)
bcc Structure $\Omega_0 = 250$, $\Phi_0 = -0.458551$	100.36	0.6	-0.456650	0.4
	198.76	0.8	-0.454737	0.5
(ERRATA: Add -0.015960 Ry to energy values)	296.26	0.4	-0.452830	0.6
bcc Structure $\Omega_0 = 256$, $\Phi_0 = -0.458447$	10.04	0.05	-0.458256	0.07
	50.37	0.2	-0.457495	0.1
(ERRATA: Add -0.016089 Ry to energy values)	100.15	0.6	-0.456546	0.4
	198.33	0.8	-0.454635	0.5
	294.28	0.3	-0.452744	0.3
	294.86	0.3	-0.452729	0.4
	343.94	0.4	-0.451768	0.4
	387.94	0.6	-0.450851	0.5
	399.13	0.5	-0.448906	0.5

	T (K)	Error (K)	Energy (Ry)	Error (x 10^{-6} Ry)
bcc Structure $\Omega_0 = 256$, $\Phi_0 = -0.458447$ (cont)	408.32		-0.449869	(not equilibrated)
	488.28	0.6	-0.447009	0.7
	587.46	1.0	-0.445122	1.0
bcc Structure $\Omega_0 = 270$, $\Phi_0 = -0.457963$ (ERRATA: Add -0.16374 Ry to energy values)	99.11	0.5	-0.456066	0.4
	199.23	0.4	-0.454153	0.4
	246.98	0.4	-0.453214	0.5
	295.08	0.3	-0.452261	0.5
	340.82	0.5	-0.451290	0.6
	374.16		-0.450357	(not equilibrated)
	404.68		-0.449395	(not equilibrated)
	411.31	0.7	-0.448432	1.0
	498.54	0.6	-0.446535	0.7
Liquid, $\Omega_0 = 232$ (ERRATA: Add -0.015559 Ry to energy values)	10.01		-0.456692	(not stable)
	12.78		-0.456693	
	19.24		-0.456538	
	31.79	0.02	-0.456269	0.01
	82.54	0.2	-0.455298	0.07
	125.17	0.2	-0.454516	0.1
	183.37	0.3	-0.453373	0.2
	248.42	0.5	-0.452092	0.3
	329.61	0.6	-0.450440	0.4
	403.75	0.5	-0.448639	0.4

	T (K)	Error (K)	Energy (Ry)	Error (x 10^{-6} Ry)
Liquid, $\Omega_0 = 256$	17.83		-0.456862	(not stable)
(ERRATA: Add -0.016089 Ry to energy values)	30.70	0.03	-0.456593	0.03
	70.47	0.2	-0.455727	0.1
	137.61	0.4	-0.454357	0.1
	229.80	0.3	-0.452499	0.2
	229.96	0.4	-0.452444	0.3
	263.39	0.4	-0.451672	0.2
	358.78	0.3	-0.449743	0.2
	374.80	0.6	-0.449574	0.4
	482.73	0.9	-0.447149	0.7
Liquid, $\Omega_0 = 270$	7.10		-0.456667	(not stable)
(ERRATA: Add -0.016374 Ry to energy values)	30.06	0.04	-0.456244	0.02
	62.04	0.1	-0.455619	0.06
	142.79	0.4	-0.454108	0.2
	194.91	0.4	-0.453033	0.2
	262.31	0.6	-0.451668	0.3
	307.33	0.6	-0.450628	0.3
	396.01	0.4	-0.448595	0.3

REFERENCES

1. Walter A. Harrison, *Pseudopotentials in the Theory of Metals* (W. A. Benjamin, Inc., New York, 1966).

2. Duane C. Wallace, *Thermodynamics of Crystals* (John Wiley and Sons, Inc., New York, 1972).

3. O. Madelung, *Introduction to Solid State Theory* (Springer-Verlag, New York, 1978).

4. J. M. Ziman, *Electrons and Phonons* (Clarendon Press, Oxford, England, 1960).

5. J. M. Ziman, *Principles of the Theory of Solids* (University Press, Cambridge, England, 1972).

6. Walter A. Harrison, *Solid State Theory* (Mc-Graw-Hill, New York, 1970).

7. *Solid State Physics*, Henry Ehrenreich, Ed. (Academic Press, New York, 1970) Vol. 24.

8. R. D. Mattuck, *A Guide to Feynman Diagrams in the Many Body Problem* (McGraw-Hill, New York, 1976) 2nd ed.

9. L. J. Sham, "A Calculation of the Phonon Frequencies in Sodium," Proc. Roy. Soc. (London) *A283*, 33 (1965).

10. J. Hubbard, "The Description of Collective Motions in Terms of Many Body Perturbation Theory, II. The Correlation Energy of a Free-Electron Gas," Proc. Roy. Soc. (London) *A243*, 336 (1958).

11. David Pines and Philippe Noziéres, *The Theory of Quantum Liquids, Vol. I: Normal Fermi Liquids* (W. A. Benjamin, Inc., New York, 1966).

12. J. P. Hansen and I. R. McDonald, *Theory of Simple Liquids* (Academic Press, New York, 1976).

13. Francis H. Ree, "Computer Calculations for Model Systems," in
    Physical Chemistry, An Advanced Treatise, D. Henderson, Ed.
    (Academic Press, New York, 1971), Vol. 8A.

14. J. L. Lebowitz and J. K. Percus, "Thermodynamic Properties of Small
    Systems," Phys. Rev. 124, 1673 (1961).

15. J. J. Erpenbeck and W. W. Wood, "Molecular Dynamics Techniques for
    Hard-Core Systems," in Statistical Mechanics, Pt. B, B. I. Berne,
    Ed. (Plenum Press, New York, 1977).

16. G. Birkhoff and R. E. Lynch, "Lagrangian Hydrodynamic Computations
    and Molecular Models of Matter," Los Alamos National Laboratory
    report LA-2618 (1961).

17. E. A. Moelwyn-Hughes, Physical Chemistry (Pergamon Press, Oxford,
    England, 1961).

18. Joseph O. Hirshfelder, Charles F. Curtiss, and R. Byron Bird,
    Molecular Theory of Gases and Liquids, (John Wiley and Sons, Inc.,
    New York, 1954 - corrected printing with notes added, 1964).

19. B. R. Martin, Statistics for Physicists (Academic Press, New York,
    1971).

20. Mario P. Tosi, "Cohesion of Ionic Solids in the Born Model," Solid
    State Physics 16, 1 (1964).

21. Duane C. Wallace, "Pseudopotential Calculation of the Thermal Ex-
    pansion Coefficient of Sodium and Potassium," Phys. Rev. 176, 832
    (1968).

22. Handbook of Mathematical Functions, Milton Abramowitz and Irene A.
    Stegun, Eds. (National Bureau of Standards Applied Mathematics
    Series - 55, 1968).

23. Marek Fisz, _Probability Theory and Mathematical Statistics_ (John Wiley and Sons, Inc., New York, 1963), 3rd ed.

24. Galen K. Straub and Duane C. Wallace, "Study of the Martensitic Phase Transition in Sodium," Phy. Rev. B $\underline{3}$, 1234 (1971).

25. N. S. Gingrich and Leroy Heaton, "Structure of Alkali Metals in the Liquid State." J. Chem. Phys. $\underline{34}$, 873 (1961).

26. T. E. Faber, _Introduction to the Theory of Liquid Metals_ (University Press, Cambridge, England, 1972).

27. _Handbook of Chemistry and Physics_, Charles D. Hodgman, Ed. (The Chemical Rubber Publishing Co., Cleveland, Ohio, 1961), 43rd ed.
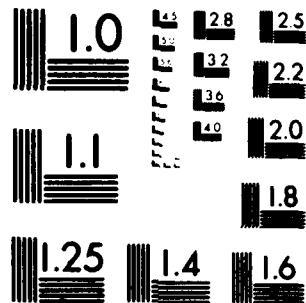
1.0

1.1

1.25 1.4 1.6

2.8 2.5
3.2 2.2
3.6
4.0 2.0

1.8

MICROCOPY RESOLUTION TEST CHART
NATIONAL BUREAU OF STANDARDS 1963-A

CURRICULUM VITAE

RICHARD E. SWANSON

BORN: 15 December 1948

EDUCATION: B.S. 1970 United States Air Force Academy
M.S. 1971 Ohio State University
Ph.D.1981 University of New Mexico

PROFESSIONAL EXPERIENCE:

1971-72 Project Physicist, Air Force Armament Laboratory,
Eglin AFB, Florida

1972-73 Armament Applications Officer, Air Force Armament
Laboratory, Eglin AFB, Florida

1973-75 Staff Scientist, Los Alamos Scientific Laboratory,
Atomic Energy Commission, Los Alamos, New Mexico

1975-76 Instructor, Department of Physics, United States
Air Force Academy, Colorado

1976-77 Instructor, Department of Physics, United States
Military Academy, West Point, New York

1977-79 Computational Laser Physicist, Advanced Laser
Technology Division, Air Force Weapons Laboratory,
Kirtland AFB, New Mexico

1979-81 Guest Scientist, Detonation Theory and Application
Group, Theoretical Division, Los Alamos National
Laboratory, Los Alamos, New Mexico

PUBLICATIONS:

1975 "One Dimensional Elastic-Plastic Calculations Involving
Strain Hardening and Strain-Rate Effects for Aluminum,"
Los Alamos Scientific Laboratory Report LA-5831

1975 "One Dimensional Calculations of Shock Loaded Polycrys-
talline Beryllium," Los Alamos Scientific Laboratory
Report LA-5943-MS

1975 "Calculations of Underwater Detonations of Military
Explosives (U)," Los Alamos Scientific Laboratory
Report LA-5985-MS (Conf)

1979 "Optical Performance of CW Chemical Laser,"AIAA 12th
Fluid and Plasma Dynamics Conference, Williamsburg, Va

1980 "GOPWR: A Computer Program to Calculate the Performance
of CW Chemical Lasers," Air Force Weapons Laboratory,
Kirtland AFB, NM, AFWL-TR-79-142

1980 "Code Anchoring: GOPWR (U),"Air Force Weapons Laboratory,
Kirtland AFB, NM, AFWL-TR-79-151 (Conf)

ATE
ME
LME
8